CHALMERS
UNIVERSITY OF TECHNOLOGY

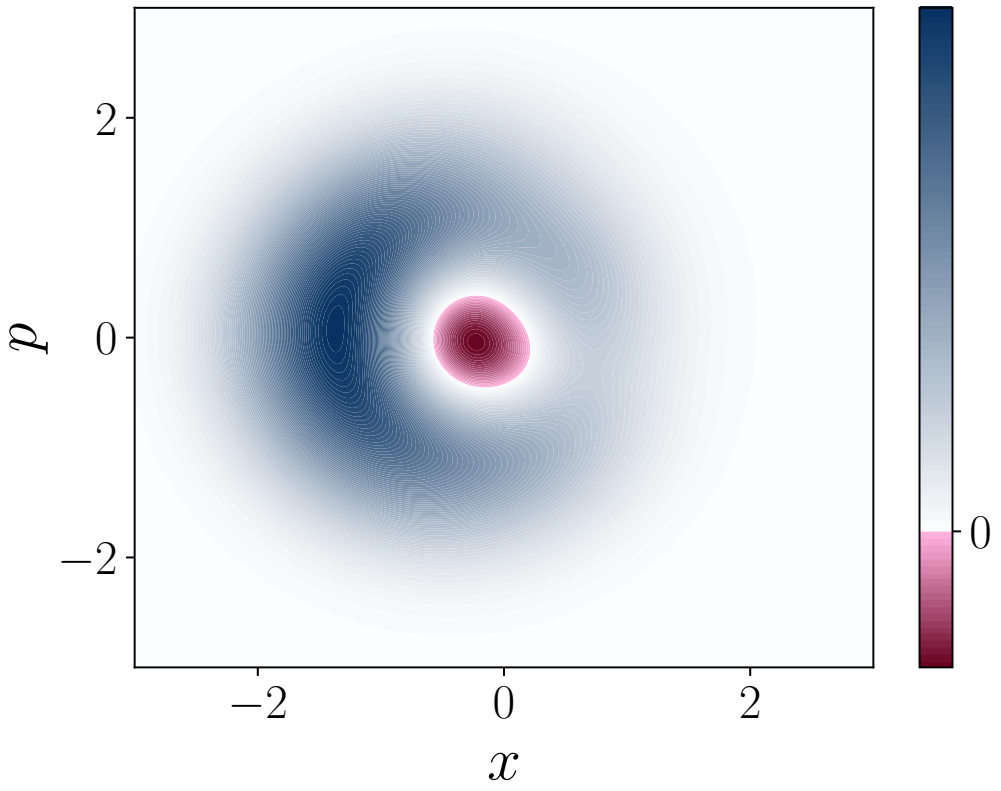

Quantum state tomography of 1D resonance fluorescence

Master's thesis in Physics and Astronomy

Ingrid Strandberg

Department of Microtechnology and Nanoscience
CHALMERS UNIVERSITY OF TECHNOLOGY
Göteborg, Sweden 2017

Master's thesis 2017

Quantum state tomography of 1D resonance fluorescence

INGRID STRANDBERG

CHALMERS
UNIVERSITY OF TECHNOLOGY

Department of Microtechnology and Nanoscience
Applied Quantum Physics Laboratory
Chalmers University of Technology
Göteborg, Sweden 2017

Quantum state tomography of 1D resonance fluorescence
INGRID STRANDBERG

Supervisor: Fernando Quijandria
Examiner: Göran Johansson

Master's Thesis 2017
Department of Microtechnology and Nanoscience
Applied Quantum Physics Laboratory
Chalmers University of Technology
SE-412 96 Göteborg
Telephone +46 31 772 1000

Cover: Contour plot of the reconstructed Wigner function for a driven two-level atom in front of a mirror. The purple color represents negative values, which is what we are looking for.

Typeset in LaTeX
Printed by Chalmers Reproservice
Göteborg, Sweden 2017

Quantum state tomography of 1D resonance fluorescence
INGRID STRANDBERG
Department of Microtechnology and Nanoscience
Chalmers University of Technology

Abstract

Tomography is the name under which all state reconstruction techniques are denoted, one of the most recognized examples being medical tomography. Quantum state tomography is a procedure to determine the quantum state of a physical system. By performing homodyne measurements on resonance fluorescence from an artificial atom coupled to a one-dimensional transmission line, its quantum state can be reconstructed. Resonance fluorescence is one of the simplest setups that results in *non-classical* states of light. If these states are non-classical in the sense that they have a negative Wigner function, they can be used as a computational resource for quantum computing.

There are many different approaches to quantum computing. Some, like gate based quantum computing using discrete variables like qubits, have been extensively researched, both theoretically and experimentally. There exists and alternative approach: continuous variable quantum computing. The continuous variables we will be concerned with are the components of the electromagnetic field that constitute the resonance fluorescence.

There are different parameters that affect the nature of the resonance fluorescence, for example, the number of transmission lines the atom is coupled to, or the strength of the driving field. In this work, we develop the tools necessary to numerically simulate homodyne detection of resonance fluorescence for different sets of parameters, and reconstruct the quantum state as well as calculating the Wigner negativity.

Keywords: quantum computing, light-matter interaction, artificial atoms, quantum measurements, stochastic master equations, quantum state reconstruction, Wigner function

Acknowledgements

First and foremost, I want to thank my supervisor Fernando Quijandria for guiding me throughout this entire project, and tirelessly answering my many questions. Your help has been invaluable.

I also want to thank my examiner Göran Johansson, for giving me an interesting project to work on, and for always being happy to answer questions or talk, no matter how busy his schedule is.

I want to thank the PhD students and postdocs at the Applied Quantum Physics Laboratory for being so very friendly, and fun to have lunch and fika with. I am very happy to have the opportunity to stay and continue working in the group.

Ingrid Strandberg, Göteborg, May 2017

Contents

1
Introduction

The main theme of this thesis is *quantum state tomography* — the reconstruction of a quantum state from measurements. In the interest of developing a quantum computer, we wish to generate non-classical states of light. We numerically simulate measurements of resonance fluorescence to find what parameters produce the most suitable states.

In this chapter we will briefly review our approach to quantum computing. Then we list the motivation and aim of this work and give an overview of the structure of the thesis.

1.1 Quantum computation

In 1994, Shor's algorithm for factoring integers [1] jump-started the interest in quantum computing, proving theoretically that quantum computers are able to outperform classical ones. It is substantially faster than the most efficient classical factoring algorithm we know of, and could break many of the cryptosystems in use today. Its invention sparked a tremendous interest in quantum computers.

Continuous variables

In a conventional computer information is stored as binary digits, bits. These can be in one of two states, 0 or 1. To represent a bit, one can use any physical system provided it allows two distinct states. A quantum bit, qubit, has the additional property that it can be in a superposition of the two quantum states $|0\rangle$ and $|1\rangle$.

Information stored in bits can be manipulated using logic gates. Correspondingly, qubits can be manipulated using quantum gates. This gate-based approach to quantum computing has been extensively researched, both theoretically and experimentally. Physical realizations include varied setups such as ion traps, optical lattices, quantum dots as well as superconducting circuits.

However, quantum computation is not restricted to discrete variable setups, such as qubits. By the end of the last century, the idea of performing quantum computation using continuous variables was presented [2]. In this approach information is encoded in observables characterized by a continuous spectrum, such as the components of an electromagnetic field. This is illustrated in Fig. 1.1

Continuous variable quantum computation has largely been studied in optical setups. In the field of quantum optics, preparation as well as individual manipulation of quantum states of light can be efficiently implemented [3]. This made continuous variable systems a very promising platform for the implementation of quantum computation. Nevertheless, progress in this field has been hindered by the difficulty of implementing interactions between photons.

However, strong photon-photon interactions have been demonstrated for propagating microwave photons in superconducting circuits. The potential of microwaves for continuous variable quantum computing has not yet been explored.

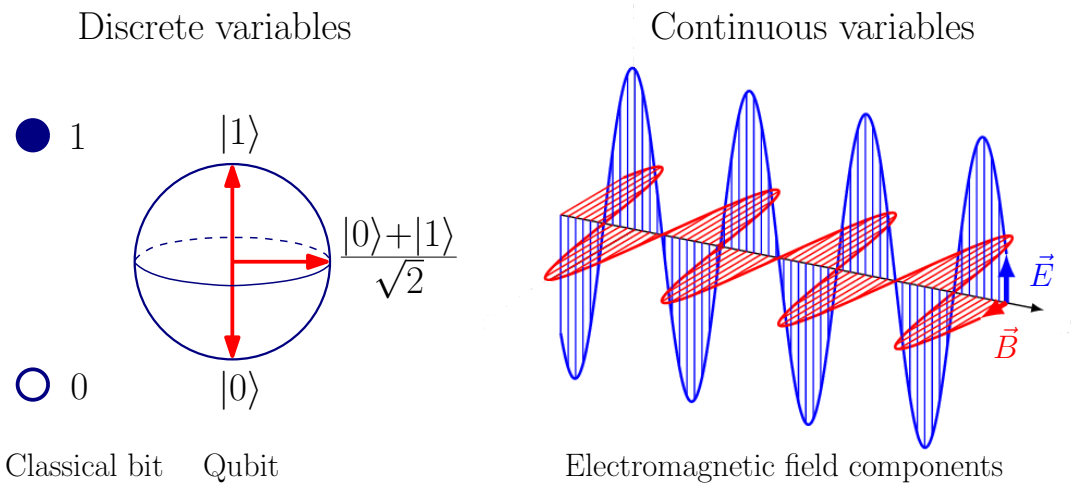

Figure 1.1

1.2 Motivation and goal

Negative Wigner functions as a resource for quantum computation

The Wigner function is a quantum phase-space distribution, containing full information of its associated quantum state. The Wigner function can take on negative values, which is identified with non-classicality. This has been identified as a computational resource. More precisely, it has been shown that quantum circuits where the initial state and all the subsequent quantum operations can be represented by positive Wigner functions can be efficiently simulated with classical resources [4]. Thus negative Wigner functions are needed to achieve a quantum advantage.

We wish to explore the generation states of light suitable for quantum information processing, that is, negative Wigner function states.

One of the simplest setups to produce non-classical states of light is to scatter

coherent light off a two-level system. Using superconducting circuits, this two-level system can be a so-called artificial atom, also known as a qubit.

Before trying to realize this experimentally, it is a good idea to investigate how to best generate negative Wigner state theoretically. That is what is done in this thesis. The work in this thesis describes how to numerically simulate the scattering of light of a two-level artificial atom and calculate the Wigner function of the resulting resonance fluorescence emitted by the atom.

We will investigate what parameters influence the negativity of the Wigner function and what settings give the most negativity.

1.3 Overview of thesis

Since resonance fluorescence is the result of photons interacting with an atom, we begin in Chapter 2 by deriving the Hamiltonian for light-matter interaction of a two-level system. The important *quadrature operators* are defined. Then we treat the dynamics of open quantum systems. More exactly, the two-level atom interacting with an environment of electromagnetic field modes. After this, we have a discussion about quantum measurement theory, most importantly *homodyne measurement* of the quadratures. This leads to a *stochastic master equation* for the time-evolution of the system. We then review two methods for numerically solving stochastic equations.

In Chapter 3 we reflect over what it means for a state to be non-classical. We explain in more detail what the Wigner function is, what it is used for, and how Wigner negativity can be obtained.

After this, Chapter 4 reviews resonance fluorescence. Also, circuit-QED is introduced. It is discussed how resonance fluorescence can be generated in superconducting circuits, and why this is beneficial.

In Chapter 5, we consider how to calculate the Wigner function of a state of light from resonance fluorescence using measurement data. Finally, we show results of the reconstruction of the Wigner function for different sets of parameters.

Lastly, we do a quick summary and discuss the results in Chapter 6.

2

Theory: light-matter interaction, open systems, quantum measurements and numerical methods

2.1 Light-matter interaction

The subject of this thesis is tomography of resonance fluorescence. Resonance fluorescence is photons being emitted from an atom, as it de-excites after being excited by an external driving field. In this Section we will begin with a derivation of the simplest model of fully quantum-mechanical light-matter interaction: the *Jaynes-Cummings* model. This describes a two-level atom interacting with a quantized electromagnetic field mode. This lays the foundation for moving into the subject of quantum system interaction with environments in Section 2.2.

2.1.1 Hamiltonian of a charged particle in an electromagnetic field

The Hamiltonian of a particle with charge e, mass m and momentum $\vec{p}$ in an electromagnetic field is given by

$$H = \frac{(\vec{p} - e\vec{A})^2}{2m} + e\phi, \tag{2.1}$$

where $\vec{A}$ is the vector potential of the magnetic field and ϕ is the scalar potential of the electric field [5]. This Hamiltonian is obtained by adding $e\phi$ and letting $\vec{p} \to \vec{p} - e\vec{A}$ in the Hamiltonian $H = p^2/2m$ for a free particle. This is the *minimal coupling* prescription.

It is interesting to note that the underlying reason for the minimal coupling is the gauge invariance of quantum electrodynamics. The electric and magnetic fields are invariant under the usual gauge transformations of electrodynamics:

$$\begin{aligned} \phi' &= \phi - \frac{\partial \chi}{\partial t}, \\ \vec{A}' &= \vec{A} + \nabla\chi, \end{aligned} \tag{2.2}$$

where χ is an arbitrary scalar function [6]. This means that the equations of motion for the fields, the Maxwell equations, must be gauge invariant. The minimal coupling Hamiltonian (2.1), from which equations of motion can be derived by use of the Euler-Lagrange equations, ensures this is the case. This is also the correct quantum mechanical Hamiltonian, as the minimal coupling Hamiltonian also ensures that the Schrödinger equation is form-invariant under the gauge transformations (2.2).

2.1.2 Interaction terms: $\vec{r}\cdot\vec{A}$ or $\vec{d}\cdot\vec{E}$

When we evaluate the square $(\vec{p}-e\vec{A})^2$ we find a cross term $\vec{p}\cdot\vec{A}$. This describes a coupling between a charged particle at position $\vec{r}$ and an electromagnetic field represented by the vector potential $\vec{A}(\vec{r},t)$. It is very common to instead express the interaction Hamiltonian as $\vec{d}\cdot\vec{E}$, where $\vec{d}$ is the dipole operator of the atom, as this can simplify calculations. These two forms of the interaction are in fact equal, under certain circumstances. The $\vec{r}\cdot\vec{A}$-representation can be transformed into the $\vec{d}\cdot\vec{E}$-representation by a unitary transformation. This procedure is named after Göppert-Mayer, who first discussed it in 1931 [7]. The circumstances that need to be fulfilled in order for the equivalence to hold is the *dipole approximation*, sometimes called the *long-wavelength approximation*. Details on the Göppert-Mayer transformation and dipole approximation can be found in Appendix A.

2.1.3 Quantization

The Hamiltonian (2.1) is the classical Hamiltonian. We now derive the fully quantized Hamiltonian, the Jaynes-Cummings Hamiltonian. First, we quantize the electromagnetic field. During this process, we define the *quadrature operators*, which are imperative for later chapters in this work. Then we quantize the two-level atom, and lastly the interaction term.

2.1.3.1 Field quantization

To quantize the electromagnetic field, we consider a radiation field inside a cavity of volume V. We will use an expansion of the vector potential $\vec{A}$ in terms of cavity modes. The problem then reduces to the quantization of the harmonic oscillator corresponding to each mode.

We do a Fourier expansion of the vector potential [8]

$$\vec{A}(\vec{r},t)=\sum_k \vec{e}_k A_k(\vec{r},t), \tag{2.3}$$

where

$$A_k(\vec{r},t)=\frac{1}{\sqrt{2\varepsilon_0 V\omega_k}}[A_k\exp\left(-\mathrm{i}\omega_k t+\mathrm{i}\vec{k}\cdot\vec{r}\right)+A_k^*\exp\left(\mathrm{i}\omega_k t-\mathrm{i}\vec{k}\cdot\vec{r}\right)]. \tag{2.4}$$

From Maxwell's equation

$$E_k = -\frac{\partial A_k}{\partial t}\,, \tag{2.5}$$

we get the electric field strength. Only looking at a single mode k, we drop the k-index. A single-mode electric field is then written as

$$E(\vec{r},t) = \mathrm{i}\sqrt{\frac{\omega}{2\varepsilon_0 V}}[A\exp\left(-\mathrm{i}\omega t + \mathrm{i}\vec{k}\cdot\vec{r}\right) - A^*\exp\left(\mathrm{i}\omega t - \mathrm{i}\vec{k}\cdot\vec{r}\right)]. \tag{2.6}$$

At this point we will follow the canonical quantization prescription. This corresponds to promoting the complex amplitudes A, A^* to operators $a, a^\dagger$ which obey the bosonic commutation relation $[a, a^\dagger] = 1$. These operators are the creation and annihilation operators of the electromagnetic field. Transforming (2.6) to its quantum mechanical counterpart, we have

$$E(\vec{r},t) = \mathrm{i}\sqrt{\frac{\omega}{2\varepsilon_0 V}}[a\exp\left(-\mathrm{i}\omega t + \mathrm{i}\vec{k}\cdot\vec{r}\right) - a^\dagger\exp\left(\mathrm{i}\omega t - \mathrm{i}\vec{k}\cdot\vec{r}\right)]. \tag{2.7}$$

We now define the *quadrature operators*

$$\begin{aligned} X &= \frac{1}{\sqrt{2}}(a^\dagger + a), \\ Y &= \frac{\mathrm{i}}{\sqrt{2}}(a^\dagger - a), \end{aligned} \tag{2.8}$$

obeying the commutation relation

$$[X, Y] = \mathrm{i}. \tag{2.9}$$

These operators will play a very important role in this work. Using these, we rewrite (2.7):

$$E(\vec{r},t) = \sqrt{\frac{\omega}{\varepsilon_0 V}}[X\sin(\omega t - \vec{k}\cdot\vec{r}) - Y\cos(\omega t - \vec{k}\cdot\vec{r})]. \tag{2.10}$$

Looking at Eq. (2.10), we can identify the quadratures with the sine and cosine components of the electric field, respectively. If we imagine a reference field $\cos(\omega t - \vec{k}\cdot\vec{r})$, the quadratures are also known as the in-phase and out-of-phase components.

Now assume the cavity has perfectly conducting walls. The electric field must vanish at the boundaries. Imposing this boundary condition on the field gives us a standing wave solution

$$E(r,t) = \sqrt{\frac{\omega}{\varepsilon_0 V}}(a^\dagger + a)\sin(\vec{k}\cdot\vec{r}). \tag{2.11}$$

We also want the quantized Hamiltonian. For the free electromagnetic field, a single-mode field is formally equivalent to a quantum harmonic oscillator of unit mass, having the Hamiltonian

$$H = \frac{\omega}{2}(a^\dagger a + aa^\dagger) = \omega(a^\dagger a + \frac{1}{2}). \tag{2.12}$$

The 1/2 is just a constant zero-point energy which does not influence the dynamics, so we can drop it.

Note that this Hamiltonian represents a single mode field. In the cavity, we will have field operators $a_k, a_k^\dagger$ corresponding to each mode satisfying the boundary condition. In the next chapter we will have an atom interacting with the electric field in free space. To achieve this, the sum over all wave vectors $\vec{k}$ will turn into an integral. For later convenience we define the integral in terms of the angular frequency ω instead, so for $V \to \infty$ we have the Hamiltonian

$$H = \int \mathrm{d}\omega \, a^\dagger(\omega) a(\omega). \tag{2.13}$$

2.1.3.2 Free Atomic Hamiltonian H_{atom}

To simplify the treatment, we assume that the system interacting with the electromagnetic field only has two energy levels. A two-level atom is of course an approximation, as a real atom has many energy levels. This approximation is however well-justified in cases where the system has a highly non-linear spectrum, so that the energy levels are unevenly spaced. If the system interacts with a narrow band of radiation that is only resonant with a transition between two specific energies, the probability amplitudes for transitions to other levels are negligible and you have an effective two-level system [9].

We denote the lower level of energy $E_g = \hbar\omega_g$ by $|g\rangle$, where the g stands for *ground state*. Denote the upper level of energy $E_e = \hbar\omega_e$ by $|e\rangle$, where e stands for *excited state*. These states are the eigenstates of the atomic Hamiltonian H_{atom}. The Hamiltonian reads in matrix form as

$$H_{\mathrm{atom}} = \begin{pmatrix} E_e & 0 \\ 0 & E_g \end{pmatrix} = \frac{1}{2}\begin{pmatrix} (E_e + E_g) + (E_e - E_g) & 0 \\ 0 & (E_e + E_g) - (E_e - E_g), \end{pmatrix},$$

or

$$H_{\mathrm{atom}} = E\mathbb{1} + \frac{1}{2}\hbar\omega_{\mathrm{A}}\begin{pmatrix} 1 & 0 \\ 0 & -1 \end{pmatrix}, \tag{2.14}$$

where $E = \frac{1}{2}(E_e + E_g)$ and $\omega_{\mathrm{A}} \equiv \omega_e - \omega_g$ denotes the transition frequency. We can remove the first term on the right hand side, which is a constant energy, by shifting the origin of energy to half-way between E_g and E_e. Then, we can rewrite (2.14) as

$$H_{\mathrm{atom}} = \frac{1}{2}\hbar\omega_{\mathrm{A}}\sigma_z, \tag{2.15}$$

with

$$\sigma_z = \begin{pmatrix} 1 & 0 \\ 0 & -1 \end{pmatrix}$$

being the Pauli Z matrix.

Finally, we have the free atom and field Hamiltonian

$$H_0 = \hbar\omega a^\dagger a + \frac{1}{2}\hbar\omega_{\mathrm{A}}\sigma_z. \tag{2.16}$$

2.1.3.3 Interaction Hamiltonian $\vec{d}\cdot\vec{E}$

Because the dipole operator is odd under parity, its diagonal matrix elements vanish (see Appendix A.3). Defining $d \equiv \langle e|\vec{d}|g\rangle$, we can then write the dipole operator as

$$\vec{d} = d\,|e\rangle\langle g| + d^*\,|g\rangle\langle e|\,, \tag{2.17}$$

with

$$\begin{aligned} |e\rangle &= \begin{pmatrix}1\\0\end{pmatrix}, \quad \langle e| = (1\,0), \\ |g\rangle &= \begin{pmatrix}0\\1\end{pmatrix}, \quad \langle g| = (0\,1). \end{aligned} \tag{2.18}$$

The operator

$$|e\rangle\langle g| = \begin{pmatrix}1\\0\end{pmatrix}(0\,1) = \begin{pmatrix}0 & 1\\0 & 0\end{pmatrix} = \sigma_+, \tag{2.19}$$

is the atomic raising operator, i.e., it raises the atom from the ground state to the excited state. The operator

$$|g\rangle\langle e| = \begin{pmatrix}0\\1\end{pmatrix}(0\,1) = \begin{pmatrix}0 & 0\\1 & 0\end{pmatrix} = \sigma_-, \tag{2.20}$$

lowers the atom from the excited state to the ground state and is therefore the atomic lowering operator. By appropriate choice of the phases in the atomic eigenstates $\{|g\rangle, |e\rangle\}$ we can always arrange so that d is real. The dipole operator is then written as

$$\vec{d} = d(\sigma_+ + \sigma_-). \tag{2.21}$$

Pseudo-Spin Operators

The Hilbert space spanned by the two states, the excited state $|e\rangle$ and the ground state $|g\rangle$, is equivalent to the Hilbert space of a spin-$\frac{1}{2}$ system [10]. The atomic raising and lowering operators σ_+ and σ_- are linear combinations of the Pauli matrices, which constitute spin operators. Since our system does not describe spin states, our atomic raising and lowering operators are called *pseudo-spin* operators.

In fact, the radiation field interacts with the electron in the atom. This means we should quantize the electron wave field (this is done in [11]), and thus end up with Fermi creation and annihilation operators for the electron. Nevertheless, a two-level atomic system described by the Fermi operators may be described by

pseudo-spin operators since the pseudo-spin operators obey same commutation relations as Fermi operators.

Note that the pseudo-spin operators $\sigma_\pm$ are eigenoperators of the atomic Hamiltonian:

$$[H_{\text{atom}}, \sigma_-] = -\hbar\omega_{\text{A}}\sigma_-, \quad [H_{\text{atom}}, \sigma_+] = \hbar\omega_{\text{A}}\sigma_+. \tag{2.22}$$

Hence, $\sigma_\pm$ changes the atomic energy by the amount $\pm\hbar\omega_{\text{A}}$, corresponding to the absorption and emission process, respectively [10].

2.1.4 Jaynes-Cummings Hamiltonian

In the interaction Hamiltonian $H_{\text{int}} = -\vec{d}\cdot\vec{E}$, we insert (2.21) and (2.11):

$$H_{\text{int}} = -\vec{d}\cdot\vec{E} = \hbar g(\sigma_+ + \sigma_-)(a + a^\dagger), \tag{2.23}$$

where $g = -d\sqrt{\omega/\varepsilon_0 V}\sin(kr)$.

So we have the full Hamiltonian

$$H = H_0 + H_{\text{int}} = \hbar\omega a^\dagger a + \frac{1}{2}\hbar\omega_{\text{A}}\sigma_z + \hbar g(\sigma_+ + \sigma_-)(a + a^\dagger). \tag{2.24}$$

This is known as the *Rabi model*. To arrive at the more easily solvable Jaynes-Cummings Hamiltonian, one must apply the *rotating wave approximation* (RWA) (see Appendix A.4).

When this is done, we get the *Jaynes-Cummings Hamiltonian*

$$H = H_0 + H_{\text{int}} = \hbar\omega a^\dagger a + \frac{1}{2}\hbar\omega_{\text{A}}\sigma_z + \hbar g(a\sigma_+ + a^\dagger\sigma_-). \tag{2.25}$$

This is the simplest model of fully quantized light-matter interaction. The atomic transition frequency is ω_{A}, and the frequency associated to the field mode is ω, while the coupling constant g quantifies the strength of the interaction between the atom and the electromagnetic field.

Further information on the subject can be found in any textbook on quantum optics, for example [12, 13, 14].

2.2 Open quantum systems

An open quantum system is a system S which interacts with another quantum system E, the environment. The latter is typically much larger or contains many more degrees of freedom than the system S. The environment is typically modelled as a collection of uncoupled harmonic oscillators. For a thorough survey of the theory of open quantum systems, see e.g. [10].

The system and environment together constitute a closed system, i.e., they obey the quantum Liouville equation (also known as the von Neumann equation), which is generalization of the Schrödinger equation for mixed states. However, we are interested in the *reduced dynamics* of the system S.

The Hilbert space of the total system $(S + E)$ is the tensor product space $\mathcal{H} = \mathcal{H}_\mathrm{S} \otimes \mathcal{H}_E$, and the full Hamiltonian governing its evolution can be written as

$$H = H_\mathrm{S} \otimes \mathbb{1}_\mathrm{E} + \mathbb{1}_\mathrm{S} \otimes H_\mathrm{E} + H_\mathrm{int}, \tag{2.26}$$

where H_S is the free Hamiltonian of the system, H_E is the free Hamiltonian of the environment, and H_int describes the interaction between them. An operator $\hat{A}$ acting in H_S is extended to $H_\mathrm{S} \otimes \mathcal{H}_E$ by the convention that it acts as the identity on $\mathcal{H}_E$: $\hat{A} = \hat{A} \otimes \mathbb{1}_E$. For notational simplicity, the identity will not be indicated from now on.

A quantum state that can be described by a state vector $|\psi\rangle$ is said to be *pure*. There are states that cannot be described by a single state vector, those are called *mixed* states. Mixed states are described by a density operator

$$\rho = \sum_i p_i \left|\psi_i\right\rangle\!\left\langle\psi_i\right|, \tag{2.27}$$

where the sum is over an ensemble of pure states $\{|\psi_i\rangle\}$, and p_i is the probability of the system being in the ith state. The density operator for a pure state is simply $\rho = |\psi\rangle\langle\psi|$. The trace of a density operator is always equal to 1,

$$\mathrm{Tr}[\rho] = 1, \tag{2.28}$$

since the diagonal elements correspond to the occupation probabilities of the different ensemble states.

We suppose that we are able to prepare the state of the total system $S + E$ (at the initial time $t = 0$) as an uncorrelated product state $\rho(0) = \rho_s(0) \otimes \rho_E(0)$. Due to the interaction H_int, in general, initial product states will evolve into entangled states:

$$\rho(t) = U^\dagger(t)\rho(0)U(t) = U^\dagger(t)\Big(\rho_s(0) \otimes \rho_E(0)\Big)U(t), \tag{2.29}$$

where $U(t) = \exp\left(-\mathrm{i}Ht\right)$ is the time-evolution operator led by (2.26). The *reduced* density matrix $\rho_s(t)$ describing the system is then obtained by taking the partial trace of the joint state over the environment degrees of freedom. This is commonly called "tracing out the environment".

Definition 1. Partial trace:

$$\rho_s(t) = \mathrm{Tr_B}\left[\rho(t)\right] = \sum_i {}_{\mathrm{E}}\langle\psi_i|\rho(t)|\psi_i\rangle_{\mathrm{E}}, \tag{2.30}$$

where $\{|\psi_i\rangle_{\mathrm{E}}\}$ is an orthonormal basis in $\mathcal{H}_E$. The equation describing the time evolution of the reduced state ρ_s is known as the *master equation*. This will be derived in Section 2.2.4.

The density operator is very useful for calculating operator averages. The average of a system operator $\hat{A}$ is given by

$$\langle\hat{A}\rangle = \mathrm{tr_S}[\rho_s A], \tag{2.31}$$

where the trace is over the system.

2.2.1 Input-Output Formalism

Quantum optics experiments are essentially scattering experiments, and input-output theory is essentially a scattering-theory description. The scattering potential is replaced by the system S, and the environment carries the incoming and outgoing fields [15]. Gardiner and Collett [16] first developed the input-output formalism for open quantum systems. We will follow a general derivation [16, 17] which does not specify the system Hamiltonian or the system operators and their commutation relations. We will however restrict to a two-level atom interacting with a reservoir of harmonic oscillators, modelling the electromagnetic field.

We are interested in studying how the interaction with the two-level system affects the field, so we will derive a boundary condition for the field before and after interacting with the atom.

The Hamiltonian of the total system, the atom interacting with the reservoir of harmonic oscillators, is

$$\begin{aligned} H &= H_{\mathrm{atom}} + H_{\mathrm{E}} + H_{\mathrm{int}}, \\ H_{\mathrm{atom}} &= \frac{1}{2}\hbar\omega_{\mathrm{A}}\sigma_z, \\ H_{\mathrm{E}} &= \hbar\int_{-\infty}^{\infty}\mathrm{d}\omega\,\omega b^\dagger(\omega)b(\omega), \\ H_{\mathrm{int}} &= \mathrm{i}\hbar\int_{-\infty}^{\infty}\mathrm{d}\omega\,\kappa(\omega)[b^\dagger(\omega)\sigma_- - \sigma_+ b(\omega)], \end{aligned} \tag{2.32}$$

where $b(\omega)$ are boson annihilation operators for the reservoir, thus satisfying

$$[b(\omega), b^\dagger(\omega')] = \delta(\omega - \omega'), \tag{2.33}$$

and σ_-, σ_+ are the lowering and raising operators for the atom.

We note that the rotating wave approximation has been made; the range of the ω integration being $(-\infty, \infty)$ rather than $[0, \infty)$. These two things are connected. The RWA argues that only terms which are almost resonant are important. Thus

we can extend the lower integration limit, since the added terms are non-resonant and thus contribute very little.

The Heisenberg equation of motion for $b(\omega)$ is

$$\dot{b}(\omega) = -\frac{\mathrm{i}}{\hbar}[b(\omega), H] = -\mathrm{i}\omega b(\omega) + \kappa(\omega)\sigma_-. \tag{2.34}$$

Note that $b(\omega)$ is a Heisenberg operator, $b(\omega) = b(\omega, t)$ with $b(\omega, t) = e^{\mathrm{i}Ht}b(\omega)e^{-\mathrm{i}Ht}$. For notational convenience we omit the time argument of operators. The solution to (2.34) can be written in two ways, in terms of a boundary condition at time t_0 (before the interaction takes place) or at t_1 (after the interaction). The two solutions are [11]

$$b(\omega) = e^{\mathrm{i}\omega(t-t_0)}b_0(\omega) + \kappa(\omega)\int_{t_0}^{t} e^{-\mathrm{i}\omega(t-t')}\sigma_-(t')\,\mathrm{d}t', \tag{2.35}$$

and

$$b(\omega) = e^{-\mathrm{i}\omega(t-t_1)}b_1(\omega) - \kappa(\omega)\int_{t}^{t_1} e^{-\mathrm{i}\omega(t-t')}\sigma_-(t')\,\mathrm{d}t', \tag{2.36}$$

where $b_0(\omega)$ is $b(\omega)$ at time $t = t_0$, and $b_1(\omega)$ is the value of $b(\omega)$ at $t = t_1$.

The equations so far are exact. Now we apply the *first Markov approximation*:

$$\kappa(\omega) = \sqrt{\gamma/2\pi}, \tag{2.37}$$

where γ is a real number, which will later be interpreted as the radiative decay rate of the two-level atom.

The first Markov approximation is named as such because it ensures that the equations of motion are simple first-order differential equations. This also means that the future time development of any operator is determined simply by the knowledge of all the system operators in the present [17].

We now *define* an input field

$$b_{\mathrm{in}}(t) = \frac{1}{\sqrt{2\pi}}\int \mathrm{d}\omega\, e^{-\mathrm{i}\omega(t-t_0)}b_0(\omega), \tag{2.38}$$

which satisfies the bosonic commutation relation

$$[b_{\mathrm{in}}(t), b_{\mathrm{in}}^\dagger(t')] = \delta(t-t'). \tag{2.39}$$

Note that $b_{\mathrm{in}}(t)$ actually means the time at which the incoming field interacts with the system, rather than specifying that $b_{\mathrm{in}}(t)$ is a time-dependent operator at time t.

Now, we integrate (2.35) over ω to get

$$\frac{1}{\sqrt{2\pi}}\int \mathrm{d}\omega\, b(\omega) = b_{\mathrm{in}}(t) + \frac{\sqrt{\gamma}}{2}\sigma_-(t), \tag{2.40}$$

where we have made use of the properties

$$\int_{-\infty}^{\infty} \mathrm{d}\omega\, e^{\mathrm{i}\omega(t-t')} = 2\pi\delta(t-t'), \tag{2.41}$$

and

$$\int_{t_0}^{t} \sigma_-(t')\delta(t-t')\,\mathrm{d}t' = \frac{1}{2}\sigma_-(t). \tag{2.42}$$

The factor 1/2 in (2.42) is because the peak of the delta function is at the end of the integration interval.

If we consider $t_1 > t$, we can similarly to (2.38) define the output field

$$b_{\text{out}}(t) = \frac{1}{\sqrt{2\pi}} \int \mathrm{d}\omega\, e^{-\mathrm{i}\omega(t-t')} b_1(\omega). \tag{2.43}$$

The output fields can be shown to satisfy exactly the same commutation relations as the input fields:

$$[b_{\text{out}}(t), b_{\text{out}}^\dagger(t')] = \delta(t-t'). \tag{2.44}$$

Furthermore,

$$\frac{1}{\sqrt{2\pi}} \int \mathrm{d}\omega\, b(\omega) = b_{\text{out}}(t) - \frac{\sqrt{\gamma}}{2}\sigma_-(t), \tag{2.45}$$

is derived similarly to (2.40). From (2.40) and (2.45) follows

$$b_{\text{out}}(t) = b_{\text{in}}(t) + \sqrt{\gamma}\sigma_-(t). \tag{2.46}$$

This is the most important result of this section. The quantities b_{in} and b_{out} are interpreted as inputs and outputs to the system. The output field is the sum of the input field and the field radiated by the source. The condition (2.46) can be viewed as a boundary condition, relating the input field, output field, and the field radiated by the system.

2.2.2 Stochastic Calculus

The commutation relation (2.39) acquired the δ-function form as a result of the Markovian approximation. Because $\delta(t-t')$ is a very singular function, one must be very careful when integrating the equations of motion. This requires us to define quantum stochastic calculus, just as one must define regular stochastic calculus when dealing with delta-correlated classical noise. [18]. Quantum stochastic differential equations can be defined rigorously and guarantee that the singular limit for the commutators is well defined [19].

For a more rigorous and extensive treatment of stochastic calculus, see e.g. [20] or [21]. Here we introduce the very basics of stochastic calculus, which is used to derive quantum stochastic equations.

The input field $b_{\text{in}}(t)$ for vacuum has some peculiar properties due to its commutation relation. For example, it has infinite variance. This is a property it shares with classical white noise, usually denoted $\xi(t)$ [22]. So, under certain circumstances $b_{\text{in}}(t)$ can be interpreted as a noise term [16]. We will use this similarity to white noise in Section 2.3.4.2.

The Wiener process is a stochastic process. More precisely, it is a mathematical idealization of Brownian motion. Despite the unusual nature of $b_{\text{in}}(t)$, we can make sense out of its integral. Namely, we define the *quantum Wiener process* $B(t)$:

$$B(t) - B(t_0) = \int_{t_0}^{t} \mathrm{d}t'\, b_{\text{in}}(t') = \int_{t_0}^{t} \mathrm{d}B(t') = B(t, t_0), \tag{2.47}$$

with the infinitesimal increment

$$\mathrm{d}B(t) = b_{\text{in}}(t)\,\mathrm{d}t. \tag{2.48}$$

This is called the *Wiener increment*. The point of defining the infinitesimal operator $\mathrm{d}B = b_{\text{in}}\,\mathrm{d}t$ is that although it appears to be of order $\mathrm{d}t$, because of the singularity of the commutation relation (2.39) it is actually of order $\sqrt{\mathrm{d}t}$.

To be able to evaluate the integral (2.47), we interpret it as an *Ito stochastic integral*. One notable thing distinguishing Ito stochastic calculus from ordinary calculus is that the chain rule of ordinary calculus

$$\mathrm{d}(x_1 x_2) = x_1\,\mathrm{d}x_2 + x_2\,\mathrm{d}x_1, \tag{2.49}$$

becomes

$$\mathrm{d}(x_1 x_2) = x_1\,\mathrm{d}x_2 + x_2\,\mathrm{d}x_1 + \mathrm{d}x_1\,\mathrm{d}x_2. \tag{2.50}$$

For more details about the Ito formulation of stochastic calculus, see Appendix B.

When the environment is in the vacuum state, we define the *Ito table* [17]

$$\begin{aligned} [\mathrm{d}B(t)]^2 &= [\mathrm{d}B^\dagger(t)]^2 = 0, \\ \mathrm{d}B(t)\,\mathrm{d}B^\dagger(t) &= \mathrm{d}t, \\ \mathrm{d}B^\dagger(t)\,\mathrm{d}B(t) &= 0. \end{aligned} \tag{2.51}$$

These properties of the stochastic process will be used to derive the *quantum Langevin equation* for the time-evolution of a system operator.

2.2.3 Quantum Langevin equation

To obtain the Heisenberg-picture dynamics of the system, one might just aim to write down the usual Heisenberg equations of motion. However, because of the singularity of the commutation relation (2.39) the situation is not so simple. There are several approaches to find the correct Heisenberg equations. Here we proceed as Wiseman and Milburn [23]. For an arbitrary system operator a, which here can be σ_- or σ_+, we define a Heisenberg operator

$$a(t + \mathrm{d}t) = U^\dagger(t + \mathrm{d}t)a(t)U(t + \mathrm{d}t), \tag{2.52}$$

which obeys the Ito differential equation

$$\mathrm{d}a = a(t + \mathrm{d}t) - a(t) = U^\dagger(t + \mathrm{d}t)a(t)U(t + \mathrm{d}t) - a(t). \tag{2.53}$$

The coupled system-bath evolves unitarily according to

$$U(t,t_0) = e^{-\mathrm{i}H(t-t_0)/\hbar}. \tag{2.54}$$

with H given by Eq. (2.32).

In order to simplify the calculations, we move to a frame rotating with the reservoir Hamiltonian H_E. The quantum states are then redefined as

$$|\psi'\rangle = e^{-\mathrm{i}H_\mathrm{E}t/\hbar}\,|\psi\rangle\,. \tag{2.55}$$

Using (A.6) with $T = \exp\left(-\mathrm{i}H_\mathrm{E}t/\hbar\right)$, the Hamiltonian in this frame is

$$H' = e^{\mathrm{i}H_\mathrm{E}t/\hbar}He^{-\mathrm{i}H_\mathrm{E}t/\hbar} - H_\mathrm{E}. \tag{2.56}$$

The system Hamiltonian H_atom is unaffected by the transformation, since its operators commute with the environment operators. We write the time-evolution operator (2.54) as

$$U(t,t_0) = \exp\left(-\frac{\mathrm{i}}{\hbar}\int_{t_0}^{t}\mathrm{d}t'\,\left[H_\mathrm{atom} + \mathrm{i}\sqrt{\frac{\gamma}{2\pi}}\int_{-\infty}^{\infty}\mathrm{d}\omega\,\left(b^\dagger(\omega)\sigma_- e^{-\mathrm{i}\omega t'} - b(\omega)\sigma_+ e^{\mathrm{i}\omega t'}\right)\right]\right),$$

or

$$U(t,t_0) = \exp\left(-\frac{\mathrm{i}}{\hbar}\int_{t_0}^{t}\mathrm{d}t'\,\left[H_\mathrm{atom} + \mathrm{i}\sqrt{\gamma}(b_\mathrm{in}^\dagger(t')\sigma_- - b_\mathrm{in}(t')\sigma_+)\right]\right). \tag{2.57}$$

Using definition (2.47), we can rewrite $U(t,t_0)$ as

$$U(t,t_0) = \exp\left(-\frac{\mathrm{i}}{\hbar}H_\mathrm{atom}(t-t_0) + \sqrt{\gamma}\left(B^\dagger(t,t_0)\sigma_- - B(t,t_0)\sigma_+\right)\right). \tag{2.58}$$

where we made use of (2.48). If we were to expand the exponential in $U(t+\mathrm{d}t,t)$ to first order in $\mathrm{d}t$, we would simply reproduce the naive Heisenberg equation. Because $\mathrm{d}B$ and $\mathrm{d}B^\dagger$are of order $\sqrt{\mathrm{d}t}$, it is necessary to expand $U(t+\mathrm{d}t,t)$ to second order:

$$\begin{aligned}
U(t+\mathrm{d}t,t) &= \mathbb{1} - \frac{\mathrm{i}}{\hbar}H_\mathrm{atom}\,\mathrm{d}t + \sqrt{\gamma}\left(\mathrm{d}B^\dagger\sigma_- - \mathrm{d}B\sigma_+\right) + \\
&+ \frac{1}{2}\Big(-\frac{\mathrm{i}}{\hbar}H_\mathrm{atom}\,\mathrm{d}t + \sqrt{\gamma}\left(\mathrm{d}B^\dagger\sigma_- - \mathrm{d}B\sigma_+\right)\Big)^2 = \\
&= \mathbb{1} - \frac{\mathrm{i}}{\hbar}H_\mathrm{atom}\,\mathrm{d}t + \sqrt{\gamma}\,\mathrm{d}B^\dagger\sigma_- - \sqrt{\gamma}\,\mathrm{d}B\sigma_+ - \frac{\gamma}{2}\sigma_+\sigma_-\,\mathrm{d}t - \frac{\gamma}{2}\left\{\sigma_+,\sigma_-\right\}\mathrm{d}B^\dagger\,\mathrm{d}B,
\end{aligned} \tag{2.59}$$

where we have used the Ito table (2.51). From here, the infinitesimal evolution (2.52) is given by

$$\begin{aligned}
U^\dagger(t+\mathrm{d}t)a(t)U(t+\mathrm{d}t) &= \Big(\mathbb{1} + \frac{\mathrm{i}}{\hbar}H_\mathrm{atom}\,\mathrm{d}t + \sqrt{\gamma}\,\mathrm{d}B\sigma_+ - \sqrt{\gamma}\,\mathrm{d}B^\dagger\sigma_- - \frac{\gamma}{2}\sigma_+\sigma_-\,\mathrm{d}t - \\
&- \frac{\gamma}{2}\left\{\sigma_+,\sigma_-\right\}\mathrm{d}B^\dagger\,\mathrm{d}B\Big)a\Big(\mathbb{1} - \frac{\mathrm{i}}{\hbar}H_\mathrm{atom}\,\mathrm{d}t + \sqrt{\gamma}\,\mathrm{d}B^\dagger\sigma_- - \sqrt{\gamma}\,\mathrm{d}B\sigma_+ - \frac{\gamma}{2}\sigma_+\sigma_-\,\mathrm{d}t - \\
&- \frac{\gamma}{2}\left\{\sigma_+,\sigma_-\right\}\mathrm{d}B^\dagger\,\mathrm{d}B\Big).
\end{aligned} \tag{2.60}$$

Only keeping terms to first order in $\mathrm{d}t$ i.e., second order in $\mathrm{d}B$ or $\mathrm{d}B^\dagger$, and again using the Ito table, we finally get the *quantum Langevin equation*

$$\begin{aligned}\mathrm{d}a = &-\frac{\mathrm{i}}{\hbar}[a, H_{\mathrm{atom}}]\,\mathrm{d}t + \frac{\gamma}{2}(2\sigma_+ a\sigma_- - a\sigma_+\sigma_- - \sigma_+\sigma_- a)\,\mathrm{d}t - \\ &- \sqrt{\gamma}[a, \sigma_+]\,\mathrm{d}B(t) + \sqrt{\gamma}[a, \sigma_-]\,\mathrm{d}B^\dagger(t).\end{aligned} \tag{2.61}$$

This is an equation for a system operator, but it can be used to derive the *master equation* which determines the time evolution of the entire system state.

2.2.4 Master equation

A master equation is a generalization of the Schrödinger equation for open systems interacting with a bath [24]. In deriving a master equation, it is necessary to make a Markovian assumption. This implies that the influence of the system on the bath is dissipated so quickly that the change in the system depends only on its present state. This was done in the derivation of the quantum Langevin equation, and we will use Eq. (2.61) to derive the master equation, following [17].

Using the relation (2.31), the mean of any operator $a(t)$ is given by

$$\langle a(t)\rangle = \mathrm{tr_S tr_B}[a(t)\rho_s(t_0)\otimes\rho_E(t_0)]) = \mathrm{tr_S tr_B}[U(t,t_0)a(t_0)U^\dagger(t,t_0)\rho_s(t_0)\otimes\rho_E(t_0)], \tag{2.62}$$

with $U(t,t_0)$ given by (2.54). Using the cyclic property of the trace, and defining the time-dependent reduced density matrix

$$\rho(t) = \mathrm{tr_B}[a(t_0)U^\dagger(t,t_0)\rho_s(t_0)\otimes\rho_E(t_0)U(t,t_0)], \tag{2.63}$$

we can write

$$\langle a(t)\rangle = \mathrm{tr_S}[a(t_0)\rho(t)]. \tag{2.64}$$

We now note that we can write (2.61) in the form

$$\mathrm{d}a(t) = A[a(t)]\,\mathrm{d}t + G^\dagger[a(t)]\,\mathrm{d}B(t) + G[a(t)]\,\mathrm{d}B^\dagger(t), \tag{2.65}$$

where we have superoperators of the form

$$A[a] = -\frac{\mathrm{i}}{\hbar}[a, H_{\mathrm{atom}}] + \frac{\gamma}{2}(2\sigma_+ a\sigma_- - a\sigma_+\sigma_- - \sigma_+\sigma_- a), \tag{2.66}$$

$$G^\dagger[a] = -\sqrt{\gamma}[a, \sigma_+], \quad G[a] = \sqrt{\gamma}[a, c].$$

For vacuum, $\langle \mathrm{d}B\rangle = \langle \mathrm{d}B^\dagger\rangle = 0$ so

$$\langle \mathrm{d}a(t)\rangle = \langle A[a(t)]\rangle\,\mathrm{d}t. \tag{2.67}$$

Using (2.64) we can evaluate the right hand side to get

$$\langle \mathrm{d}a(t)\rangle = \mathrm{tr_S}[A[a(t_0)]\rho(t)]\,\mathrm{d}t. \tag{2.68}$$

For simplicity and notational clarity, we now denote $a = a(t_0)$ for the operators, which are the Schrödinger picture operators. Using (2.66) in (2.68), and the cyclicity of the trace, we get

$$\frac{\mathrm{d}\,\langle a(t)\rangle}{\mathrm{d}t} = \mathrm{tr_S}\Big[a\Big(\frac{\mathrm{i}}{\hbar}[\rho, H_{\mathrm{atom}}] + \frac{\gamma}{2}(2c\rho c^\dagger - c^\dagger c\rho - \rho c^\dagger c)\Big)\Big]. \tag{2.69}$$

On the other hand, from (2.64) we get

$$\frac{\mathrm{d}\,\langle a(t)\rangle}{\mathrm{d}t} = \mathrm{tr_S}\left[a\,\frac{\mathrm{d}\rho(t)}{\mathrm{d}t}\right]. \tag{2.70}$$

Both equation (2.69) and (2.70) are valid for any system operator a, hence we derive the master equation

$$\frac{\mathrm{d}\rho}{\mathrm{d}t} = \frac{\mathrm{i}}{\hbar}[\rho, H_{\mathrm{atom}}] + \frac{\gamma}{2}(2c\rho c^\dagger - c^\dagger c\rho - \rho c^\dagger c) \equiv \mathcal{L}\rho. \tag{2.71}$$

This is the *quantum optical master equation*. It is considered to define the superoperator $\mathcal{L}$, called the *Liouvillian*. This equation describes the time-evolution of the system. The second term on the right hand side describes spontaneous radiative decay transitions $|e\rangle \to |g\rangle$. The coupling strength between the atom and the environment is given by γ, which can also be interpreted as the radiative decay rate.

We can also introduce the Lindblad superoperator

$$\mathcal{D}[\hat{A}]\rho \equiv A\rho A^\dagger - \frac{1}{2}(A^\dagger A\rho + \rho A^\dagger A). \tag{2.72}$$

This operator is also called the *dissipator*. In this case it represents the radiative decay, giving the non-unitary evolution. The master equation (2.71) then looks like

$$\frac{\mathrm{d}\rho}{\mathrm{d}t} = \frac{\mathrm{i}}{\hbar}[\rho, H_{\mathrm{atom}}] + \gamma\mathcal{D}[\sigma_-]\rho. \tag{2.73}$$

The total system $S + E$ evolves unitarily with the Hamiltonian H. The open system S has a unitary evolution part governed by the Hamiltonian H_{atom} and a non-unitary evolution described by the dissipator $\mathcal{D}$, due to the coupling to the reservoir.

2.2.5 Multiple decay channels

We have the master equation (2.73) for a two-level atom interacting with a reservoir of harmonic oscillators, representing the electromagnetic field. This reservoir serves as a *decay channel*, as the atom dissipates energy into the environment.

We now generalize this into a situation with multiple environments. The master equation then becomes

$$\frac{\mathrm{d}\rho}{\mathrm{d}t} = \frac{\mathrm{i}}{\hbar}[\rho, H_{\mathrm{atom}}] + \sum_i \gamma_i\mathcal{D}[\sigma_-]\rho, \tag{2.74}$$

In this work we will consider the case of an atom coupled to two non-interacting electromagnetic fields, modelling two transmission lines. The master equation for this system is

$$\frac{\mathrm{d}\rho}{\mathrm{d}t} = \frac{\mathrm{i}}{\hbar}[\rho, H_{\mathrm{atom}}] + \gamma_1 \mathcal{D}[\sigma_-]\rho + \gamma_2 \mathcal{D}[\sigma_-]\rho. \tag{2.75}$$

where the different γ_i describe the coupling strength to each transmission line. In this particular case of two identical decay channels, the master equation looks identical to the one-channel equation (2.73) as the dissipator terms add up: $\gamma_1 + \gamma_2 = \gamma$.

With two environments to couple to, we can also have two different sets of input and output relations.

2.2.6 Driving the system

The derivation of the quantum Langevin equation and the master equation in the previous sections assumed that the environment was in the vacuum state: $\mathrm{d}B\,|0\rangle = 0 \implies \langle \mathrm{d}B\rangle = 0$. There are still vacuum fluctuations, but their mean is zero.

When the input field b_{in} is a coherent drive, we have $\langle \mathrm{d}B(t)\rangle = \beta\,\mathrm{d}t$ [23]. Redoing the derivation of the master equation using this, we get

$$\begin{aligned}
\dot{\rho} &= -\frac{\mathrm{i}}{\hbar}[H_{\mathrm{atom}}, \rho] + \gamma\mathcal{D}[\sigma_-]\rho - \sqrt{\gamma}[\sigma_+, \rho]\,\langle \mathrm{d}B\rangle + \sqrt{\gamma}[\sigma_-, \rho]\,\langle \mathrm{d}B^\dagger\rangle = \\
&= -\frac{\mathrm{i}}{\hbar}[H_{\mathrm{atom}}, \rho] - \mathrm{i}\sqrt{\gamma}[-\mathrm{i}\sigma_+\beta - \sigma_-\beta^*, \rho] + \gamma\mathcal{D}[\sigma_-]\rho = \\
&= -\frac{\mathrm{i}}{\hbar}[H', \rho] + \gamma\mathcal{D}[\sigma_-]\rho,
\end{aligned} \tag{2.76}$$

where the new Hamiltonian H'

$$H' = H_{\mathrm{atom}} - \mathrm{i}\sqrt{\gamma}(\sigma_+\beta - \sigma_-\beta^*), \tag{2.77}$$

has a driving term $-\mathrm{i}\sqrt{\gamma}(\sigma_+\beta - \sigma_-\beta^*)$. We can choose β to be real. To conform with the notational standard in literature, we replace β with Ω and write the driving Hamiltonian as

$$H_{\mathrm{drive}} = -\mathrm{i}\sqrt{\gamma}\Omega(\sigma_+ - \sigma_-). \tag{2.78}$$

2.3 Quantum measurement theory

In quantum mechanics, measurement theory and open-system theory are intimately connected, as an observed system is certainly open with respect to the measuring apparatus. We have reviewed open system dynamics in Section 2.2, where we also introduced stochastic calculus. This will also be used in this section; as the outcomes of quantum measurements are probabilistic in nature, it is natural that a quantum theory of continuous measurements gives rise to stochastic processes. [25].

We begin with defining quantum measurement operators, and then describe different measuring schemes. For more information about quantum measurement theory, see for example the books [23] or [10]. Or for a more brief survey, see [26].

2.3.1 Projective Measurements

The traditional description of measurement in quantum mechanics is in terms of projective measurements, sometimes called von Neumann measurements. Consider an observable A. We can label its eigenstates as $|a\rangle$ where a is the eigenvalue of A: $A|a\rangle = a|a\rangle$. These states fulfill the completeness relation

$$\mathbb{1} = \sum_a |a\rangle\langle a| . \tag{2.79}$$

Acting from the left with A, we get its spectral decomposition:

$$A = \sum_a A|a\rangle\langle a| = \sum_a a|a\rangle\langle a| = \sum_a a\Pi_a, \tag{2.80}$$

where $\Pi_a = |a\rangle\langle a|$ is a projection operator. The projectors are idempotent, $\Pi_a^2 = \Pi_a$, and mutually orthogonal, $\Pi_a\Pi_a' = \Pi_a\delta_{aa'}$.

The projective measurement postulate states that if the system is originally in the state ρ, the normalized state after a measurement with result a is

$$\rho_a = \frac{\Pi_a\rho\Pi_a}{p_a} = |a\rangle\langle a| , \tag{2.81}$$

and this result is found with probability $p_a = \mathrm{Tr}[\Pi_a\rho]$. This probability rule need not be postulated, it can actually be derived from assuming that the measurements are described by a complete set of projectors. This is Gleason's theorem [23].

Due to the idempotency of the projection operators, it is easily seen that subsequent measurements of A will yield the same result a as the first measurement, that is, projective measurements are repeatable.

However, many important measurements in quantum mechanics are not repeatable, and thus not projective. One simple example of such a measurement is counting the number of photons in a cavity. This inevitably involves detecting the photons by absorbing them, leaving the system in a different state than before the measurement.

Another reason why we need to consider a larger class of measurements is so we can describe measurements that extract only partial information about an observable. Projective measurement provides complete information: after the measurement is performed we know exactly what the value of the observable is, since the system is projected into an eigenstate. However, there exist many measurements which, while reducing on average our uncertainty regarding the observable of interest, do not remove it completely.

2.3.2 General Quantum Measurements

A more general measurement postulate is able to describe a wider range of measurements than the projection postulate. The idea is to model a measurement by a set of measurement operators Ω_m where the subscript m represents the different possible results of the measurement. The measurements we will be interested in involve continuous monitoring of a quantum system.

After a measurement yielding the result m, the state *conditioned on the result* is

$$\rho_m = \frac{\Omega_m \rho \, \Omega_m^\dagger}{\mathrm{pr}(m)} = \frac{\mathcal{O}_m \rho}{\mathrm{pr}(m)}, \tag{2.82}$$

where $\mathcal{O}$ is a *completely positive* superoperator

$$\mathcal{O}_m \rho = \Omega_m \rho \Omega_m^\dagger, \tag{2.83}$$

called an *operation*, which maps positive operators into positive operators.

The result m occurs with probability

$$\mathrm{pr}(m) = \mathrm{Tr}[\Omega_m \rho \Omega_m^\dagger] = \mathrm{Tr}[\Omega_m^\dagger \Omega_m \rho] = \mathrm{Tr}[E_m \rho]. \tag{2.84}$$

Here we have introduced a positive operator

$$E_m = \Omega_m^\dagger \Omega_m, \tag{2.85}$$

called the *effect*, which satisfies the normalization condition

$$\sum_m E_m = \mathbb{1}, \tag{2.86}$$

so that the sum of all probabilities is one. The set of all effects $\{E_m\}$ constitutes an *effect-valued measure* (EVM) more commonly known as *positive operator valued measure* (POVM). This description in terms of operations and effects gives the most general form of quantum measurements.

Note that the von Neumann projection postulate corresponds to the special case where the E_m are orthogonal projection operators.

The most general measuring process is not represented by a complete set of orthogonal projection operators, but by a non-orthogonal, positive, operator-valued measure.

The non-selective evolution is obtained by averaging over all possible measurement results [24]:

$$\rho = \sum_a \mathrm{pr}(a)\rho_a. \tag{2.87}$$

This is the unconditional state, with time-evolution determined by the master equation (2.73). The time-evolution of the conditioned state, on the other hand, is governed by a *stochastic master equation*. This will be described in Section 2.3.4.2. But before this, we identify some crucial properties of the operation $\mathcal{O}_m$.

2.3.2.1 Completely positive maps

The class of operations $\mathcal{O}_m$ can be identified with the class of superoperators that map density operators to density operators. This important class of operators is known as *completely positive maps*. The Kraus representation theorem [27] now states that a completely positive map $\mathcal{O}_m$ can be be written in the *Kraus representation*

$$S(\rho) = \sum_m \Omega_m \rho \, \Omega_m^\dagger, \tag{2.88}$$

while the effects satisfy

$$E_m = \sum_m \Omega_m^\dagger \Omega_m \leq \mathbb{1}. \tag{2.89}$$

These are the most general forms of operations and effects for a Markovian system.

It can be interesting to note that a POVM measurement can be realized by a projective measurement in an extended Hilbert space — this is Neumark's theorem [28].

2.3.3 Direct photodetection

As a first example of a quantum measurement, we will discuss photon detection, where a detector "clicks" every time it registered a single photon. We have measurement operators Ω_m, where $m = 0, 1$, representing the two outcomes of a single measurement — either we register a photon, or we do not register it. The operator Ω_1 is associated with the detection of one photon, and Ω_0 is associated with the absence of a detection, i.e. the detection of zero photons. With the environment in the vacuum state $|0\rangle$, the measurement operators are [29]

$$\begin{aligned} \Omega_0(\mathrm{d}t) &= \langle 0|U(t+\mathrm{d}t)|0\rangle = \mathbb{1} - \frac{\mathrm{i}}{\hbar} H_{\mathrm{atom}}\,\mathrm{d}t - \frac{\gamma}{2}\sigma_+\sigma_-\,\mathrm{d}t, \\ \Omega_1(\mathrm{d}t) &= \langle 1|U(t+\mathrm{d}t)|0\rangle = \sqrt{\gamma}\sigma_-\sqrt{\mathrm{d}t}. \end{aligned} \tag{2.90}$$

After an infinitesimal detection time $\mathrm{d}t$, the conditional state of the density operator depending on the measurement result m is

$$\rho_m(t+\mathrm{d}t) = \frac{\Omega_m(\mathrm{d}t)\rho(t)\Omega_m^\dagger(\mathrm{d}t)}{p_m(\mathrm{d}t)}, \tag{2.91}$$

from which a stochastic equation for $\mathrm{d}\rho_c = \rho_c(t+\mathrm{d}t) - \rho_c(t)$ can be calculated:

$$\mathrm{d}\rho_c = \Big(-\frac{\mathrm{i}}{\hbar}[H_{\mathrm{atom}},\rho_c]+\gamma\mathrm{Tr}[\sigma_+\sigma_-\rho_c]\rho_c-\frac{\gamma}{2}\left\{\sigma_+\sigma_-,\rho_c\right\}\Big)\,\mathrm{d}t+\Big(\frac{\sigma_-\rho_c\sigma_+}{\mathrm{Tr}[\sigma_-\rho_c\sigma_+]}-\rho_c\Big)\,\mathrm{d}N. \tag{2.92}$$

The subscript c emphasizes that this density operator is conditioned on the measurement result.

The second term in the stochastic master equation (2.92) gives the stochastic contribution. The stochastic increment $\mathrm{d}N$ can be either 1 or 0. In any given time interval $\mathrm{d}t$, the probability to detect a photon is $\gamma/2\,\langle\sigma_+\sigma_-\rangle\,\mathrm{d}t$, so $\mathrm{d}N$ is unity with the same probability, and zero otherwise.

2.3.4 Balanced homodyne detection

Homodyne detection is the textbook example of a scheme for measuring field quadratures, and is experimentally realized in quantum optics setups. In homodyne detection, the incoming signal is mixed with the signal of a local oscillator.

Here we will derive the stochastic master equation, which gives the evolution of the system state conditioned on the measurement outcome. This equation has the form of a stochastic differential equation. The stochasticity arises due to the randomness of the measurement outcomes [30].

2.3.4.1 Photocurrent and quadratures

We introduced the quadrature operators in Eq. (2.8). We can define the *generalized* quadrature operators [31]

$$\begin{aligned} X_\theta &= \frac{1}{\sqrt{2}}(a^\dagger e^{\mathrm{i}\theta} + a\, e^{-\mathrm{i}\theta}),\\ Y_\theta &= \frac{\mathrm{i}}{\sqrt{2}}(a^\dagger e^{\mathrm{i}\theta} - a\, e^{-\mathrm{i}\theta}). \end{aligned} \tag{2.93}$$

Similar to (2.8), these operators correspond to the in- and out-of-phase components of the electric field with respect to a source dephased by θ from the original one. We may express X_θ and P_θ through the original quadrature components $X = X_0$ and $Y = Y_0$:

$$\begin{aligned} X_\theta &= X\cos\theta + Y\sin\theta,\\ Y_\theta &= -X\sin\theta + Y\cos\theta. \end{aligned} \tag{2.94}$$

This transformation describes a rotation by an angle θ in the phase-space (X,Y-plane). It follows from (2.94) that $Y_\theta = X_{\theta+\pi/2}$. Hence X_θ comprises the whole manifold of quadrature components if we have $\theta \in [0,\pi]$.

Since X and Y are Hermitian, X_θ is Hermitian as well, which guarantees that it is an observable. Homodyne detection corresponds to a measurement of this

operator. A schematic sketch of a homodyne measurement experiment is shown in Fig. 2.1. In homodyne detection, the input field a is mixed with a signal b from a local oscillator (LO). These fields impinge on a 50:50 beam splitter, which is the reason for the name *balanced* homodyne detection. With an added phase shift of

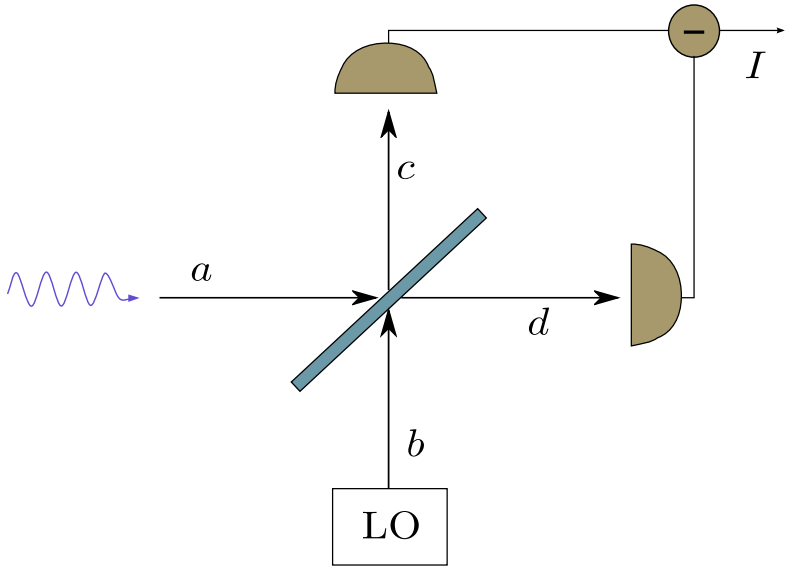

Figure 2.1: The setup for balanced homodyne detection. The resonance fluorescence is the incoming field a, and the signal of a local oscillator (LO) is the second incoming field b. These two fields impinge on a 50:50 beam splitter. The output fields c and d are detected separately. The measured quantity I is the photocurrent from one detector subtracted from the other.

$\pi/2$ for reflection, the output fields from the beam splitter are

$$c = \frac{1}{\sqrt{2}}(\mathrm{i}a + b), \quad d = \frac{1}{\sqrt{2}}(a + \mathrm{i}b). \tag{2.95}$$

The detected current consists of subtracting the photocurrent of one detector from the photocurrent of the other. If we assume the photocurrent to be proportional to the number of photons reaching the detector, we can calculate the detector response using the field number operators:

$$I = \langle c^\dagger c - d^\dagger d \rangle \,. \tag{2.96}$$

With

$$\begin{aligned} c^\dagger c &= \frac{1}{2}(-\mathrm{i}a^\dagger + b^\dagger)(\mathrm{i}a + b) = \frac{1}{2}(a^\dagger a - \mathrm{i}a^\dagger b + \mathrm{i}b^\dagger a + b^\dagger b), \\ d^\dagger d &= \frac{1}{2}(a^\dagger a - \mathrm{i}b^\dagger a + \mathrm{i}a^\dagger b + b^\dagger b), \end{aligned} \tag{2.97}$$

we get

$$I = \mathrm{i}\,\langle b^\dagger a - a^\dagger b \rangle \,. \tag{2.98}$$

Now b represents the coherent drive from the local oscillator, so we can set $b = |\beta|e^{\mathrm{i}\alpha}$. We are free to set the phase, so we use $\alpha = \theta + \pi/2$, where θ will be the phase of the local oscillator. This gives $\mathrm{i}|\beta|e^{\mathrm{i}\theta}$. Inserting this in (2.98) gives

$$I = |\beta| \left\langle a\, e^{-\mathrm{i}\theta} + a^\dagger e^{\mathrm{i}\theta} \right\rangle = |\beta|\sqrt{2} \left\langle X_\theta \right\rangle . \tag{2.99}$$

Here we have explicitly shown how optical homodyne detection measures the generalized quadrature operator X_θ.

It can be worth mentioning that homodyne detection is a *weak measurement*. Most of the measurement signal comes from the LO, meaning that only a small amount of information about the quantum system is gained. Therefore, the measurement disturbs the system very little. Observing a two-level system via direct photodetection gives a very sharp jump of the state when a photon is observed. But during homodyne detection, the state evolution shows a more diffusive behaviour, as seen in Figures 2.2.

By using the input-output relation we can derive the stochastic differential equation for the photocurrent $\mathrm{d}j(t) = j(t)\,\mathrm{d}t$. We can associate a stochastic process $\mathrm{d}X$ with the quadrature X, defined as

$$\mathrm{d}X = \frac{1}{\sqrt{2}}(\mathrm{d}B_{\mathrm{out}} + \mathrm{d}B_{\mathrm{out}}^\dagger) = \frac{1}{\sqrt{2}}(b_{\mathrm{out}}\,\mathrm{d}t + b_{\mathrm{out}}^\dagger\,\mathrm{d}t). \tag{2.100}$$

For simplicity, we exclude the phase angle θ. Using the input-output relation (2.46) in (2.100), we get

$$\langle \mathrm{d}X \rangle = \frac{1}{\sqrt{2}}\Big(\sqrt{\gamma}\,\langle \sigma_- + \sigma_+ \rangle\,\mathrm{d}t + \langle b_{\mathrm{in}} + b_{\mathrm{in}}^\dagger \rangle\,\mathrm{d}t\Big). \tag{2.101}$$

Recalling from Section 2.2.2 that the input field has the statistics of vacuum white noise, we can rewrite (2.101) as

$$\langle \mathrm{d}X \rangle = \frac{1}{\sqrt{2}}\left(\sqrt{\gamma}\,\langle \sigma_- + \sigma_+ \rangle\,\mathrm{d}t + \xi(t)\,\mathrm{d}t\right). \tag{2.102}$$

We relate this to the photocurrent by

$$\mathrm{d}j(t) = \langle \mathrm{d}X \rangle = \frac{1}{\sqrt{2}}\left(\sqrt{\gamma}\,\langle \sigma_- + \sigma_+ \rangle\,\mathrm{d}t + \mathrm{d}W(t)\right). \tag{2.103}$$

Here we identified $\xi\,\mathrm{d}t$ with $\mathrm{d}W$, where the latter is a Wiener increment. The Wiener increment is a Gaussian random variable, with mean zero, $\mathbb{E}[W] = 0$, and variance 1.

The signal from the local oscillator is a coherent state, which has Poissonian photon counting statistics. But in the limit of a large number of photon detections, the Poissonian distribution approaches a Gaussian. And as homodyne detection can be seen as the limit of infinite amplitude of the local oscillator, $|\beta| \to \infty$, we certainly have a large number of photons. This is the reason for using a Gaussian random variable.

White noise ξ is called the derivative of the Wiener process. You might wonder how this is possible, seeing as W is not differentiable. The resolution to this conundrum is simply to remember that this expression in terms of a derivative is just symbolic, the corresponding integral equation can be interpreted consistently [22].

2.3.4.2 Stochastic master equation

A derivation of the stochastic homodyne master equation starting from the equation for direct photodetection (2.92) is done in [23], and another version can be found in [32]. Here we instead follow [26].

We utilize that, as we have learned in Section 2.3.2.1, the most general form of a completely positive map is

$$X \to \sum_n A_n X A_n^\dagger. \tag{2.104}$$

Now, consider a stochastic operator A of the form

$$A = 1 - \frac{\mathrm{i}}{\hbar} H \,\mathrm{d}t + b \,\mathrm{d}t + c \,\mathrm{d}W \tag{2.105}$$

where b and c are operators, and $\mathrm{d}W$ is a Wiener increment. Since any operator can be decomposed into a Hermitian and anti-Hermitian part, we may assume b to be Hermitian since we can absorb any anti-Hermitian part into $-\mathrm{i}H$. Inserting this A into the transformation (2.104) we find

$$\mathrm{d}\rho = -\frac{\mathrm{i}}{\hbar}[H, \rho] \,\mathrm{d}t + \{b, \rho\} \,\mathrm{d}t + c\rho c^\dagger \,\mathrm{d}t + (c\rho + \rho c^\dagger) \,\mathrm{d}W. \tag{2.106}$$

We define $\tilde{\rho} = \mathbb{E}[\rho]$, and take the average of Eq. (2.106):

$$\mathrm{d}\tilde{\rho} = -\frac{\mathrm{i}}{\hbar}[H, \tilde{\rho}] \,\mathrm{d}t + \{b, \tilde{\rho}\} \,\mathrm{d}t + c\tilde{\rho} c^\dagger \,\mathrm{d}t. \tag{2.107}$$

Since the operator $\tilde{\rho}$ is an average over valid density operators, it is also a valid density operator and must satisfy $\mathrm{Tr}[\tilde{\rho}] = 1$ Hence we must have $\mathrm{dTr}[\tilde{\rho}] = \mathrm{Tr}[\mathrm{d}\tilde{\rho}] = 0$. Using the cyclic property of the trace, this gives

$$\mathrm{Tr}[\tilde{\rho}(2b + cc^\dagger)] = 0. \tag{2.108}$$

This holds for an arbitrary density operator only if

$$b = -\frac{c^\dagger c}{2}. \tag{2.109}$$

Thus we obtain the Lindblad form of the master equation

$$\mathrm{d}\tilde{\rho} = -\frac{\mathrm{i}}{\hbar}[H, \tilde{\rho}] \,\mathrm{d}t + \mathcal{D}[c]\tilde{\rho} \,\mathrm{d}t. \tag{2.110}$$

This is the most general (Markovian) form of the unconditioned master equation for a single dissipation process. The full transformation from Eq. (2.106) then becomes

$$\mathrm{d}\rho_c = -\frac{\mathrm{i}}{\hbar}[H, \rho_c] \,\mathrm{d}t + \mathcal{D}[c]\rho_c \,\mathrm{d}t + (c^\dagger c \rho_c + \rho_c c^\dagger c) \,\mathrm{d}W, \tag{2.111}$$

where we with the subscript c emphasize that this density operator is conditioned on the measurement result.

This form of the master equation does not preserve the trace, since the condition $\mathrm{Tr}[\mathrm{d}\rho] = 0$ implies

$$\mathrm{Tr}[\rho_c(c + c^\dagger)\,\mathrm{d}W] = 0. \tag{2.112}$$

We could interpret this relation as a constraint on c, but instead we keep c an arbitrary operator and explicitly normalize ρ_c at each time step by adding a term to cancel out the left hand side of (2.112). The result is a stochastic master equation of the form

$$\mathrm{d}\rho_c = -\frac{\mathrm{i}}{\hbar}[H, \rho_c]\,\mathrm{d}t + \mathcal{D}[c]\rho_c\,\mathrm{d}t + \mathcal{H}[c]\rho_c\,\mathrm{d}W, \tag{2.113}$$

where the *measurement superoperator* is

$$\mathcal{H}[c]\rho = c\rho + \rho c^\dagger - \langle c + c^\dagger \rangle\,\rho. \tag{2.114}$$

This superoperator represents the measurement process.

Using our system operator and coupling constants, the equation we will use is

$$\mathrm{d}\rho_c = -\frac{\mathrm{i}}{\hbar}[H_{\mathrm{drive}}, \rho_c]\,\mathrm{d}t + \gamma\mathcal{D}[\sigma_-]\rho_c\,\mathrm{d}t + \sqrt{\gamma'}\mathcal{H}[e^{-\mathrm{i}\theta}\sigma_-]\rho_c\,\mathrm{d}W. \tag{2.115}$$

By transforming to a frame rotating with the system, we can omit the system Hamiltonian and only use the drive Hamiltonian defined in Eq. (2.78).

If we have one decay channel, then $\gamma' = \gamma$. If we have two channels, $\gamma' = \gamma_1$ or $\gamma' = \gamma_2$ from Eq. (2.75). This is because we will only observe one channel. Also, the σ_- in the measurement operator $\mathcal{H}$ is exchanged for $e^{-\mathrm{i}\theta}\sigma_-$ because we want to measure the generalized quadratures.

The stochastic master equation is solved numerically to simulate individual measurement records.

2.3.5 Quantum Trajectories

A quantum trajectory is the path followed by the state of the system in time. If you formulate an equation tracking the evolution of the state of the system then the solution is a quantum trajectory. Note that this solution is not a solution to the master equation, but a solution to the *stochastic* master equation.

Stochastic master equations arise when a system interacts with an environment which is subsequently measured. A single measurement provides only a single data point. Quantum mechanics is a statistical theory and therefore cannot predict the outcome of this single measurement. This gives rise to stochasticity. The solution of a trajectory equation gives the evolution of the density operator conditioned on the measurement results, as the density operator ρ_c is randomly replaced by

$$\rho_c \to \frac{\Omega_m \rho_c \Omega_m^\dagger}{\mathrm{Tr}[\Omega_m \rho_c \Omega_m^\dagger]}, \tag{2.116}$$

when the measurement result m is recorded. In essence, quantum trajectories are a consequence of continuous measurement of a quantum system [24].

Averaging over a large number of trajectories one should recover the deterministic solution of the master equation

$$\rho(t) = \mathbb{E}[\rho_c(t)], \tag{2.117}$$

where ρ_c is the conditioned density operator and $\mathbb{E}$ denotes the ensemble average. We can see that our stochastic equation (2.115) reduces to (2.71) when taking the average.

This is illustrated in Fig. 2.2. The plots show the probability of being in the excited state, $\langle \sigma_- \sigma_+ \rangle = \mathrm{Tr}[\sigma_- \sigma_+ \rho_c] = \mathrm{Tr}[|e\rangle\langle e| \, \rho_c]$, over time. In the top row we show simulated trajectories for an un-driven atom initially starting in the excited state. We see that as we average over more and more trajectories, we approach the solution of the master equation, which is the familiar exponential decay. An atom starting in the ground state driven with driving strength $\Omega = 1$ is displayed in the bottom row. Here we see that when the atom is driven, more trajectories are needed to reach the correct solution of the master equation.

Different measurement schemes give rise to different stochastic master equations, as we can see from the direct detection equation (2.92) and the homodyne equation (2.115). Despite being different. they describe the same quantum system, so their averages $\mathbb{E}[\rho_c] = \rho$ will obey the same master equation (2.71). Different stochastic equations are called different *unravellings* of the master equation [33].

We will solve the stochastic equation instead of the master equation because we want to simulate homodyne measurements. One trajectory simulation represents one measurement.

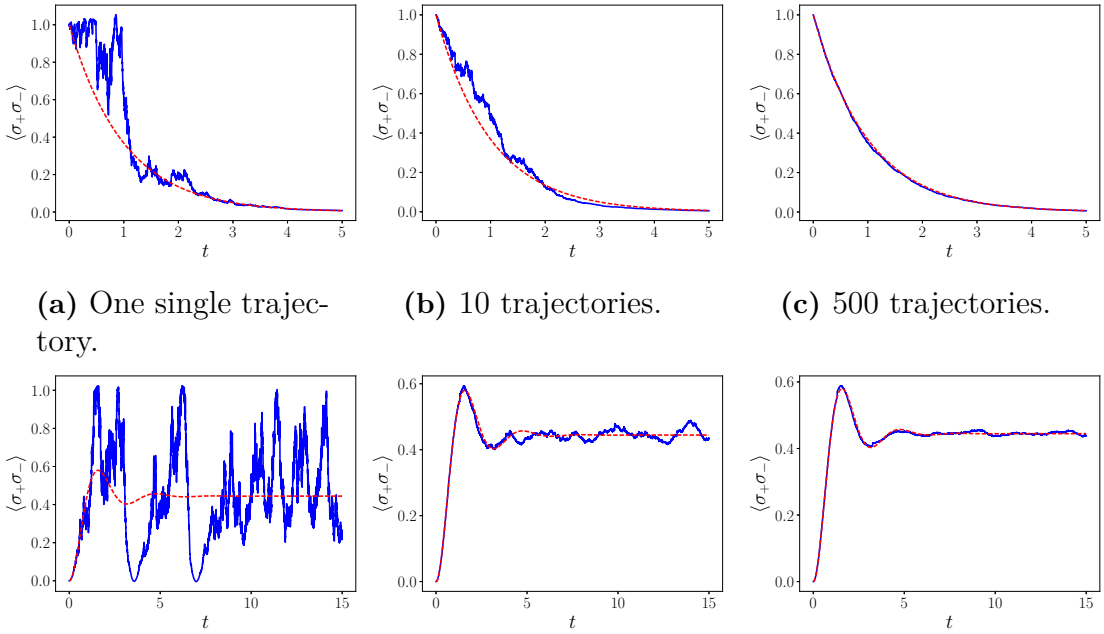

(a) One single trajectory.

(b) 10 trajectories.

(c) 500 trajectories.

(d) One single trajectory.

(e) 500 trajectories.

(f) 5000 trajectories.

Figure 2.2: Probability of the atom being in the excited state as a function of time. The dashed line is the solution of the master equation. The filled line shows trajectories. As more and more trajectories are averaged over, the solution of the master equation is approached.

In Figures (a), (b) and (c) the atom starts in the excited state $|e\rangle\langle e|$ and no driving is applied, $\Omega = 0$.

In Figures (d), (e), (f) the atom starts in the ground state $|g\rangle\langle g|$ and is driven with strength $\Omega = 1$. Comparing with (a), (b) and (c) above, we note that more trajectories are needed to reach the master equation solution than when the atom is not driven.

2.4 Numerical Methods

Several investigations have shown that one cannot in general take a numerical method for solving ordinary differential equations and apply it to stochastic differential equations (SDEs) [34]. Not all discrete-time approximations of SDEs converge to the correct stochastic process solution, and SDEs with well-behaved and bounded analytical solutions can render numerical simulations unstable, and produce unbounded solutions [35].

Ways to handle SDEs numerically have been developed. The simplest discrete-time method for SDEs is a generalization of the simple Euler method, called the Euler-Maruyama method [36]. For a higher order of convergence, the Milstein method can be used. For a more in-depth review on these two methods, see [37].

2.4.1 Euler-Maruyama

The Euler-Maruyama (EM) scheme is the simplest recursive algorithm to get an approximation for the density matrix. Although we are studying a quantum system, we can use an ordinary, classical method like EM to solve the stochastic master equation. This is because the Wiener increment, which is the stochastic part of the master equation (2.115), is classical — i.e. not an operator.

We simply use

$$\rho_{i+1} = \rho_i + \Delta\rho. \tag{2.118}$$

For a general SDE

$$\mathrm{d}X = h\,\mathrm{d}t + g\,\mathrm{d}W, \tag{2.119}$$

the discretized Ito integration gives the Euler-Maruyama approximation

$$X_{i+1} = X_i + h\Delta t + g\Delta W. \tag{2.120}$$

For a stochastic master equation of the form (2.113), we have

$$\rho_{i+1} = \rho_i + \left(-\mathrm{i}[H,\rho_i]\Delta t + \mathcal{D}[c]\rho_i\Delta t + \mathcal{H}[c]\rho_i\Delta W\right). \tag{2.121}$$

The Wiener increments ΔW are independent Gaussian random variables with zero mean and variance Δt. We can write $\Delta W = \sqrt{\Delta t}\xi$, where ξ is a Gaussian distributed random variable with zero mean and unit variance, produced by a random number generation algorithm.

This method has a strong convergence of 0.5, whereas the underlying deterministic Euler method converges with order 1. It is possible to raise the strong order of EM to 1 by adding a correction to the stochastic increment, giving Milstein's method. The correction arises because the traditional Taylor expansion must be modified in the case of Ito calculus. For information about convergence orders for stochastic equation solvers, see e.g. [34].

2.4.2 Milstein

A stochastic Taylor expansion up to order dt is derived in Appendix B.1.3. There we arrive at the Milstein algorithm:

$$X_{i+1} = X_i + h(X_i)\Delta t + g(X_i)\Delta W + \frac{1}{2}g(X_i)g'(X_i)\Big((\Delta W)^2 - \Delta t\Big). \tag{2.122}$$

Comparing with Eq. (2.120), we see that the Milstein method amounts to adding a correction

$$\frac{1}{2}g(X_i)g'(X_i)\Big((\Delta W)^2 - \Delta t\Big), \tag{2.123}$$

to the Euler-Maruyama algorithm.

The main difficulty for implementing this algorithm is to calculate the derivative g' in the correction term. In our case, the function $g(X)$ is the measurement superoperator term, as defined in Eq. (2.114). In order not to get confused by the notation, we here write it as $\mathcal{H}(\rho)$ to emphasize that it is a function of our stochastic variable $X = \rho$. Our correction term $gg'/2$ is given by

$$\frac{1}{2}\sum_{mn}\mathcal{H}(\rho)_{mn}\frac{\partial\mathcal{H}(\rho)_{pq}}{\partial\rho_{mn}}\,. \tag{2.124}$$

With

$$\mathcal{H}(\rho)_{pq} = \sum_k\Big(c_{pk}\rho_{kq} + \rho_{pk}c^\dagger_{kq}\Big) - \mathrm{Tr}[c\rho + \rho c^\dagger]\rho_{pq}, \tag{2.125}$$

the derivative is

$$\frac{\partial\mathcal{H}(\rho)_{pq}}{\partial\rho_{mn}} = c_{pm}\delta_{qn} + \delta_{mp}c^\dagger_{nq} - (c_{nm} + c^\dagger_{nm})\rho_{pq} - \mathrm{Tr}[c\rho + \rho c^\dagger]\delta_{mp}\delta_{nq}. \tag{2.126}$$

Inserting this in (2.124) gives

$$\begin{aligned}\frac{1}{2}\sum_{mn}\Big(\sum_\ell\Big(c_{m\ell}\rho_{\ell n} + \rho_{m\ell}c^\dagger_{\ell n}\Big) - \mathrm{Tr}[c\rho + \rho c^\dagger]\rho_{mn}\Big)\Big(c_{pm}\delta_{qn} + \delta_{mp}c^\dagger_{nq} - (c_{nm} + c^\dagger_{nm})\rho_{pq} - \\ - \mathrm{Tr}[c\rho + \rho c^\dagger]\delta_{mp}\delta_{nq}\Big).\end{aligned} \tag{2.127}$$

Now we go term by term. The first two terms from both factors gives

$$\sum_{mn\ell}\Big(c_{m\ell}\rho_{\ell n} + \rho_{m\ell}c^\dagger_{\ell n}\Big)\Big(c_{pm}\delta_{qn} + \delta_{mp}c^\dagger_{nq}\Big) = cc\rho + 2c\rho c^\dagger + \rho c^\dagger c^\dagger. \tag{2.128}$$

The last term in the first factor, and two first terms in the second factor gives

$$-\sum_{mn}\mathrm{Tr}[c\rho + \rho c^\dagger]\rho_{mn}\Big(c_{pm}\delta_{qn} + \delta_{mp}c^\dagger_{nq}\Big) = -\mathrm{Tr}[c\rho + \rho c^\dagger](c\rho + \rho c^\dagger). \tag{2.129}$$

The first two terms from he first factor and the two last terms from the second factor gives

$$\begin{aligned} &-\sum_{mn\ell}\Big(c_{m\ell}\rho_{\ell n}+\rho_{m\ell}c^\dagger_{\ell n}\Big)\Big((c_{nm}+c^\dagger_{nm})\rho_{pq}+\mathrm{Tr}[c\rho+\rho c^\dagger]\delta_{mp}\delta_{nq}\Big)= \\ &=-\mathrm{Tr}[cc\rho+2c\rho c^\dagger+\rho c^\dagger c^\dagger]\rho-\mathrm{Tr}[c\rho+\rho c^\dagger](c\rho+\rho c^\dagger). \end{aligned} \tag{2.130}$$

Finally, the last term in the first factor and the two last terms from the second factor:

$$\mathrm{Tr}[c\rho+\rho c^\dagger]\sum_{mn}\rho_{mn}\Big((c_{nm}+c^\dagger_{nm})\rho_{pq}+\mathrm{Tr}[c\rho+\rho c^\dagger]\delta_{mp}\delta_{nq}\Big)=2\mathrm{Tr}[c\rho+\rho c^\dagger]^2\rho. \tag{2.131}$$

Adding up all of these terms, and reinserting the $1/2$ and the increments, gives the correction (2.123)

$$\begin{aligned} &\frac{1}{2}\Big(cc\rho_i+2c\rho_i c^\dagger+\rho_i c^\dagger c^\dagger-\mathrm{Tr}[cc\rho_i+2c\rho_i c^\dagger+\rho_i c^\dagger c^\dagger]- \\ &-2\mathrm{Tr}[c\rho_i+\rho_i c^\dagger](c\rho_i+\rho_i c^\dagger)+2\mathrm{Tr}[c\rho_i+\rho_i c^\dagger]^2\rho_i\Big)\Big((\Delta W)^2-\Delta t\Big). \end{aligned} \tag{2.132}$$

Note that we moved away from matrix index notation; above i is a time-step index.

3

Wigner function

A quantum state is said to be *non-classical* if it cannot be described using methods of classical physics. There are several ways to characterize non-classicality. Typically this will depend on the problem at hand. One of such measures are photon correlations, which we will review later in Chapter 4. Another measure that will turn out to be more useful for us, however, is the negativity of the Wigner function.

3.1 Quantum phase-space distribution

The Wigner function is a quantum phase-space distribution function, introduced in 1932 by Wigner [38]. Phase-space is spanned by the canonically conjugate variables x and p. In general, we identify them with position and momentum, however, they could also refer to the quadratures X and Y of the electromagnetic field.

The Wigner function belongs to a family of so-called *quasi-probability distributions* [17]. Unlike genuine probability distributions, such quasi-distributions can take on negative values. This property turns out to be essential for our purposes, because the negativity of the Wigner function is an indicator of non-classicality.

The uncertainty principle makes the formulation of a phase-space probability distribution in quantum mechanics problematic. Because position and momentum correspond to non-commuting operators, a particle cannot simultaneously have a well defined position and momentum. This means one cannot define the probability that a particle has a position x and a momentum p, i.e. one cannot define a phase-space probability distribution in the classical sense for a quantum mechanical particle.

Quantum phase-space distributions have proven to be of great use in the study of quantum mechanical systems [39]. They are useful as calculational tools, since they allow the use of classical phase-space methods. They also provide insights into the connections between classical and quantum mechanics.

The Wigner phase-space distribution associates a real function $W(x,p)$ in phase-space with a density operator ρ in Hilbert space:

$$W(x,p) = \frac{1}{2\pi}\int_{-\infty}^{\infty} \mathrm{d}y\, e^{-\mathrm{i}py/\hbar}\, \langle x + \frac{y}{2}|\rho|x - \frac{y}{2}\rangle\,. \tag{3.1}$$

Note that the arguments x and p in the Wigner function are c-numbers, not operators. The relation (3.1) can be inverted; there is a one-to-one correspondence between the Wigner function and the density operator, which means the Wigner function contains complete information about the quantum system. Mathematically, this corresponds to the Weyl transform of ρ. Weyl quantization in the phase-space formulation is one of three equivalent paths of quantization, besides the standard canonical quantization using operators in Hilbert space, and the path integral formalism of quantum mechanics. It is based on the Wigner function, and Weyl's correspondence between ordinary c-number functions in phase-space and quantum mechanical operators in Hilbert space [40]. As a result of this, quantum mechanical expectation values can be written in a classical-looking form as phase-space integrals.

3.1.1 Probability distributions from the Wigner function

Integrating the Wigner function over the momentum variable yields the probability distribution for the position variable. To see this, integrate both sides of (3.1) over p and interchange the integrations over y and p:

$$\int_{-\infty}^{\infty} \mathrm{d}p\, W(x,p) = \int_{-\infty}^{\infty} \mathrm{d}y\ \langle x + \frac{y}{2}|\rho|x - \frac{y}{2}\rangle\, \frac{1}{2\pi\hbar} \exp\left(-\mathrm{i}py/\hbar\right). \tag{3.2}$$

The relation

$$\int_{-\infty}^{\infty} \mathrm{d}p \exp\left(-\mathrm{i}py/\hbar\right) = \delta(y), \tag{3.3}$$

allows to reduce (3.2) to

$$\int_{-\infty}^{\infty} \mathrm{d}p\, W(x,p) = \int_{-\infty}^{\infty} \mathrm{d}y\ \langle x + \frac{y}{2}|\rho|x - \frac{y}{2}\rangle\, \delta(y) = \langle x|\rho|x\rangle = W(x). \tag{3.4}$$

Analogously, we get the momentum distribution by integrating over the position x. This shows that even though the Wigner function itself can be negative, its phase-space integrals correspond to well-behaved probability distributions. In fact, you can integrate over any angle θ in phase-space, see Fig. 3.1, and get a true probability distribution for the conjugate quadrature $X_{\theta+\pi/2}$.

3.1.2 Wigner negativity as a resource for quantum computation

We mentioned already in Section 1.2 that a negative Wigner function is a necessary condition for quantum computing displaying a so-called *quantum advantage* over classical computers. This is based on a theorem due to Eisert and Mari [4], which helps discern the boundary between systems that can be efficiently simulated classically, and those that cannot. The role of the negativity of the Wigner function is identified as a quantum computational resource: if the basic elements of a circuit exhibit a positive Wigner function, the circuit can be efficiently simulated classically.

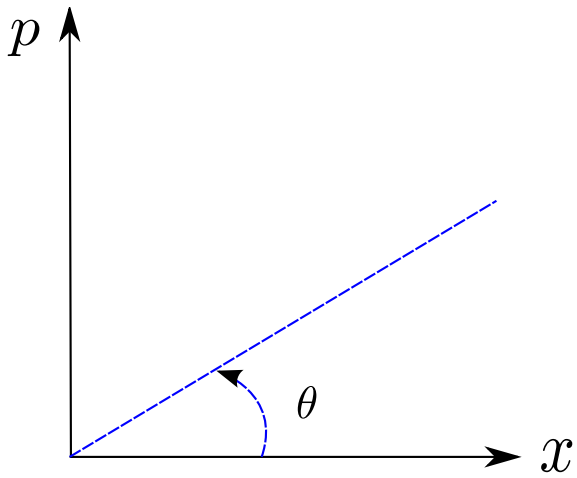

Figure 3.1: Phase-space. The axes x and p correspond to generalized quadratures with $\theta = 0$ (X) and $\theta = \pi/2$ (Y). It is possible to integrate the Wigner function for a generalized quadrature with any angle θ and get its probability distribution.

A schematic sketch of a quantum circuit is displayed in Fig. 3.2. It shows an input block, a processing block and a measuring block. Either one of these

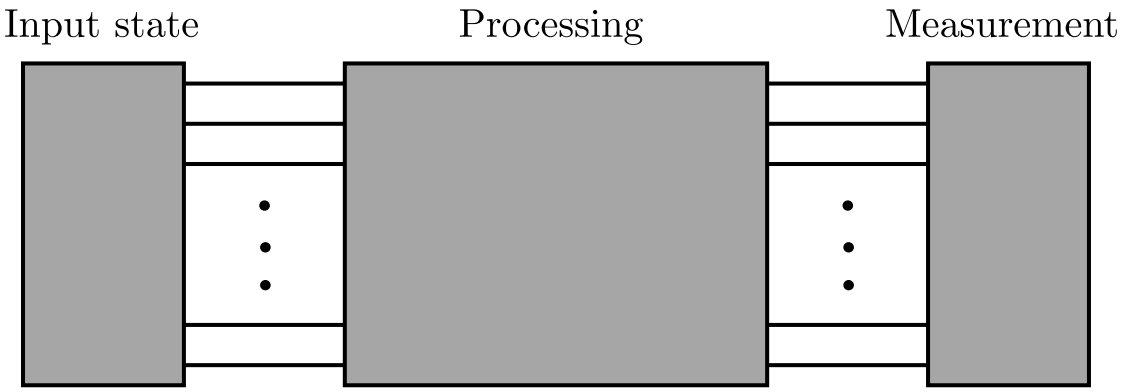

Figure 3.2: Quantum circuit. At least one of these blocks must produce a negative Wigner function, otherwise the circuit can be efficiently simulated on a conventional computer.

blocks can introduce negativity. If none of them do, the circuit can be efficiently simulated on a classical computer, with efficiently meaning that the running time is polynomial in the number of input states and processing operations.

At least for pure states, Wigner negativity is restricted to non-Gaussian states [41]. Starting from a Gaussian state, like a coherent state, a non-linear interaction during either the processing or the measurement is required to generate a negative Wigner state.

Homodyne measurement does not contribute to negativity, so in our case, it is the two-level atom that provides the non-linearity to produce the negative Wigner function states, as incoming coherent light is scattered by the atom. The atom

represents for the coherent field a Kerr-like medium (non-linear), in that the reflection and transmission of light from the atom depend on the intensity of the incoming field.

Finally, as an example of how the Wigner function can look, we show in Figures 3.3a and 3.3b surface plots of the Wigner functions for vacuum (0-photon state) and a one-photon state, respectively. We note that the vacuum Wigner function is positive all over phase-space, while the one-photon Wigner function displays some negativity.

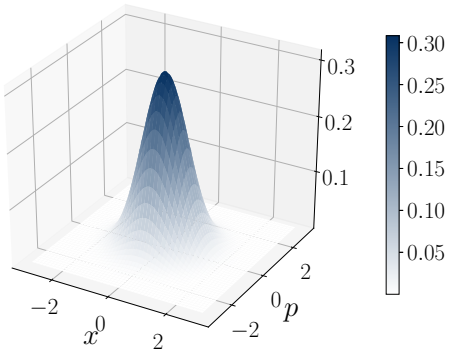

(a) Wigner function for vacuum. It is shaped like a 3D Gaussian, and is positive everywhere.

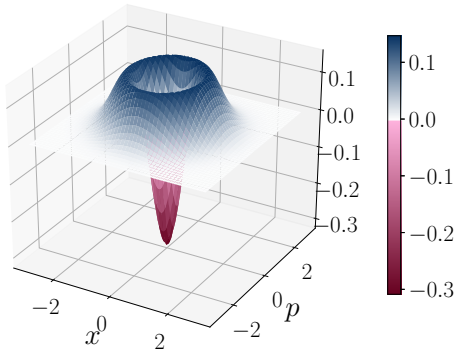

(b) Wigner function for one photon. It is negative near the phase-space origin. The negative part is emphasized by the shift of color in the colormap.

Figure 3.3

In Fig. 3.4 the Wigner state for a coherent state is displayed. Like the vacuum Wigner function, it is positive everywhere.

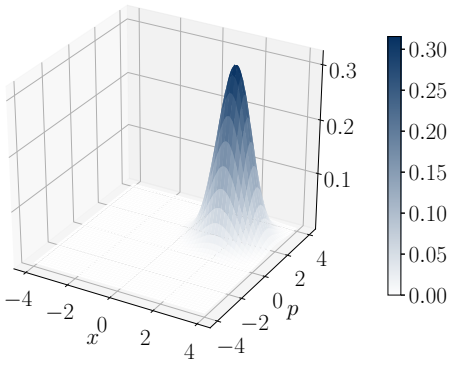

Figure 3.4: Surface plot of the Wigner function for a coherent state. The Wigner function is positive all over phase-space. It is shaped like the vacuum state (Gaussian), but is displaced from the origin so that its average is non-zero.

4

Resonance fluorescence

Resonance fluorescence, the emission from a two-level atom driven by a resonant coherent drive field, is a basic process in light-matter interactions, and has thus been investigated extensively. See e.g. [42] for a review of the experimental studies, and [43] for detailed theory. Also [11] has an excellent chapter on resonance fluorescence.

Resonance fluorescence exhibits quantum properties, and it could possibly be used as a resource for quantum computation. This has been investigated in quantum optics, with ordinary atoms. But there are issues that make this an experimentally difficult task. These problems could potentially be overcome by using microwave frequencies and artificial atoms in superconducting circuits instead.

In this Chapter, we will give an overview of circuit-QED. Then we discuss resonance fluorescence, and present the models we will study in this thesis.

4.1 Circuit QED

The field known as circuit quantum electrodynamics, or circuit QED for short, deals with on-chip implementations of quantum electrodynamics [44]. In order to minimize losses due to electrical resistance, the circuits are designed with superconducting materials — for this reason it is common to refer to this field as *superconducting circuits* as well.

Here, excitations confined to coplanar waveguides, or propagating through open transmission lines, will play the role of photons, their frequencies being in the microwave regime. Artificial atoms correspond to non-linear resonators, the non-linearity due to a Josephson junction. The non-linearity makes it possible to isolate two or more energy levels from the rest of the spectrum. Two-level artificial atoms, also known as qubits, play a major role in quantum computing implementations. Fig. 4.1 displays a transmon artificial atom.

Superconducting circuits provide not only the possibility to reproduce QED scenarios for visible light and real atoms, but it also enables us to engineer configurations way beyond any possibility in optical setups. This is mainly because of low-dimensionality, tunability and the flexibility in circuit design.

Confining the field to lower dimensions has proven to enhance the light-matter interaction achieving the so-called strong-coupling regime [46]. This in turn can be used to engineer effective strong photon-photon interactions. The tunability of

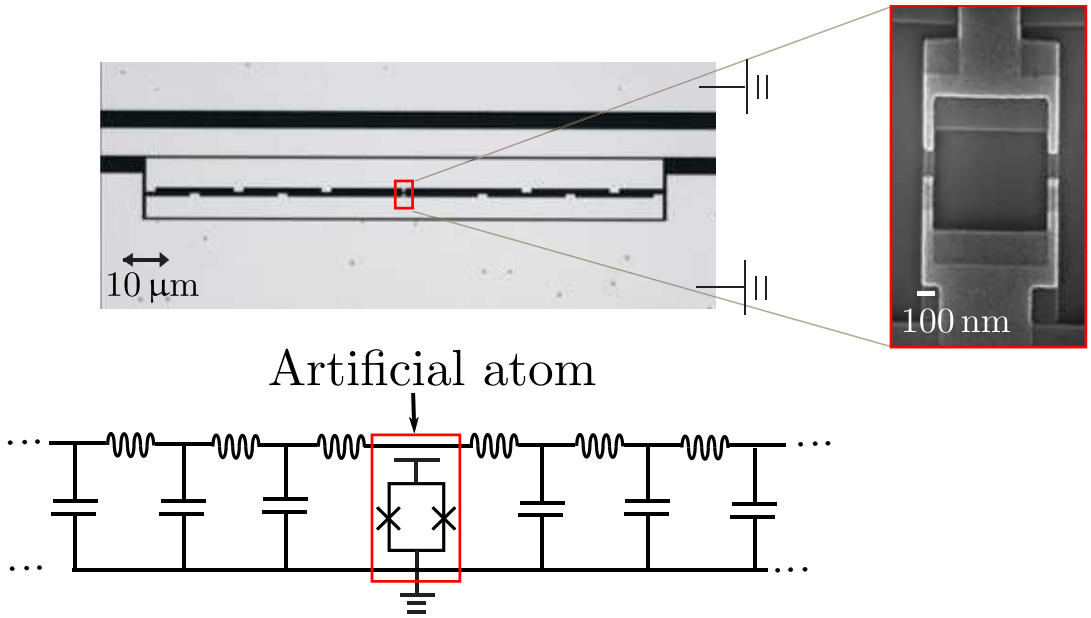

Figure 4.1: Top: Micrograph of an artificial atom, a superconducting transmon qubit embedded in a 1D open transmission line. Magnified section: Scanning-electron micrograph of the superconducting quantum interference device (SQUID) loop of the transmon. Bottom: the corresponding circuit model. Figure adapted from [45].

system parameters not only allows to tailor the energy levels of an artificial atom, but also to modify the boundary condition of a field very fast in order to observe relativistic effects such as the dynamical Casimir effect [47], or to probe the effects of vacuum fluctuations on an artificial atom [48].

Resonant coherent excitation of a two-level system has been broadly studied in superconducting circuits [45]. Here, interference effects such as extinction of propagation in the transmitted component were observed due to confinement of the microwave field to a single spatial dimension.

Quadrature measurement schemes, such as the one required for the protocol presented in this thesis, are also possible. In the microwave regime, this relies on parametric amplification of the quadrature field X_θ (2.93). Amplification is performed via a Josephson parametric amplifier (JPA). The phase θ defining the probed quadrature is selected by means of a pump tone injected on the JPA.

Tomography of a continuous variable field has already been reported [49]. Therefore, the physics studied in this work is within current experimental possibilities and, as we consider, relevant for the future implementation of quantum computation with continuous variables.

4.2 Resonance fluorescence in circuit-QED

In a three-dimensional configuration, the atom non-linearity is lost due to the fact that the atom couples to modes in a 4π solid angle. In order to enhance this non-linearity it is desirable to confine the electromagnetic field to a single spatial dimension — a common scenario in superconducting circuits where fields propagate through (quasi) one-dimensional transmission lines. This enhanced non-linearity was observed experimentally in [50] and [45].

We will look at resonance fluorescence for two different configurations, shown in Fig. 4.2. A setup with two decay channels is shown in 4.2a, and with a single decay channel in 4.2b. With two channels, we have the option to look at the reflected field $b_{\text{out,R}}$ or the transmitted field $b_{\text{out,T}}$. We will restrict ourselves to look at the reflected radiation.

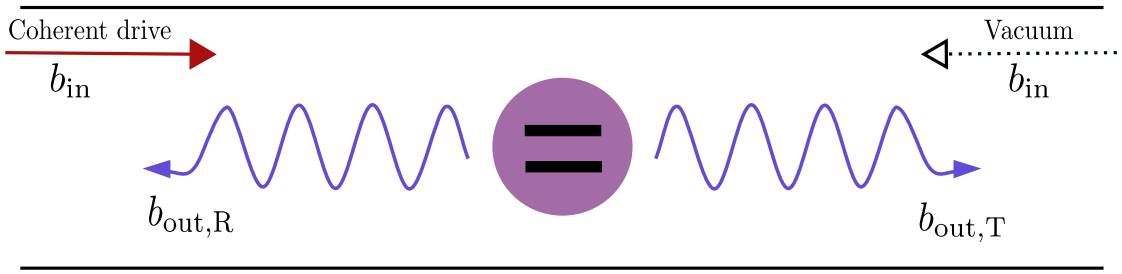

(a) Two-level atom coupled to two decay channels via a waveguide. The atom is being driven from the left. The emitted radiation is either reflected or transmitted. These fields are characterized by the output operators $b_{\text{out,R}}$ and $b_{\text{out,T}}$.

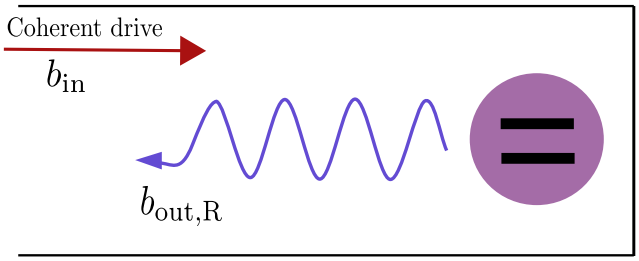

(b) Two-level atom in front of a mirror (single decay channel). he atom is being driven from the left, and the only available output is the reflected field $b_{\text{out,R}}$.

Figure 4.2: Display of the two different setups we will investigate.

We will drive the atom from one channel with coherent light, which could come from a laser. This will be the b_{in}. The input field from the other channel is just vacuum. The two different b_{out} for the channels will represent the reflected and the transmitted field, resulting from the driving field. This is illustrated later in Fig. 4.2.

This rather simple setup exhibits very interesting quantum properties such as anti-bunching and squeezing. In this thesis we will not concern ourselves with squeezing, because while squeezing is a quantum phenomenon, it does not affect the Wigner negativity of a state [51]. In addition, the atom behaves as a non-linear medium for the incident coherent field, the reflectance and transmittance (the fraction of the incident field being reflected and transmitted, respectively) being dependent on the driving strength. It is this non-linearity we wish to exploit in order to generate negative Wigner states of the electromagnetic field — recall from Section 3.1.2 that starting from a Gaussian state, such as a coherent state, a non-linear interaction is required to generate a non-classical state in the Wigner sense.

4.2.1 The Mollow triplet

Following our introduction to light-matter interactions, the Hamiltonian governing the resonance fluorescence is the Jaynes-Cummings Hamiltonian (2.25). The electromagnetic field acts as an environment to the two-level system. Therefore, the atom follows a non-unitary evolution described by the quantum master equation (2.71).

Exhaustive mathematical treatments of this problem can be found in the literature, so instead, we would like to comment on some properties of the solutions which may be relevant later in this work. One of this is the shape of the resonance fluorescence spectrum, called the *Mollow triplet*, after Mollow who first described the phenomenon in 1969 [52].

For low light intensities the interaction is linear and the scattering is elastic. If the excitation field is monochromatic and on resonance with the atom, the atom absorbs a photon at the excitation frequency, and energy conservation demands that the emitted photon has the same frequency. The emitted fluorescence has the same spectral profile, and in particular the same narrow width, as the excitation.

In a strong resonant field, non-linear scattering occurs. In the ideal case of scattering from an isolated atom at rest the theory predicts a three peak spectrum. The spectrum of resonance fluorescence is derived rigorously in [43, 11].

4.2.2 Anti-bunching

A striking feature of resonance fluorescence is *anti-bunching*, that is, the tendency of a source to emit photons one by one. This is a purely quantum-mechanical effect. The opposite effect of anti-bunching is *bunching* — the tendency of photons to be emitted in correlated pairs. It turns out that bunching is a property of thermal light, and can be explained classically [53]. Anti-bunching, on the other hand, is an exclusively quantum phenomenon with no classical explanation.

Bunching or anti-bunching can be characterized via two-time intensity correlations. Experimentally, this amounts to measuring the joint probability of detecting

two photons with a time delay τ between the detections. Typically, this is quantified by the Glauber $g^{(2)}$ function defined as [54]

$$g^{(2)}(\tau) = \frac{\langle b^\dagger(0) b^\dagger(\tau) b(\tau) b(0)\rangle}{\langle b^\dagger(0) b(0)\rangle^2}, \tag{4.1}$$

where the two-time correlation is normalized over the number of photons. For the resonance fluorescence case, the field b corresponds to either the reflected or transmitted b_{out}. These fields relate to the state of the atom by the input-output relation (2.46).

In Fig. 4.3 the $g^{(2)}$ function for the reflected field of steady-state resonance fluorescence from an atom coupled to two decay channels is displayed. We see that starting from $g^{(2)}(0) = 0$, the probability of detecting a second correlated photon build up with time: $g^{(2)}(\tau) > g^{(2)}(0)$. This inequality is a defining property of anti-bunching. During a short time interval following the first detection, the probability of detecting another photon remains small — this is photon anti-bunching. This effect is rapidly lost as we increase the driving strength.

The effect of anti-bunching from resonance fluorescence was predicted by [55], and observed first by [56]. Physically, anti-bunching in the field scattered of a two-level atom occurs because in order to be able to emit a second photon, the atom must be re-excited by the laser light which requires a certain amount of time [12, 11, 13].

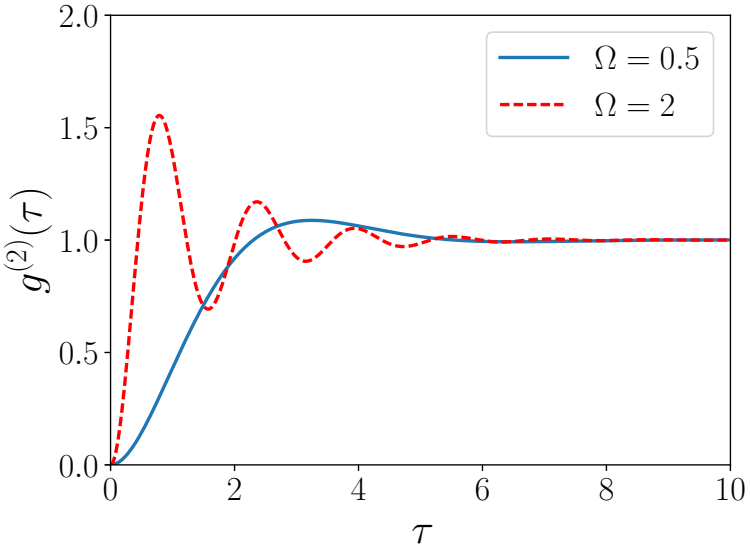

Figure 4.3: Intensity correlation function $g^{(2)}$ for resonance fluorescence from an atom coupled to two decay channels, for two different driving strengths. Note that when a photon has been detected at time $\tau = 0$, the probability of detecting a second photon is zero. This is perfect anti-bunching. A value of $g^{(2)}$ below 1 indicates non-classicality.

4.2.3 Steady-state generation

Steady-state generation of negative Wigner function states is sought after. In the field of quantum optics, current available methods for producing them are highly probabilistic [57]. Therefore, we will look at resonance fluorescence in the steady state. From Fig. 4.4 we can estimate when steady-state is reached after starting to drive an atom in the ground state.

The strong driving regime is when $\Omega \gg \gamma/4$, and the weak driving regime is when $\Omega \ll \gamma/4$, according to [11]. Here γ is, as in Section 2.2, the decay rate of the system, and Ω is the driving strength in the driving Hamiltonian (2.78). We will consistently use $\gamma = 1$. For $\Omega = 5$, which is strong driving in our case, we are in steady-state after $t = 10$. Thus, waiting this amount of time before commencing measurements should be sufficient in the parameter regime we will investigate later in Chapter 5.

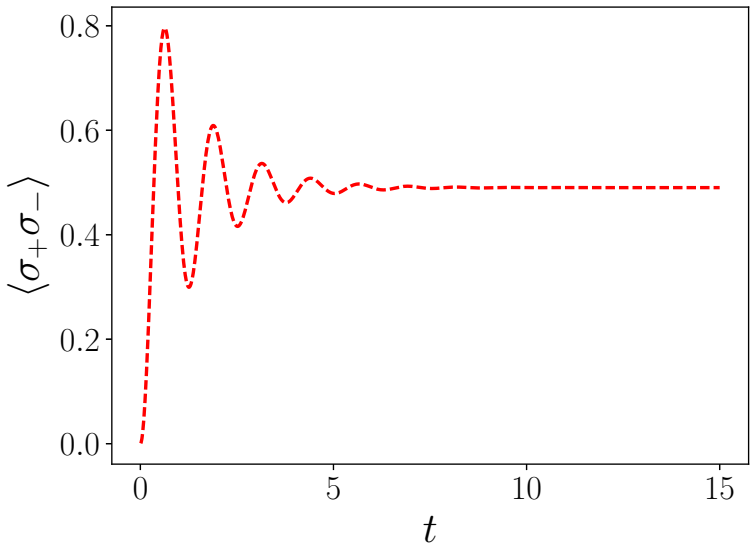

Figure 4.4: Probability of the atom to be in the excited state. Even for fairly strong driving, here $\Omega = 5$, the system is certainly in steady state after $t = 10$.

5

Quantum state tomography

Classical tomography is an experimental method for examining the density distribution inside an object. An example everyone is familiar with is from medicine; the interior of the human body can be reconstructed using the method of CT (Computed Tomography) scans.

In quantum tomography, the subject of interest is not the density distribution inside a physical object, but rather the state of a quantum system. If we know the quantum state, we can calculate the probability distribution for any observable.

Any scheme making measurements on a quantum system can only provide probability distributions — could it be possible to use a set of measured probability distributions to reconstruct the quantum state? This is an old problem in quantum mechanics. In 1933, Pauli wondered if it was possible to find the wave function amplitude *and* phase from the probability distributions in position and momentum. It turns out that it is not possible in general to reconstruct the quantum state knowing only these two distributions [58].

Fortunately, through homodyne detection it becomes possible to measure not only two canonically conjugate field quadratures, but any linear combination of them, corresponding to a rotation by an angle θ [31] in phase-space. That is, we can measure all generalized quadratures (2.93) by setting the local oscillator phase θ. Knowing all the distributions corresponding to a range of θ, it is possible to reconstruct the state of the field [59].

A generalized quadrature is a linear combination of the Hermitian position and momentum operators, and is thus Hermitian itself. Let's denote its eigenstates $|\theta, x\rangle$ and the corresponding eigenvalues x_θ, such that

$$X_\theta \, |\theta, x\rangle = x_\theta \, |\theta, x\rangle \, . \tag{5.1}$$

Note that the eigenvalues x_θ are real numbers, as opposed to an n-level system where the spectrum is discrete. Hence the quadrature eigenvalues are functioning as our continuous variables, potentially to be used for continuous variable quantum computing.

For a system in the state ρ, the probability that a measurement of the generalized quadrature X_θ yields the eigenvalue x_θ is

$$\mathrm{pr}(\theta, x) = \mathrm{Tr}[\Pi(\theta, x)\rho] = \langle \theta, x|\rho|\theta, x\rangle \, , \tag{5.2}$$

where $\Pi(\theta, x) = |\theta, x\rangle\langle\theta, x|$ is the projector onto this quadrature eigenstate.

Originally, this was done by *Wigner tomography*, as the probability distribution of a given quadrature can be expressed directly in terms of the Wigner function [60]

$$\mathrm{pr}(\theta, x) = \int_{-\infty}^{\infty} W(x_\theta \cos\theta - y_\theta \sin\theta, x_\theta \sin\theta + y_\theta \cos\theta)\, \mathrm{d}y_\theta. \tag{5.3}$$

From this expression, one can perform the *inverse Radon transformation* to obtain the Wigner function. This method, which is the same as used for medical tomography, was proposed by Vogel and Risken [60], and successfully realized by Faridani et al. [61].

5.1 Maximum Likelihood Estimation

Quantum state reconstruction can never be perfect, due to uncertainties in the estimation of the measured statistical distributions. The inverse transform method only works well when these uncertainties are negligible. Otherwise, errors can lead to inaccurate, and even unphysical, features in the reconstructed density matrix. For example, the diagonal elements of the density matrix, which represent occupation probabilities, may be found to be negative, and its trace is not guaranteed to equal 1 [62]. Although errors cannot be eliminated completely, we would like a reconstruction method that guarantees a physically plausible density matrix and minimizes artifacts. This led to the development of a reconstruction method based on a *maximum likelihood estimation* [63]. This seems sensible, as when considering the probabilistic nature of quantum mechanics and the uncertainties of measurement, instead of asking "Which quantum state is determined by that set of measurements?", it is more appropriate to ask "What quantum state seems to be most likely for that measurement?" .

An interval of the real axis is discretized into equally sized bins, the photocurrent measurement data is sorted into the bins, and the number of events $f(\theta, x)$ belonging to each bin is counted.

We remember from Section 2.3.4.1 that measuring the photocurrent corresponds to measuring the quadrature. The probability $\mathrm{pr}(\theta, j)$ of observing the quadrature variable x_θ within the jth bin (x_j, x_{j+1}) is

$$\mathrm{pr}(\theta, j) = \int_{x_j}^{x_{j+1}} \mathrm{pr}(\theta, x)\, \mathrm{d}x = \int_{x_j}^{x_{j+1}} \mathrm{Tr}[|\theta, x\rangle\langle\theta, x|\, \rho]\, \mathrm{d}x = \mathrm{Tr}[\Pi(\theta, j)\rho], \tag{5.4}$$

where

$$\Pi(\theta, j) = \int_{x_j}^{x_{j+1}} |\theta, x\rangle\langle\theta, x|\, \mathrm{d}x, \tag{5.5}$$

is the projection operator for the jth bin.

In the Fock (photon number state) basis, the matrix representation of the projection operator is

$$\Pi_{mn}(\theta, j) = \langle m|\Pi(\theta, j)|n\rangle = \int_{x_j}^{x_{j+1}} \langle m|\theta, x\rangle\, \langle\theta, x|n\rangle\, \mathrm{d}x, \tag{5.6}$$

where the overlap between the number and quadrature eigenstates is given by the harmonic oscillator eigenfunctions in the position basis [64]

$$\langle x|n\rangle = \psi_n(x) = \frac{1}{\sqrt{2^n n!}} \left(\frac{1}{\pi}\right)^{1/4} \exp\left(-x^2/2\right) H_n(x), \tag{5.7}$$

multiplied by a phase [65]:

$$\langle \theta, x|n\rangle = \psi_n(\theta, x) = \exp\left(-\mathrm{i}n\theta\right) \frac{1}{\sqrt{2^n n!}} \left(\frac{1}{\pi}\right)^{1/4} \exp\left(-x^2/2\right) H_n(x). \tag{5.8}$$

Here H_n denotes the nth Hermite polynomial. So we have

$$\Pi_{mn}(\theta, j) = \int_{x_j}^{x_{j+1}} \psi_m(\theta, x)^* \psi_n(\theta, x)\, \mathrm{d}x. \tag{5.9}$$

Note that here the integration over x is an integration over photocurrents.

With $f(\theta, j)$ observations in bin j, the likelihood function is defined as [66]

$$L(\rho) = \prod_{\theta,j} \mathrm{Tr}[\Pi(\theta, j)\rho]^{f(\theta,j)}. \tag{5.10}$$

The likelihood is the joint probability of obtaining a particular set of measurements. Note that this is a function of the state ρ which we aim to determine. The central idea behind this method is that the state we observe experimentally is the one which maximizes this quantity. This optimization procedure can be performed iteratively as it is described below.

In order to reconstruct the quantum state, we define the operator

$$R(\rho) = \sum_{\theta,j} \frac{N_\theta}{N} \frac{f(\theta, j)}{pr(\theta, j)} \Pi_{\theta,j}, \tag{5.11}$$

where N_θ is the number of measurements per angle θ, and N is the total number of measurements. It can be shown that the state ρ^* that maximizes the likelihood (5.10) obeys [67]

$$R(\rho^*)\rho^* R(\rho^*) = \rho^*. \tag{5.12}$$

Choosing some initial density matrix ρ_0, we can apply repetitive iterations

$$\rho_{k+1} = \mathcal{N}[R(\rho_k)\rho_k R(\rho_k)], \tag{5.13}$$

where $\mathcal{N}$ denotes normalization to unity trace. Each iteration will increase the likelihood, $L(\rho_{k+1}) > L(\rho_k)$, and the density matrix estimate asymptotically approaches the maximum-likelihood state ρ^* [62].

We determine when to stop the iterative process by specifying that the reconstruction is finished when

$$\Delta\rho = \|\rho_{k+1} - \rho_k\| \leq \varepsilon, \tag{5.14}$$

where ε is a small number. We will use $\varepsilon = 10^{-3}$. As the matrix norm we use the *Frobenius norm*, sometimes called the *Hilbert-Schmidt norm*, defined as

$$\|A\| \equiv \sqrt{\mathrm{Tr}[A^\dagger A]}. \tag{5.15}$$

We will work in the Fock basis, and the dimension of the projector Π_{mn}, and the reconstructed density matrix $\rho_{mn} = \langle m|\rho|n\rangle$, is set by the dimension of the Fock space. To perform numerical calculations we must truncate the Fock space. The dimension we choose for the Fock space is dependent on the driving strength. For stronger driving, we expect to observe more photons, and the Fock space must be large enough to accommodate all photons.

5.2 Calculating the Wigner function

Knowing the density matrix, we can calculate the Wigner function of the state by [66]

$$W(x,p) = \sum_{m,n} \rho_{mn} W_{mn}(x,p), \tag{5.16}$$

with

$$W_{mn}(x,p) = \frac{1}{2\pi}\int_{-\infty}^{\infty} \mathrm{d}y\, e^{-\mathrm{i}py/\hbar} \left\langle x + \frac{y}{2}\right| |m\rangle\langle n| \left| x - \frac{y}{2}\right\rangle . \tag{5.17}$$

Sometimes the function (5.17) is called the diagonal or generalized Wigner function, as in the literature the Wigner function often only refers to the diagonal elements W_{nn} [68], which is the ordinary Wigner function for a Fock state $\rho = |n\rangle\langle n|$. This can be seen by inserting this density matrix into the definition (3.1) of the Wigner function and comparing it with W_{nn} from Eq. (5.17).

The off-diagonal form was introduced by Moyal [69], and it is therefore also known as the Moyal function. In the Fock basis, the Moyal function is

$$\begin{cases} W_{mn} = \frac{1}{\pi} e^{-(x^2+p^2)} (-1)^m \sqrt{\frac{m!}{n!}} (2x^2+2p^2)^{\frac{n-m}{2}} e^{\mathrm{i}(n-m)\phi} L_m^{n-m}(2x^2+2p^2), & n \geq m, \\ W_{mn} = \frac{1}{\pi} e^{-(x^2+p^2)} (-1)^n z \sqrt{\frac{n!}{m!}} (2x^2+2p^2)^{\frac{m-n}{2}} e^{\mathrm{i}(m-n)\phi} L_n^{m-n}(2x^2+2p^2), & n < m. \end{cases} \tag{5.18}$$

For a detailed derivation of these expressions, see Appendix C.

5.3 Filter function

The Wigner function is defined for a set of observables such as (2.8), that fulfill the commutation relation (2.9). For this to hold, the creation and annihilation operators must fulfill $[a, a^\dagger] = 1$. This relation implies that the operators $a, a^\dagger$ are dimensionless.

Looking back at section 2.3.4, more specifically Eq. (2.100) and (2.103), we see that the relation between the photocurrent and detected output field is

$$\mathrm{d}j(t) = \frac{1}{\sqrt{2}} \left\langle b_{\mathrm{out}}\, \mathrm{d}t + b_{\mathrm{out}}^\dagger\, \mathrm{d}t \right\rangle . \tag{5.19}$$

But as we learned in Section 2.2.1, the output field is time-dependent, and has the commutation relation (2.44). This means that b_{out} has the dimension of $1/\sqrt{t}$. We can define a dimensionless mode A from b_{out} by filtering the latter with an appropriate function f, also having dimension $1/\sqrt{t}$:

$$A = \int_0^T f(t) b_{\text{out}}(t)\, \mathrm{d}t. \tag{5.20}$$

The condition that f is normalized such that

$$\int_0^T \mathrm{d}t\, |f(t)|^2 = 1, \tag{5.21}$$

guarantees that A is a dimensionless bosonic mode with commutation relation $[A, A^\dagger] = 1$.

Meaning of the filter function

The filter function also has a physical meaning. The one-photon state

$$|1_f\rangle = A^\dagger |0\rangle = \int \mathrm{d}t f(t) b_{\text{out}}^\dagger(t) |0\rangle\,, \tag{5.22}$$

corresponds to a single photon in a well defined envelope $f(t)$. In other words, $f(t)$ is the probability amplitude to detect a photon at time t.

Importance of mode-matching

Whenever the filter function does not match the envelope of the detected photon, vacuum noise is added to the signal. This can be understood in the following way: consider the vector space of square integrable functions, with a scalar product

$$(\psi, \phi) = \int_0^T \mathrm{d}t\, \psi^*(t)\phi(t). \tag{5.23}$$

Select f_k as an orthonormal basis: $f_k f_k' = \delta_{k'k}$. Then, any square integrable function f can be decomposed as

$$f(t) = \sum_k (f_k, f) f_k. \tag{5.24}$$

Normalization of f implies

$$\sum_k |(f_k, f)|^2 = 1. \tag{5.25}$$

The creation operator $a_f^\dagger$ of a mode f is

$$a_f^\dagger = \int \mathrm{d}t f(t) a^\dagger(t) = \int \mathrm{d}t \sum_k (f_k, f) f_k a^\dagger(t) = \sum_k (f_k, f) a_{f_k}^\dagger, \tag{5.26}$$

which is a multi-mode state.

Consider again the single photon $|1_f\rangle$. In density matrix formulation, this single-mode state is

$$\rho = |1_f\rangle\langle 1_f| = \sum_{k\ell}(f_k, f)(f_\ell, f)^* a^\dagger_{f_k} |\Omega\rangle\langle\Omega| a_{f_\ell}, \tag{5.27}$$

where $|\Omega\rangle = \otimes_k |0\rangle_k$. A single photon in a given envelope can be seen as a superposition of photons in the basis functions f_k.

The density operator corresponding to a mode $f_1 \neq f$ is obtained by tracing out the other modes:

$$\rho_1 = \mathrm{Tr}_{k\leq 2}\rho = \sum_{m\geq 2} \langle\Omega| a_{f_m} \left(\sum_k |(f_k, f)|^2 a^\dagger_{f_k} |\Omega\rangle\langle\Omega| a_{f_k} \right) a^\dagger_{f_m} |\Omega\rangle . \tag{5.28}$$

- if $k = 1$, the sum yields $|(f_1, f)|^2 |1_{f_1}\rangle\langle 1_{f_1}|$,
- if $k \neq 1$, we have $\sum_{m\geq 2} |(f_m, f)|^2 |0\rangle\langle 0|$

so

$$\rho_1 = |(f_1, f)|^2 |1_{f_1}\rangle\langle 1_{f_1}| + \sum_{m\geq 2} |(f_m, f)|^2 |0\rangle\langle 0| . \tag{5.29}$$

Imposing the normalization condition (5.25) gives

$$\rho = |(f_1, f)|^2 |1_{f_1}\rangle\langle 1_{f_1}| + \left(1 - |(f_1, f)|^2\right) |0\rangle\langle 0| . \tag{5.30}$$

We immediately see that only for $f_1 = f$ do we recover $\rho = |1_f\rangle\langle 1_f|$. Otherwise, the state ρ will contain a factor of $|0\rangle\langle 0|$, i.e. vacuum.

For an alternative derivation of this property of the filter function for homodyne detection, see [70].

Filtered photocurrent

In general, the filter function f is complex valued. Nevertheless, for the rest of the discussion we will restrict ourselves to real-valued functions.

The time-independent generalized quadrature

$$X_\theta = \int \mathrm{d}t f(t) X_\theta(t), \tag{5.31}$$

corresponds to the measurement of quadrature $X_\theta(t)$ in the temporal mode defined by f. Thus, it suffices to filter the photocurrent (2.103) in order to determine the quadratures of the mode A. The integrated, filtered photocurrent

$$\int \mathrm{d}j(t) f(t) = \int \frac{f(t)}{\sqrt{2}} \left(\sqrt{\gamma} \langle \sigma_+ e^{\mathrm{i}\theta} + \sigma_- e^{-\mathrm{i}\theta} \rangle \, \mathrm{d}t + \mathrm{d}W \right) . \tag{5.32}$$

is recorded for each simulated trajectory.

5.4 Calibration test

Before we begin to reconstruct states of resonance fluorescence, we try to reconstruct already well-known states: vacuum (zero photons) and a single photon. Since we know that the maximum amount of photons that could possibly be observed is one, a two-dimensional Fock space is sufficient.

To begin with, we use only one decay channel. We use $\gamma = 1$, matching the decay parameter γ in the master equation (2.115). Also, there is no external driving applied — we set $\Omega = 0$ in the driving Hamiltonian (2.78), making it vanish. The stochastic master equation we will solve then looks like

$$\mathrm{d}\rho = \gamma \mathcal{D}[\sigma_-]\rho \,\mathrm{d}t + \sqrt{\gamma}\mathcal{H}[e^{-\mathrm{i}\theta}\sigma_-]\rho \,\mathrm{d}W. \tag{5.33}$$

We solve Eq. (5.33) using Milstein's method, described in Section 2.4.2. As can be seen in the top row of Fig. 2.2, even only 500 trajectories seems adequate for an undriven system, but we use 1000 trajectories just to have a safe margin.

5.4.1 Reconstructing vacuum

With the two-level system initially in the ground state, and in the absence of a driving field, the photocurrent consists only of vacuum fluctuations. The vacuum state is defined as $A\,|0\rangle = 0$, independent of the mode A — therefore, an arbitrary filter function should be able to reconstruct the vacuum state.

For the calibration tests 20 angles θ in the range $[0, \pi]$ were used. A photocurrent histogram for $\theta = 0$ is shown in Fig. 5.1, along with the theoretical prediction indicated by the dashed line. The prediction is given by Eq. (5.2), being $|\langle \theta, x|0\rangle|^2$ for the vacuum state $|0\rangle$. Looking at Equations (5.7) and (5.8) we see that this is the same as $|\langle x|0\rangle|^2$, so the shape of the distribution is expected to follow the modulus square of the harmonic oscillator ground state wave function. The measured histogram is in excellent agreement.

The probability distribution $|\langle x|0\rangle|^2$ is independent of θ, and we did indeed observe that the current histograms had the same shape for every angle.

The vacuum fluctuations come solely from the Wiener increment in Eq. (2.103), giving the stochastic photocurrent $\mathrm{d}j = \mathrm{d}W/\sqrt{2}$. The photocurrents in Fig. 5.1 form a Gaussian distribution with a fitted standard deviation of approximately $1/\sqrt{2}$, which stems from the factor $1/\sqrt{2}$ in the expression for the photocurrent. The fact that the results match the theory validates that the random number generation works correctly.

The reconstructed density matrix is shown in Eq. (5.34), besides the exact density matrix, for comparison.

$$\rho_{\text{reconstructed}} = \begin{pmatrix} 0.9960 & 0.0073 \\ 0.0073 & 0.0040 \end{pmatrix}, \quad \rho_{\text{exact}} = \begin{pmatrix} 1 & 0 \\ 0 & 0 \end{pmatrix}. \tag{5.34}$$

The Wigner function for the reconstructed density matrix is shown in Fig. 5.2. We can see that it is positive everywhere. Due to the independence of θ, it is also completely symmetric around the origin.

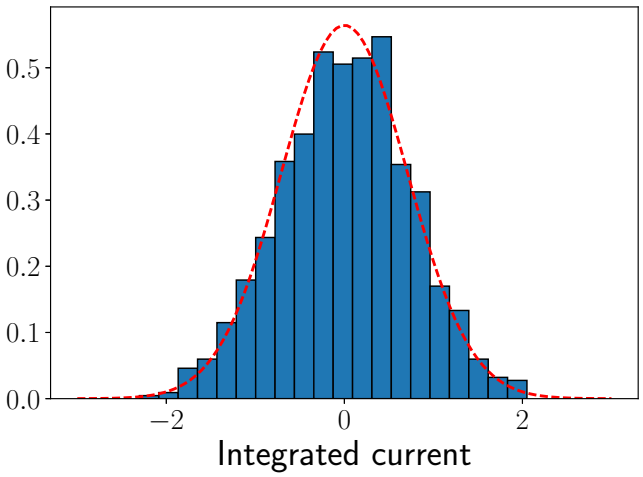

Figure 5.1: Photocurrents from 1000 trajectories of the vacuum state, with integration time $T = 20$. The dashed line is the modulus square of the vacuum wave function.

The Wigner function of the reconstructed state is very nearly identical to the Wigner function of the exact state. To show this, a cut of both functions at $p = 0$ is displayed in Fig. 5.3. The result is similar for all other values of p.

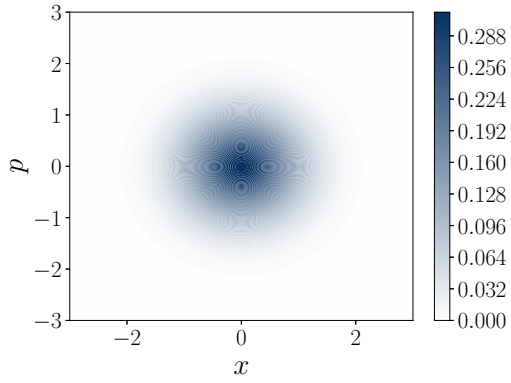

(a) Contour plot of the reconstructed density matrix for vacuum. It is symmetric around the origin, illustrating the phase independence.

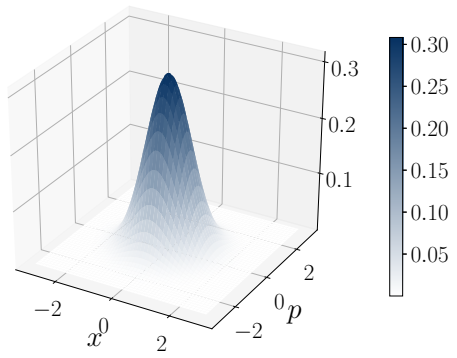

(b) Surface plot of the reconstructed density matrix for vacuum.

Figure 5.2

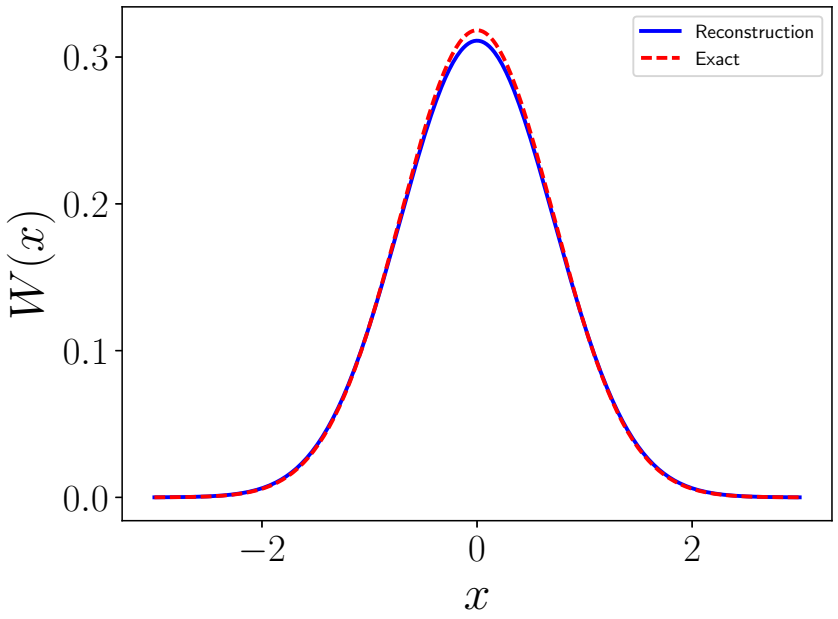

Figure 5.3: Cut of the Wigner function for vacuum at $p = 0$. The solid line is the cut of the exact Wigner function, and the dashed line is the Wigner function for the reconstructed density matrix. The lines overlap everywhere except at the top.

5.4.2 Reconstructing one photon

We set the two-level atom density matrix to be in the excited state at $t = 0$. Following our light-matter interaction discussion, in the rotating wave approximation a qubit and a light field can exchange a single excitation. If coupled to the many degrees of freedom of the electromagnetic field, which is the environment, and in the absence of excitations (zero temperature), the initially excited atom will decay to the ground state by emitting a photon. This is the photon we are aiming to see.

If there are multiple decay channels, then the photon can leak through all of them with different probabilities. To be assured that we will observe the whole photon when it is emitted, we use a single decay channel.

The normalized filter function used for reconstructing the one-photon state is

$$f_1(t) = \sqrt{\frac{\gamma}{1 - e^{-\gamma T}}} \exp\left(-\gamma t/2\right). \tag{5.35}$$

This is the filter in the time domain. In the frequency domain, the filter is the Fourier transform of $f(t)$, which is a Lorentzian, matching the spectrum of spontaneous decay of an excited atom. To match the decay parameter γ in the master equation, we use (5.35) with $\gamma = 1$.

The integration time is set to $T = 6$. The integration time is chosen long enough that the excited atom will have decayed and released a photon by the end of that

time. As can be verified by looking at Fig. 2.2, $T = 6$ is sufficiently lengthy. If a too short integration time is chosen, the atom may not decay and some vacuum will be observed, which will degrade the negativity of the state. In general, if T is on the other hand too long, the atom will have decayed at an earlier time and vacuum is again observed. However, the filter function (5.35) matches the one-photon decay perfectly — it decays sufficiently fast in time so that no extra negativity is observed.

When using the correct filter function for the single-photon state, the observed photocurrents from the decaying atom look like Fig. 5.4a. The shape of the distribution is $|\langle x|1\rangle|^2$, the modulus squared of the single-photon wave function. While the reconstruction is made using data for 20 angles, the histogram only shows the result for one angle. But just like the vacuum state, the one-photon state is phase independent.

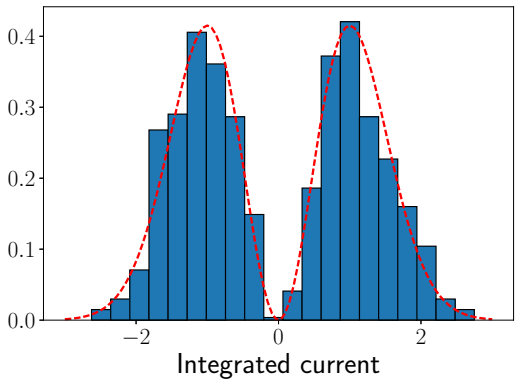

(a) Photocurrents from 1000 trajectories. The dashed line is the modulus square of the one-photon wave function.

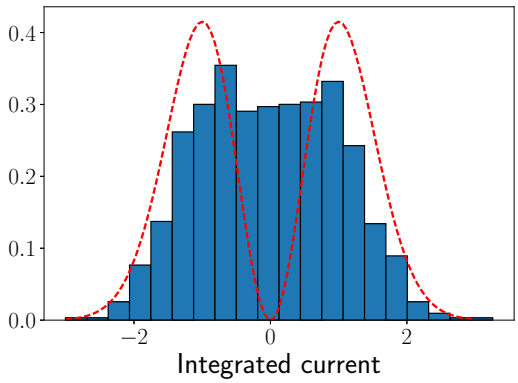

(b) Photocurrent from observing the excited atom, with the wrong filter function, $\gamma = 5$, instead of $\gamma = 1$. The current distribution is in the shape of a mix between vacuum (Fig. 5.1) and one photon (Fig. 5.4a). The dashed line is the modulus square of the one-photon wave function.

Figure 5.4: Photocurrent distributions from simulations of a one-photon decay, using different filter functions.

The reconstructed density matrix is shown in Eq. (5.36), besides the exact density matrix for comparison.

$$\rho_{\text{reconstructed}} = \begin{pmatrix} 0.0010 & -0.0006 \\ -0.0006 & 0.9990 \end{pmatrix}, \quad \rho_{\text{exact}} = \begin{pmatrix} 0 & 0 \\ 0 & 1 \end{pmatrix}. \tag{5.36}$$

The Wigner function calculated from the reconstructed density matrix can be seen in Fig. 5.5. The relative error between the matrix elements of the exact and

reconstructed states is of the order of 10^{-4}. This yields no significant differences between the corresponding Wigner functions as can be seen in Fig. 5.6. There we plot a section ($p = 0$) of both the theoretical Wigner function and the reconstructed one for a single photon. We can see that the agreement is perfect.

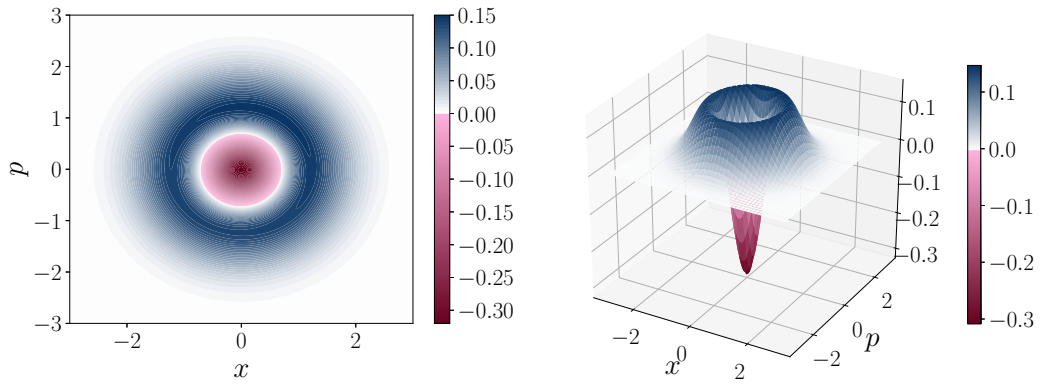

(a) Contour plot of the reconstructed density matrix for one photon. It is symmetric around the origin, illustrating the phase independence.

(b) Surface plot of the reconstructed density matrix for one photon.

Figure 5.5

Effect of filtering

Using a filter function $f \neq f_1$ by setting $\gamma \neq 1$ in (5.35), more precisely $\gamma = 5$ in this example, we get a photocurrent distribution that does not look like the theoretical prediction, shown in Fig. 5.4b. This means we observe currents from vacuum fluctuations, as can be understood from the discussion about mode-matching in Section 5.3.

The reconstructed density matrix looks like

$$\rho_{\text{reconstructed}} = \begin{pmatrix} 0.4845 & -0.0026 \\ -0.0026 & 0.5155 \end{pmatrix}. \tag{5.37}$$

This can actually be calculated, by evaluating the scalar product (f_1, f) as defined in Eq. (5.23) and inserting the result into (5.30). With f being (5.35) with $\gamma = 1$, and f_1 the same except with $\gamma = 5$ gives $|(f_1, f)|^2 = 0.555$, in reasonable agreement with the matrix element ρ_{22} in (5.37).

The Wigner distribution for this erroneous reconstruction is shown in Fig. 5.7. The negativity is markedly reduced in comparison with the true one-photon state. This can be understood in the following way: from definition (3.1) the Wigner function of (5.30) will be

$$W = |(f_1, f|)^2 W_1 + \left(1 - |(f_1, f)|^2\right) W_0, \tag{5.38}$$

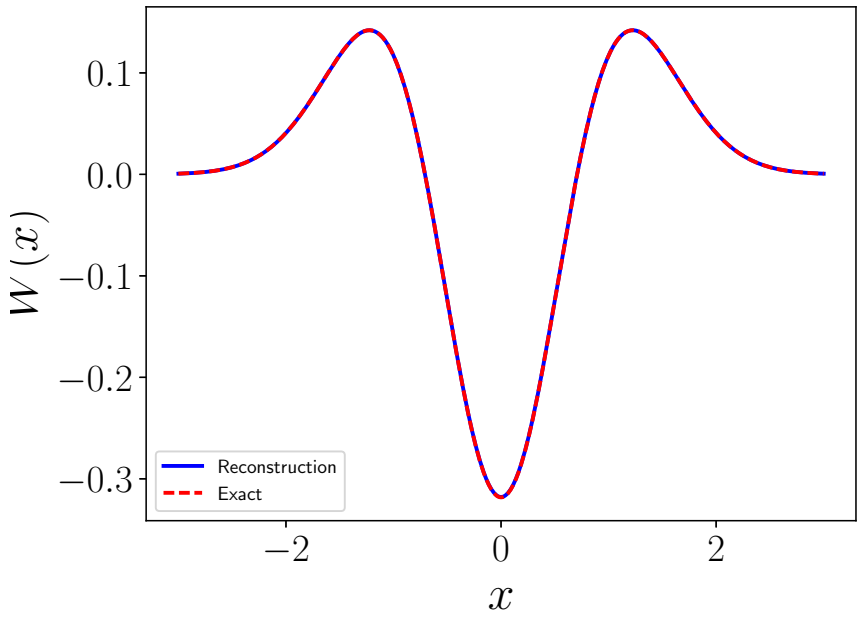

Figure 5.6: Cut of the Wigner function for a one-photon state at $p = 0$. The solid line is the cut of the exact Wigner function, and the dashed line is the Wigner function for the reconstructed density matrix. The lines overlap completely. The result is similar for all other values of p.

where W_0 and W_1 are the Wigner functions for vacuum and a one-photon state, respectively. Recalling that the Wigner function of vacuum is positive everywhere, we realize that by choosing a wrong filter function, the negativity of the single photon state is reduced. We can conclude that it is important to use the right filter function to retain Wigner negativity.

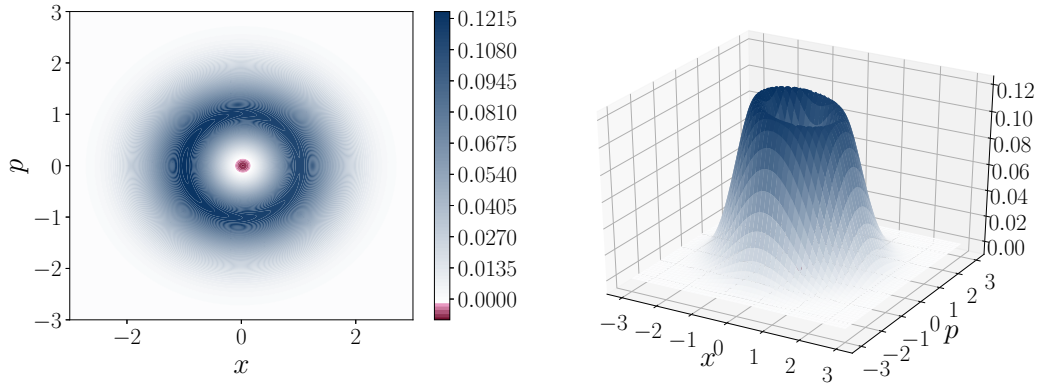

Figure 5.7: Reconstructed Wigner function for a one-photon state using the wrong filter function, with $\gamma = 5$ instead of $\gamma = 1$ in Eq. (5.35). Compare with Fig. 5.5 which is the correct result. With the wrong filter function, the Wigner negativity is reduced.

If we add an additional decay channel, we can never obtain a one-photon state. If the atom is coupled to both decay channels with equal strengths, as it is in our case, the atom has equal probability of emitting the photon to the left or to the right. So on average we will observe half a photon when observing only one channel. This is reflected in the reconstructed density matrix, which shows approximately 50/50 vacuum and one-photon.

$$\begin{pmatrix} 0.4888 & 0.0022 \\ 0.0022 & 0.5112 \end{pmatrix}. \tag{5.39}$$

Maximum likelihood convergence

We also look at the convergence of the maximum likelihood algorithm (5.13). The plots in Fig. 5.8 show up to 2000 iteration steps, but for the presented reconstructions we terminate the iteration process when the matrix difference (5.14) becomes smaller than 10^{-3}. We note that convergence is slower for a larger Fock space.

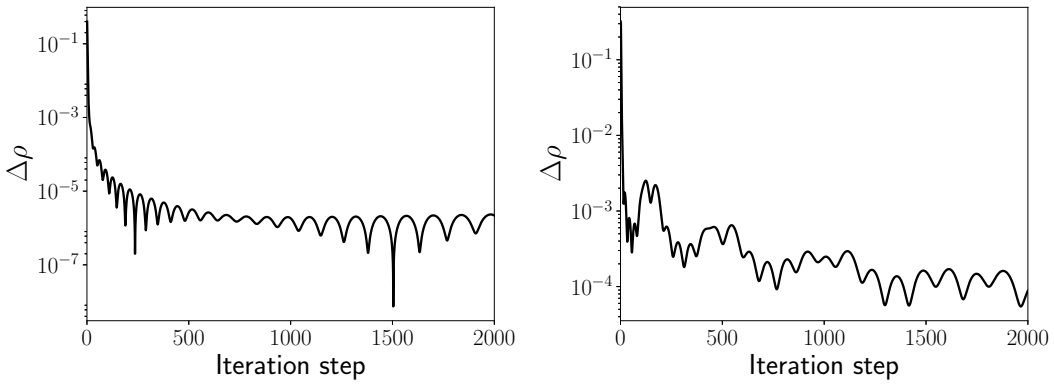

(a) Fock space dimension $N = 2$. It took 227 seconds for 2000 iterations.

(b) Fock space dimension $N = 8$. It took 1622 seconds for 2000 iterations.

Figure 5.8: Graphs of the Frobenius matrix difference (5.14) during iterations of the maximum likelihood algorithm while reconstructing a single-photon state.

5.5 Results

Here we look at reconstructed states from steady-state resonance fluorescence with different parameters. We present results for a few different combinations of integration time T and driving strength Ω.

As discussed in Chapter 4, we will study two configurations. Namely, the atom in 1D open space (two decay channels) and the atom in front of a mirror (one decay channel).

In all instances 20 angles evenly spaced between 0 and π were used — this range of angles covers phase-space, as we learned in Section 2.3.4.1. We run 1000 trajectories per angle. Since we want steady-state generation, we wait until $t = 10$ before we start integrating. As can be seen in Fig. 4.4, even for very strong driving the state has stabilized by that time. Note that this time is suitable for the parameter regime explored here, but if even stronger driving were to be applied, or different decay rates selected, a different stabilization time may need to be selected.

For weaker driving one does not expect to observe that many photons, especially for a short integration time. This suggests that we can use a rather small Fock space, which is beneficial for computational reasons. To obtain the optimal Fock space dimension, one can start with a small space, say $N = 2$. Then, increase N and run the simulation again. If the results differ, progressively increase N until the results are the same. Then you can conclude that a higher dimension is not necessary. For the results presented below a Fock space dimension $N = 8$ was used.

We want to produce negative Wigner function states in steady-state. Nothing dictates which filter function is the best for our problem, we have complete freedom to choose. As we have time-independent emission, it makes sense to choose a time-independent filter function. We use the constant, but normalized, filter function $f(t) = 1/\sqrt{T}$. Note that while this function is constant, i.e. independent of t, we can select different modes by varying the integration time T.

The results are shown as contour plots of the Wigner function.

5.5.1 Two decay channels

First, we look at the Wigner functions in the case to two identical decay channels. This corresponds to $\gamma' = \gamma_1 = \gamma_2 = 0.5\gamma = 0.5$ in the stochastic master equation (2.115). In Fig. 5.9 we show the numerically reconstructed states for three different integration times $T = 1$, $T = 5$ and $T = 10$. The atom is driven with $\Omega = 0.5$, which is in the regime of weak driving.

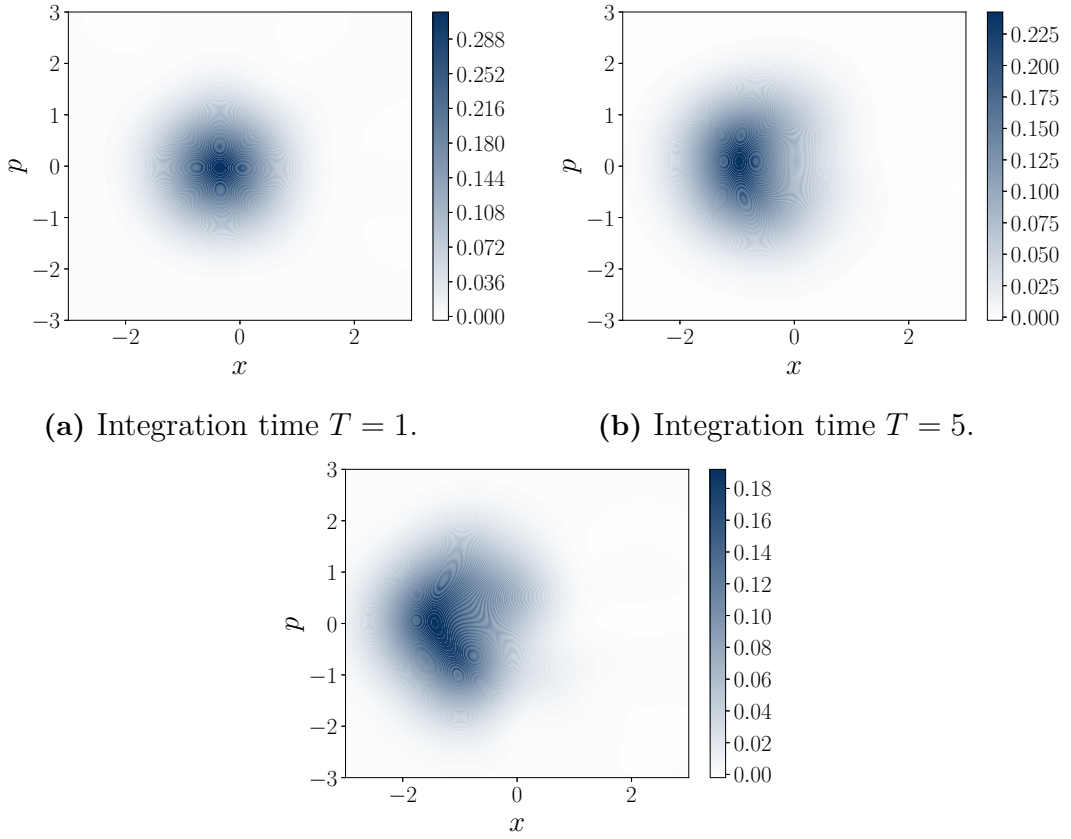

(a) Integration time $T = 1$.

(b) Integration time $T = 5$.

(c) Integration time $T = 10$.

Figure 5.9: Driving strength $\Omega = 0.5$. Two decay channels. No negativity is observed for any integration time.

In Fig. 5.10 below, we show the results for the same integration times as in Fig. 5.9, but in the strong driving regime with $\Omega = 2$. Still with two decay channels.

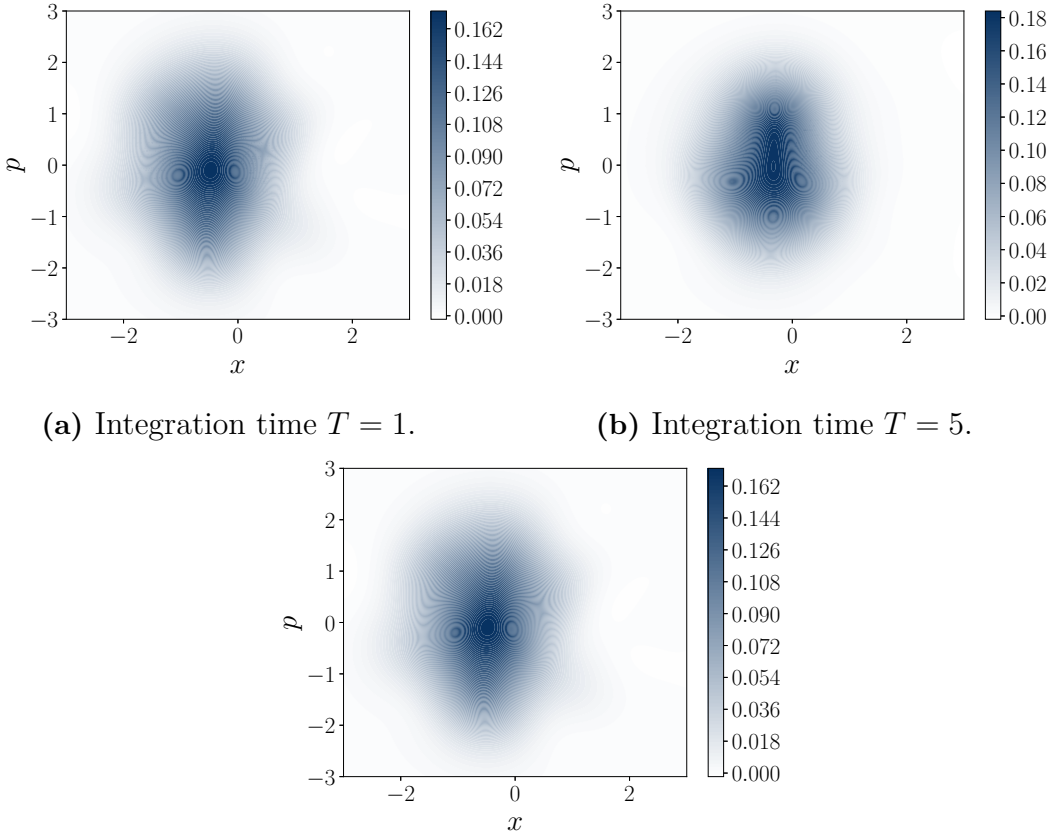

(a) Integration time $T = 1$.

(b) Integration time $T = 5$.

(c) Integration time $T = 10$.

Figure 5.10: Driving strength $\Omega = 2$. Two decay channels. No negativity is observed for any integration time.

We note that no negativity whatsoever is observed when having two decay channels. This can be understood by the following reasoning. As explained in conjunction with the density matrix (5.39), if there are two equal decay channels and only one is observed, there is a 50 % chance of observing only vacuum. Denote the vacuum and single photon density matrices ρ_0 and ρ_1, respectively. We know from Section 5.4.1 that $W(\rho_0) > 0$, meaning that the the Wigner function corresponding to ρ_0 is positive. We also know from Section 5.4.2 that the single-photon state takes on negative values: $W(\rho_1) < 0$. With a 50/50 incoherent mix of these, we have $W(\rho_0/2 + \rho_1/2) > 0$ everywhere in phase space.

The drive Ω is inducing Rabi oscillations in the system, i.e. the state of the two-level atom oscillates between the ground and excited state [12]. Therefore, driving the two-level atom is actually enhancing the vacuum contribution, adding to the vacuum contribution from the unobserved channel. In other words, we are

not going to get more negativity than from $W(\rho_0/2 + \rho_1/2)$, which is already a positive-Wigner state.

5.5.2 Atom in front of a mirror

We now look at the Wigner functions in the case of a single decay channel, i.e., an atom in front of a mirror. This corresponds to $\gamma' = \gamma = 1$ in the stochastic master equation (2.115). In Fig. 5.11 we show the reconstructed Wigner functions for the same integration times as in Section 5.5.1 above. The driving strength is $\Omega = 0.5$.

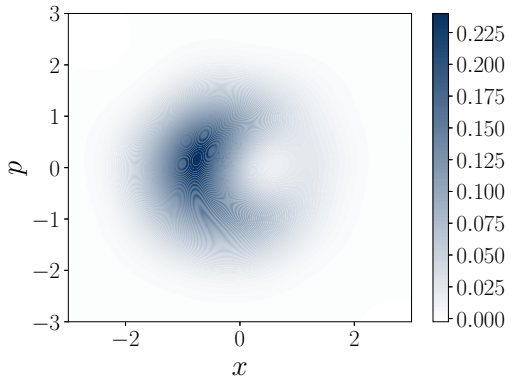

(a) Integration time $T = 1$.

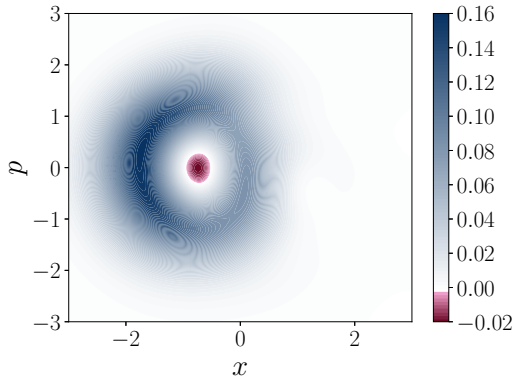

(b) Integration time $T = 5$. Negativity is observed!

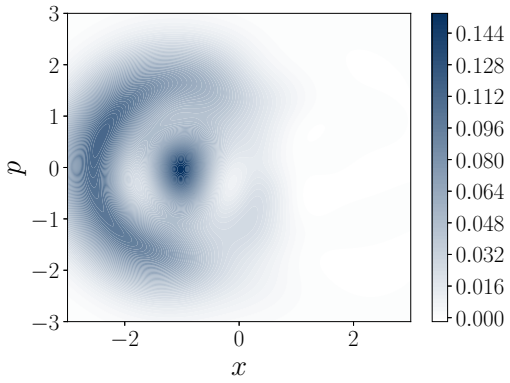

(c) Integration time $T = 10$.

Figure 5.11: Driving strength $\Omega = 0.5$. One decay channel. Negativity in the Wigner function is observed for integration time $T = 5$.

Results for driving strength $\Omega = 2$ are displayed in Fig. 5.12.

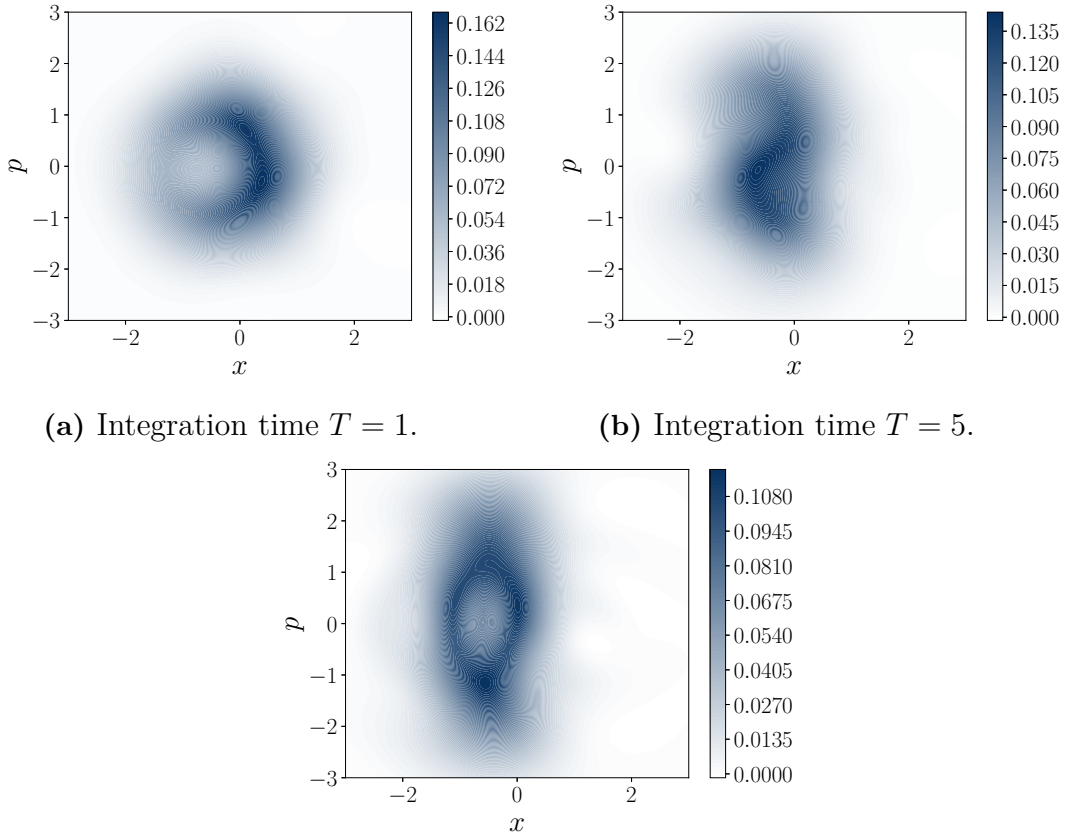

(a) Integration time $T = 1$.

(b) Integration time $T = 5$.

(c) Integration time $T = 10$.

Figure 5.12: Driving strength $\Omega = 2$. One decay channel. No negativity is observed for any integration time.

As can be seen in Fig. 5.11b, it is possible to observe a Wigner-negative state, i.e., a state whose corresponding Wigner function takes on negative values in some region of phase space, in the weak driving regime $\Omega = 0.5$ and for an integration time $T = 5$. This can be understood qualitatively. For a short integration time, the atom has not had enough time to decay, so vacuum is observed. On the other hand, for long integration times, observation is continued well after the atom has already decayed, again resulting in observation of vacuum.

Also, the fact that it is possible to observe Wigner-negative states in the configuration with an atom in front of a mirror can be understood by an argument similar to the one for the opposite case with two decay channels. For a single decay channel, in the absence of driving and for the atom initially in the excited state, it is possible to observe a single photon, as shown in Section 5.4.2. In the presence of a driving field, as already discussed at the end of Section 5.10, we will have a contribution from the vacuum state due to the atom periodically being in the ground state due to Rabi oscillations. Nevertheless, we can expect that in a

certain parameter regime the contribution from the single photon will be larger, and therefore, expect the observed state to be Wigner-negative. We verified numerically that in the strong driving regime no negativity was observed.

6
Conclusion

Quantum computers could solve problems that are intractable on conventional classical computers. The allure of this so-called *quantum advantage* has garnered a substantial interest in quantum computing. Several approaches to quantum computing have been investigated, but one avenue that has not been explored as of yet is continuous variable quantum computing using microwave photons in superconducting circuits. Superconducting qubits is one of the most extensively researched methods of quantum computing, but this set-up can also be used to create continuous variable quantum states. Since the experimental possibility is available, we want to investigate how to set up an experiment to produce continuous variable states, namely quadrature states, that can be used as computational resources.

The necessary condition for these states to have the "quantumness" which allows them to be used for calculations a classical computer cannot perform, is that they should have a negative Wigner function.

Before doing experiments in a laboratory, we can do numerical simulations of homodyne measurements of resonance fluorescence, and using the technique of quantum state tomography we can calculate the Wigner function of the state that was measured.

The aim of this work was to characterize what parameters provide negative Wigner functions. We tested different integration times, driving strengths and number of decay channels. We studied two configurations of resonance fluorescence, namely placing the atom in front of mirror and in a one-dimensional continuum. We found that for the latter configuration, only positive Wigner functions were obtained. We also found that negativity only occurred for rather weak driving strengths with the atom in front of a mirror. The next step in continuing this work would be to explore a larger parameter space of different driving strengths and integration times. There are more effects that could be studied —for example, the role of dephasing. Dephasing, and decoherence in general, is a more or less unavoidable phenomena that occurs in open quantum systems. It would be interesting to see how this affects the negativity of the Wigner function. Also, in this thesis we assumed 100 % efficient detectors. Since this is an idealization, it would be very relevant to see how the Wigner function is affected by more realistic detector efficiencies.

We aim to explore the possibility of generating suitable states for continuous variable quantum computing by continually driving a two-level atom. Our rather simple setup provides the non-linearity required to generate negative Wigner

states, which according to the Eisert-Mari theorem is a requirement to outperform a classical computer.

The idea is that a theoretical investigation, continuing the work in this thesis, will provide parameters to be used in a future experimental implementation of the setup. In this work a quantum state was reconstructed using simulated data, but a reconstruction from experimental results can just as well be done with the methods covered in this thesis.

A

Light-matter interaction

A.1 Göppert-Mayer transformation

The *Göppert-Mayer transformation* allows one to go from the point of view where the interaction Hamiltonian between the system of charges and the field is proportional to $A \cdot p$, to the electric dipole point of view where the interaction Hamiltonian is proportional to $r \cdot E$. These points of view are equal, and can be derived from one another using a unitary transformation T:

$$T = e^{-\frac{\mathrm{i}}{\hbar} e\vec{r}\cdot\vec{A}(r,t)} = e^{-\frac{\mathrm{i}}{\hbar}\vec{d}\cdot\vec{A}(r,t)}, \tag{A.1}$$

where $d = er \cdot E$ is the dipole operator. This transformation is equivalent to choosing $\chi = \vec{r} \cdot \vec{A}(r,t)$ in the gauge transformations (2.2) [71].

We now show how the $A \cdot p$ Hamiltonian can be transformed into the $r \cdot E$ Hamiltonian. The original Schrödinger equation is

$$\mathrm{i}\hbar \frac{\partial \psi}{\partial t} = H\psi. \tag{A.2}$$

The transformed wave function satisfies the Schrödinger equation

$$\mathrm{i}\hbar \frac{\partial \tilde{\psi}}{\partial t} = H'\tilde{\psi}. \tag{A.3}$$

Inserting the transformed wave function $\tilde{\psi} = T\psi$ we get

$$\mathrm{i}\hbar \frac{\partial T\psi}{\partial t} = \mathrm{i}\hbar T \frac{\partial \psi}{\partial t} + \mathrm{i}\hbar \frac{\partial T}{\partial t}\psi = H'T\psi. \tag{A.4}$$

Noting that T is a unitary operator, so that $T^\dagger T = \mathbb{1}$, we multiply with $T^\dagger$ from the left:

$$\underbrace{\mathrm{i}\hbar \frac{\partial \psi}{\partial t}}_{=H\psi} + \mathrm{i}\hbar T^\dagger \frac{\partial T}{\partial t}\psi = T^\dagger H'T\psi. \tag{A.5}$$

This is valid for every ψ, so

$$\begin{aligned} H + \mathrm{i}\hbar T^\dagger \frac{\partial T}{\partial t} &= T^\dagger H'T \\ \implies H' &= THT^\dagger + \mathrm{i}\hbar \frac{\partial T}{\partial t} T^\dagger. \end{aligned} \tag{A.6}$$

Now we manipulate the expression $T^\dagger pT$:

$$T^\dagger pT = T^\dagger pT - T^\dagger Tp + p = T^\dagger [p, T] + p \tag{A.7}$$

using the following commutator identity for any position dependent function $F(x)$ [64]

$$[p, F(x)] = -\mathrm{i}\hbar\nabla F$$

we get

$$T^\dagger pT = -\mathrm{i}\hbar T^\dagger \nabla T + p = -e\nabla\left(\vec{r}\cdot\vec{A}(r,t)\right) + p \tag{A.8}$$

We will use the vector identity

$$\nabla\left(\vec{r}\cdot\vec{A}\right) = (\vec{r}\cdot\nabla)\vec{A} + (\vec{A}\cdot\nabla)\vec{r} + \vec{r}\times(\nabla\times\vec{A}) + \vec{A}\times(\nabla\times\vec{r}). \tag{A.9}$$

In our case the last term is zero and the second term is $\vec{A}$. So far everything is exact. Now we need to use the dipole approximation.

A.2 Dipole approximation

This is also known as the *long wavelength approximation*, which is relevant when the wavelength of the electromagnetic field is much larger than the atomic dimension. In that case, the spatial variation of the electromagnetic field over the size of the atom is very small and can thus be neglected. This approximation simplifies the calculations significantly.

We can neglect the spatial variation of $\vec{A}(r,t)$ in the Hamiltonian. Replace $\vec{A}(r,t)$ with $\vec{A}(R,t)$, where we choose R to be the origin at the center of mass. This amounts to ignoring any displacements of the atom. This means the spatial derivatives of $\vec{A}$ are zero, and thus the first and third terms in Eq. (A.9) are also zero, and we are left with only $\nabla\left(\vec{r}\cdot\vec{A}\right) = \vec{A}$, which gives

$$T^\dagger pT = p - e\vec{A} \tag{A.10}$$

from Eq. (A.8).

This transformation translates p by an amount eA. With $H = (p - eA)^2/2m + V(r)$, where $V(r)$ is the Coulomb potential We have

$$THT^\dagger = \frac{p^2}{2m} + V(r) \tag{A.11}$$

and since in the Coulomb gauge, we have from Maxwell's equations

$$\vec{E} = -\frac{\partial\vec{A}}{\partial t}\,. \tag{A.12}$$

we get

$$\mathrm{i}\hbar\frac{\mathrm{d}T}{\mathrm{d}t}T^\dagger = \vec{d}\cdot\dot{\vec{A}} = -\vec{d}\cdot\vec{E}. \tag{A.13}$$

The transformed Hamiltonian of the atom in the electromagnetic field in the dipole approximation is

$$H' = \frac{p^2}{2m} - \vec{d} \cdot \vec{E} + V(r). \tag{A.14}$$

We have found that in the long-wavelength approximation, the interaction with the external field is simply described by a coupling term between the dipole moment d of the atom and the external electric field evaluated at the position of the atom center of mass.

Validity of formula

The validity of the dipole approximation is crucial for the equivalence of the $p \cdot \vec{A}$ and $r \cdot E$ interactions. The equivalence of the two interaction Hamiltonians is based on the gauge transformation (A.1) in which, by the dipole approximation, the relative position r of the electron does not enter in the vector potential $\vec{A}$, and that the center-of-mass R is not time-dependent. If center-of-mass motion is taken into account, additional terms appear in the Hamiltonian [68]. Fortunately artificial atoms in superconducting circuits are fixed in position.

A.3 Dipole operator

For the electric dipole transition between the states $|i\rangle$ and $|k\rangle$, the states must be of opposite parity since the dipole operator $\vec{d}$ is proportional to $\vec{r}$, which is an odd operator with respect to parity transformations, $\Pi\vec{r}\,\Pi^{-1} = -\vec{r}$, and parity is conserved in electromagnetic interactions.

We follow [64]. Parity is conserved, thus parity commutes with the Hamiltonian and the energy eigenstates are parity eigenstates. Suppose $|\alpha\rangle$ and $|\beta\rangle$ are parity eigenstates:

$$\begin{aligned} \Pi\,|\alpha\rangle &= \varepsilon_\alpha\,|\alpha\rangle\,, \\ \Pi\,|\beta\rangle &= \varepsilon_\beta\,|\beta\rangle\,, \end{aligned} \tag{A.15}$$

where ε_α, ε_β are the parity eigenvalues (± 1). Calculating the matrix element,

$$\langle\beta|\vec{r}|\alpha\rangle = \langle\beta|\Pi^{-1}\Pi\vec{r}\,\Pi^{-1}\Pi|\alpha\rangle = -\varepsilon_\alpha\varepsilon_\beta\,\langle\beta|\vec{r}|\alpha\rangle \tag{A.16}$$

shows that the matrix element can only be non-zero if $|\alpha\rangle$ and $|\beta\rangle$ have opposite parity, i.e. $\varepsilon_\alpha = -\varepsilon_\beta$. In other words, the parity-odd operator $\vec{d}$ connects states of opposite parity. This is known as *Laporte's rule*. This means we have the diagonal matrix elements $\langle g|\vec{d}|g\rangle = \langle e|\vec{d}|e\rangle = 0$.

A.4 Rotating wave approximation

The rotating wave approximation (RWA) is based on the fact that some operators evolve in different time-scales. For this reason, we need to look at the time-evolution of field and atomic operators.

A.4.1 Time evolution of field operators

The Heisenberg equation for the annihilation operator a reads

$$\frac{\mathrm{d}a}{\mathrm{d}t} = \frac{\mathrm{i}}{\hbar}[H, a]. \tag{A.17}$$

This equation has the solution

$$a(t) = a(0)e^{-\mathrm{i}\omega t}. \tag{A.18}$$

Taking the adjoint yields

$$a^\dagger(t) = a^\dagger(0)e^{\mathrm{i}\omega t}. \tag{A.19}$$

A.4.2 Time evolution of atomic operators

The time dependence of the operators σ_+ and σ_- is most easily appreciated in the interaction picture. We define operators in the interaction picture as

$$\hat{O}_I \equiv e^{\mathrm{i}H_0 t/\hbar}\hat{O}_S e^{-\mathrm{i}H_0 t/\hbar}. \tag{A.20}$$

The difference to the connection between the Schrödinger and the Heisenberg pictures

$$\hat{O}_H \equiv e^{\mathrm{i}Ht/\hbar}\hat{O}_S e^{-\mathrm{i}Ht/\hbar}, \tag{A.21}$$

is that now only H_0 rather than H appears in the exponential; in the interaction picture the system evolution is governed by the non-interacting part of the Hamiltonian.

The interaction picture interaction Hamiltonian is

$$H_I(t) = e^{\mathrm{i}H_0 t/\hbar}H_{\mathrm{int}}e^{-\mathrm{i}H_0 t/\hbar}. \tag{A.22}$$

Noting that the atomic and the field operators commute, we arrive at

$$H_I = e^{\mathrm{i}\omega a^\dagger a}(a + a^\dagger)e^{-\mathrm{i}\omega a^\dagger a}e^{\mathrm{i}\omega_{\mathrm{A}}\sigma_z/2}(\sigma_+ + \sigma_-)e^{-\mathrm{i}\omega_{\mathrm{A}}\sigma_z/2}. \tag{A.23}$$

From (A.18) and (A.19) we already know the time evolution of the field operators:

$$e^{\mathrm{i}\omega a^\dagger a}(a + a^\dagger)e^{-\mathrm{i}\omega a^\dagger a} = ae^{-\mathrm{i}\omega t} + a^\dagger e^{\mathrm{i}\omega t}. \tag{A.24}$$

The atomic part: Since $\sigma_z$is diagonal, we get:

$$\begin{aligned} e^{\mathrm{i}\omega_\mathrm{A}\sigma_z/2}\sigma_+ e^{-\mathrm{i}\omega_\mathrm{A}\sigma_z/2} &= \begin{pmatrix} e^{\mathrm{i}\omega_\mathrm{A}/2} & 0 \\ 0 & e^{-\mathrm{i}\omega_\mathrm{A}/2} \end{pmatrix} \begin{pmatrix} 0 & 1 \\ 0 & 0 \end{pmatrix} \begin{pmatrix} e^{-\mathrm{i}\omega_\mathrm{A}/2} & 0 \\ 0 & e^{\mathrm{i}\omega_\mathrm{A}/2} \end{pmatrix} = \\ &= \begin{pmatrix} 0 & e^{\mathrm{i}\omega_\mathrm{A}} \\ 0 & 0 \end{pmatrix} = \sigma_+ e^{\mathrm{i}\omega_\mathrm{A} t}. \end{aligned} \tag{A.25}$$

Similarly, we get $\sigma_-(t) = \sigma_- e^{-\mathrm{i}\omega_\mathrm{A} t}$. The interaction Hamiltonian in the interaction picture is then

$$H_I = \hbar g \left(a\sigma_+ e^{-\mathrm{i}(\omega-\omega_\mathrm{A})t} + a\sigma_- e^{-\mathrm{i}(\omega_\mathrm{A}+\omega)t} + a^\dagger \sigma_+ e^{\mathrm{i}(\omega_\mathrm{A}+\omega)t} + a^\dagger \sigma_- e^{\mathrm{i}(\omega-\omega_\mathrm{A})t} \right). \tag{A.26}$$

A.4.3 The approximation

The four terms in Eq. (A.26) have the following interpretation:

$a\sigma_+$: one photon is absorbed and the atom is excited: $|g, n\rangle \to |e, n-1\rangle$.
$a^\dagger\sigma_-$: emission of a photon and de-excitation of the atom: $|e, n\rangle \to |g, n+1\rangle$.

Note that these terms oscillate slowly when near resonance, with the frequency of the detuning $\Delta = \omega - \omega_\mathrm{A}$.

The other two terms:

$a^\dagger\sigma_+$: one photon is emitted and the atom is excited: $|g, n\rangle \to |e, n+1\rangle$.
$a\sigma_-$: one photon is absorbed and the atom gets de-excited: $|e, n\rangle \to |g, n-1\rangle$.

These terms oscillate much faster than the other two terms. Near resonance, $\omega \approx \omega_\mathrm{A}$, they oscillate with roughly twice the optical frequency ω. In the rotating wave approximation we neglect the rapidly oscillating terms. The fast rotating terms typically have frequencies of order $\sim 10^{15}\,\mathrm{s}^{-1}$, and will average to zero over the time-scale of radiative decay, that is $\sim 10^{-8}\,\mathrm{s}$. This approximation leads to significant simplifications [23].

The RWA implies that just near-resonant terms are effective in describing the interaction between radiation and matter.

In the literature it is commonly stated that the fast-rotating/anti-resonant terms do not conserve energy. This is not true. The Schrödinger picture Hamiltonian is time-independent, this means that energy is conserved. The misconception is based on considering the energy of transitions between states of the form $|e, n\rangle$, $|g, n+1\rangle$. While these are eigenstates of the free Hamiltonian, they are *not* energy eigenstates of the Jaynes-Cummings Hamiltonian which includes interactions between the atom and field [72].

B

Stochastic calculus

B.1 Stochastic Integrals

The general form of a stochastic differential equation is [22]

$$\mathrm{d}X_t = h(X_t, t)\,\mathrm{d}t + g(X_t, t)\,\mathrm{d}B_t. \tag{B.1}$$

This is in fact only a formal expression — its meaning is given by the corresponding stochastic integral equation

$$X_t = X_0 + \int_{t_0}^{t} h(X_s, s)\,\mathrm{d}s + \int_{t_0}^{t} g(X_s, s)\,\mathrm{d}B_s, \tag{B.2}$$

as only the integral equation can be interpreted consistently. The second integral is the stochastic integral.

In this notation, $X_t \equiv X(t)$. If the Wiener process $B(t)$ was differentiable, we could define this integral in the ordinary Riemann-Stieltjes sense. But $B(t)$ is nowhere differentiable (although it is continuous), and the integral can not be defined in the ordinary way [20]. Instead, we proceed as follows.

B.1.1 Mathematical Definition of the Stochastic integral

Suppose $g(t)$ is an arbitrary function of time and $B(t)$ is the Wiener process. We define the stochastic integral $\int_{t_0}^{t} g(t')\,\mathrm{d}B(t')$ as a kind of Riemann-Stieltjes integral. Namely, we divide the interval $[t_0, t]$ into n sub-intervals by means of partitioning points as in Fig. B.1.

$$t_0 \le t_1 \le t_2 \le \ldots \le t_{n-1} \le t_n$$

and define intermediate points τ_i such that

$$t_{i-1} \le \tau_i \le t_i.$$

The stochastic integral $\int_{t_0}^{t} g(t')\,\mathrm{d}B(t')$ is defined as a limit of the partial sums

$$S_n = \sum_{i=1}^{n} g(\tau_i)[B(t_i) - B(t_{i-1})]. \tag{B.3}$$

Unlike the ordinary Riemann-Stieltjes integral, in general the integral defined as the limit of S_n depends on the particular choice of intermediate point τ_i. The choice $\tau_i = t_{i-1}$ defines the *Ito stochastic integral* [22].

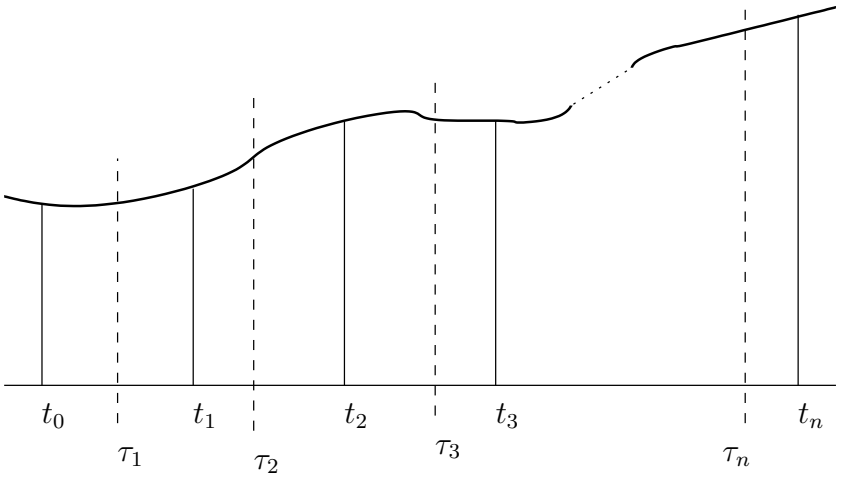

Figure B.1: Partitioning of the time interval used in the definition of stochastic integration.

B.1.1.1 Ito stochastic Integral

If $g(t)$ is any system operator, we define the (quantum) Ito integral by

$$\mathrm{I}\int_{t_0}^{t} g(t')\,\mathrm{d}B(t') = \lim_{n\to\infty}\sum_i g(t_i)[B(t_{i+1},t_0) - B(t_i,t_0)], \tag{B.4}$$

where the I stands for Ito, and $t_0 < t_1 < t_2 < \ldots < t_n = t$.

B.1.2 Ito's formula

In the previous section we defined the Ito stochastic integral. Just as for ordinary integrals, we do not use the basic definition but rather the fundamental theorem of calculus plus the chain rule in the explicit calculations. It turns out that it is possible to establish an Ito integral version of the chain rule, called the Ito formula. This formula differs from the one of classical calculus.

Consider an arbitrary function of $X(t)$: $f(X)$, where we omit the t argument for notational clarity. The function f has the Taylor expansion

$$\begin{aligned} &f(X+\mathrm{d}X) = f(X) + f'(X)\,\mathrm{d}X + \frac{1}{2}f''(X)(\mathrm{d}X)^2 + \ldots \\ &\implies f(X+\mathrm{d}X) - f(X) = \mathrm{d}f(X) = f'(X)\,\mathrm{d}X + \frac{1}{2}f''(X)(\mathrm{d}X)^2 + \ldots \end{aligned} \tag{B.5}$$

Now insert (B.1):

$$\mathrm{d}f(X) = f'(X)[h(X)\,\mathrm{d}t + g(X)\,\mathrm{d}B] + \frac{1}{2}f''(X)[h(X)\,\mathrm{d}t + g(X)\,\mathrm{d}B]^2. \tag{B.6}$$

Higher order terms are discarded. Using the Ito results $\mathrm{d}B\,\mathrm{d}t = 0$, $[\mathrm{d}t]^2 = 0$ and $[\mathrm{d}B]^2 = \mathrm{d}t$, we get

$$\mathrm{d}f(X) = \Big(h(X)f'(X) + \frac{1}{2}g(X)^2 f''(X)\Big)\,\mathrm{d}t + g(X)f'(X)\,\mathrm{d}B. \tag{B.7}$$

We see that because $\mathrm{d}B$ is only of order $\sqrt{\mathrm{d}t}$, we get an extra term that would not be present otherwise.

Solving $\mathrm{d}f(X)\,\mathrm{d}t = \mathrm{d}f - g(X)\,\mathrm{d}B$ from (B.1) and inserting that in the first term in (B.7), as well as using that $[\mathrm{d}X]^2 = g^2[\mathrm{d}B]^2 = g^2\,\mathrm{d}t$ in the second term (neglecting terms of order higher that dt) we can rewrite the Ito formula as

$$\mathrm{d}f(X) = f'(X)\,\mathrm{d}X + \frac{1}{2}f''(X)\,\mathrm{d}X^2. \tag{B.8}$$

Considering a multivariate function $f(X_1, X_2) = X_1X_2$, and inserting this in (B.8), we get

$$\mathrm{d}(X_1X_2) = X_1\,\mathrm{d}X_2 + X_2\,\mathrm{d}X_1 + \mathrm{d}X_1\,\mathrm{d}X_2. \tag{B.9}$$

Here we clearly see the difference between the Ito rule and the ordinary chain rule, where we would get only $\mathrm{d}(X_1X_2) = X_1\,\mathrm{d}X_2 + X_2\,\mathrm{d}X_1$.

B.1.3 Stochastic Taylor Expansions

Consider the Ito stochastic differential equation (B.1) and its solution in integral form (B.2). To obtain the stochastic Ito-Taylor expansion, we iteratively apply the Ito formula. For any twice differentiable function f, starting with the Ito formula (B.8), inserting (B.1), and integrating, gives us

$$\begin{aligned} f(X_t) = f(X_{t_0}) &+ \int_{t_0}^{t} \Big(h(X_s)\,\frac{\partial}{\partial x}\,f(X_s) + \frac{1}{2}g^2(X_s)\,\frac{\partial^2}{\partial X^2}\,f(X_s)\Big)\,\mathrm{d}s + \\ &+ \int_{t_0}^{t} g(X_s)\,\frac{\partial}{\partial X}\,f(X_s)\,\mathrm{d}W_s. \end{aligned} \tag{B.10}$$

Using (B.10) for the functions h and g in (B.2), with $t_0 < s < t$, gives

$$\begin{aligned} X_t = X_{t_0} &+ \int_{t_0}^{t} \Big[h(X_{t_0}) + \int_{t_0}^{s} \Big(h(X_u)\,\frac{\partial}{\partial x}\,h(X_u) + \frac{1}{2}g^2(X_u)\,\frac{\partial^2}{\partial X^2}\,h(X_u)\Big)\,\mathrm{d}u + \\ &+ \int_{t_0}^{s} g(X_u)\,\frac{\partial}{\partial X}\,h(X_u)\,\mathrm{d}W_u\Big]\,\mathrm{d}s + \\ &+ \int_{t_0}^{t} \Big[g(X_{t_0}) + \int_{t_0}^{s} \Big(h(X_u)\,\frac{\partial}{\partial x}\,g(X_u) + \frac{1}{2}g^2(X_u)\,\frac{\partial^2}{\partial X^2}\,g(X_u)\Big)\,\mathrm{d}u + \\ &+ \int_{t_0}^{s} g(X_u)\,\frac{\partial}{\partial X}\,g(X_u)\,\mathrm{d}W_u\Big]\,\mathrm{d}W_s. \end{aligned} \tag{B.11}$$

Neglecting terms of higher order than $\mathrm{d}t$ leaves us with

$$X_t = X_{t_0} + h(X_{t_0}) \int_{t_0}^{t} \mathrm{d}s + g(X_{t_0}) \int_{t_0}^{t} \mathrm{d}W_u + \int_{t_0}^{t} \int_{t_0}^{s} g(X_u) \frac{\partial}{\partial X} g(X_u) \, \mathrm{d}W_u \, \mathrm{d}W_s. \tag{B.12}$$

Now, using (B.10) for the function $g(X_u) \dfrac{\partial}{\partial X} g(X_u)$, and again neglecting higher order terms gives [73]

$$X_t = X_{t_0} + h(X_{t_0}) \int_{t_0}^{t} \mathrm{d}s + g(X_{t_0}) \int_{t_0}^{t} \mathrm{d}W_u + g(X_{t_0}) \frac{\partial}{\partial X} g(X_{t_0}) \int_{t_0}^{t} \int_{t_0}^{s} \mathrm{d}W_u \, \mathrm{d}W_s. \tag{B.13}$$

The final integral evaluates to [73]

$$\int_{t_0}^{t} \int_{t_0}^{s} \mathrm{d}W_u \, \mathrm{d}W_s = \frac{1}{2} \left[(W_t - W_{t_0})^2 - (t - t_0) \right]. \tag{B.14}$$

We now have

$$\begin{aligned} X_t = X_{t_0} + h(X_{t_0})(t - t_0) + g(X_{t_0}) \Big(W_t - W_{t_0} \Big) + \\ + g(X_{t_0}) \frac{\partial}{\partial X} g(X_{t_0}) \frac{1}{2} \left[(W_t - W_{t_0})^2 - (t - t_0) \right]. \end{aligned} \tag{B.15}$$

After discretizing, we thus arrive at

$$X_{i+1} = X_i + h(X_i)\Delta t + g(X_i)\Delta W + \frac{1}{2} g(X_i) \frac{\partial}{\partial X} g(X_i) \Big((\Delta W)^2 - \Delta t \Big). \tag{B.16}$$

This is the Milstein algorithm for solving stochastic differential equations.

C

Moyal function in the Fock basis

The Moyal function is a generalization of the Wigner function, introduced by Moyal [69]. It is also called the generalized or off-diagonal Wigner function. We begin the derivation following [74]. For another approach, see [75].

In the Fock basis, the Moyal function is

$$\begin{aligned} W_{mn}(x,p) &= \frac{1}{2\pi}\int_{-\infty}^{\infty} \mathrm{d}y\, e^{-\mathrm{i}py/\hbar}\,\langle x-\frac{y}{2}|m\rangle\,\langle n|x-\frac{y}{2}\rangle = \\ &= \frac{1}{2\pi}\int \mathrm{d}y\, e^{\mathrm{i}yp}\psi_m^*(x+y/2)\psi_n(x-y/2) \end{aligned} \tag{C.1}$$

Inserting the wave functions ψ_m, ψ_n defined in (5.7), we have

$$W_{mn}(x,p) = \frac{1}{2\pi}\frac{1}{\sqrt{2^{n+m}n!m!\pi}}\int \mathrm{d}y\, e^{\mathrm{i}yp}e^{-\frac{(x+y/2)^2}{2}}e^{-\frac{(x-y/2)^2}{2}}H_m(x+y/2)H_n(x-y/2). \tag{C.2}$$

Now we utilize the generating function for Hermite polynomials:

$$e^{-\xi^2+2\xi y} = \sum_{n=0}^{\infty}\frac{1}{n!}\xi^n H_n(y). \tag{C.3}$$

We complete the square in the exponential, and get

$$e^{-(\xi-y)^2+y^2} = \sum_{n=0}^{\infty}\frac{1}{n!}\xi^n H_n(y). \tag{C.4}$$

Multiplying Eq. (C.2) with $\sum_{n,m=0}^{\infty}\frac{1}{n!m!}\eta^m\xi^n$ we can rewrite it as

$$\begin{aligned} &2\pi\sum_{m,n}\sqrt{\frac{2^{n+m}}{n!m!}}\xi^m\eta^n W_{mn} = \\ &= \frac{1}{\sqrt{\pi}}\int \mathrm{d}y\, e^{\mathrm{i}yp}e^{-\frac{(x+y/2)^2}{2}}e^{-\frac{(x-y/2)^2}{2}}e^{-(\xi-(x+y/2))^2+(x+y/2)^2}e^{-(\eta-(x-y/2))^2+(x-y/2)^2} = \\ &= \frac{1}{\sqrt{\pi}}\int \mathrm{d}y\, e^{\mathrm{i}yp}e^{\frac{(x+y/2)^2}{2}}e^{\frac{(x-y/2)^2}{2}}e^{-(\xi-x-y/2)^2}e^{-(\eta-x+y/2)^2}. \end{aligned} \tag{C.5}$$

Evaluating the integral and rearranging some terms, we get

$$2\pi\sum_{m,n}\sqrt{\frac{2^{n+m}}{n!m!}}\xi^m\eta^n W_{mn} = 2e^{-(x^2+p^2)}e^{2\eta(x-\mathrm{i}p)+2\xi(x+\mathrm{i}p)-2\eta\xi}. \tag{C.6}$$

Taylor expanding the last exponential, we have

$$2\pi \sum_{m,n} \sqrt{\frac{2^{n+m}}{n!m!}} \xi^m \eta^n W_{mn} = 2e^{-(x^2+p^2)} \sum_{jk\ell} \frac{1}{j!k!\ell!} \left[2\eta(x-\mathrm{i}p)\right]^j \left[2\xi(x+\mathrm{i}p)\right]^k \left[-2\eta\xi\right]^\ell =$$
$$= 2e^{-(x^2+p^2)} \sum_{jk\ell} \frac{1}{j!k!\ell!} (-1)^\ell 2^\ell \left[2(x-\mathrm{i}p)\right]^j \left[2(x+\mathrm{i}p)\right]^k \eta^{j+\ell} \xi^{k+\ell}. \tag{C.7}$$

For fixed m and n, we see that we must set $j+\ell \to n \implies j \to n-\ell$ and $k+\ell \to m \implies k \to m-\ell$ to solve for W_{mn}. We are then left with

$$\pi \sqrt{\frac{2^{n+m}}{n!m!}} W_{mn} = e^{-(x^2+p^2)} \sum_{\ell}^{min(m,n)} \frac{1}{(n-\ell)!(m-\ell)!\ell!} (-1)^\ell 2^\ell \left[2(x-\mathrm{i}p)\right]^{n-\ell} \left[2(x+\mathrm{i}p)\right]^{m-\ell}. \tag{C.8}$$

Now set $z = \sqrt{2}(x+\mathrm{i}p)$, and the right hand side becomes

$$\begin{aligned} &e^{-\frac{zz^*}{2}} \sum_{\ell} \frac{1}{(n-\ell)!(m-\ell)!\ell!} (-1)^\ell 2^\ell 2^{(n-\ell)/2} 2^{(m-\ell)/2} z^{*n-\ell} z^{m-\ell} = \\ &= e^{-\frac{zz^*}{2}} \sum_{\ell} \frac{1}{(n-\ell)!(m-\ell)!\ell!} (-1)^\ell 2^{\frac{m+n}{2}} z^{*n-\ell} z^{m-\ell}. \end{aligned} \tag{C.9}$$

So we have

$$\begin{aligned} &\pi \sqrt{\frac{2^{n+m}}{n!m!}} W_{mn} = e^{-\frac{zz^*}{2}} \sum_{\ell} \frac{1}{(n-\ell)!(m-\ell)!\ell!} (-1)^\ell \sqrt{2^{m+n}} z^{*n-\ell} z^{m-\ell} \\ &\implies \pi W_{mn} = e^{-\frac{zz^*}{2}} \sum_{\ell} \frac{\sqrt{n!m!}}{(n-\ell)!(m-\ell)!\ell!} (-1)^\ell z^{*n-\ell} z^{m-\ell} \end{aligned} \tag{C.10}$$

We now use an identity for associated Laguerre polynomials L_α^β [76]:

$$\sum_{j}^{\max(m,n)} \frac{\sqrt{n!m!}}{(n-j)!(m-\ell)!\ell!} (-1)^j z^{*n-j} z^{m-j} = (-1)^n \sqrt{\frac{n!}{m!}} z^{m-n} L_n^{m-n}(zz^*) =$$
$$= (-1)^m \sqrt{\frac{m!}{n!}} z^{*n-m} L_m^{n-m}(zz^*), \tag{C.11}$$

This finally gives us an expression for the Wigner function for a Fock state:

$$\begin{cases} W_{mn} = \frac{1}{\pi} e^{-\frac{zz^*}{2}} (-1)^m \sqrt{\frac{m!}{n!}} z^{*n-m} L_m^{n-m}(zz^*), & n \geq m \\ W_{mn} = \frac{1}{\pi} e^{-\frac{zz^*}{2}} (-1)^n, \sqrt{\frac{n!}{m!}} z^{m-n} L_n^{m-n}(zz^*), & n < m. \end{cases} \tag{C.12}$$

We can also replace z with $\sqrt{2}(x+\mathrm{i}p)$:

$$\begin{cases} W_{mn} = \frac{1}{\pi} e^{-(x^2+p^2)} (-1)^m \sqrt{2^{n-m} \frac{m!}{n!}} (x-\mathrm{i}p)^{n-m} L_m^{n-m}(2x^2+2p^2)), & n \geq m, \\ W_{mn} = \frac{1}{\pi} e^{-(x^2+p^2)} (-1)^n \sqrt{2^{m-n} \frac{n!}{m!}} (x+ip)^{m-n} L_n^{m-n}(2x^2+2p^2), & n < m. \end{cases} \tag{C.13}$$

Another common form of representing this particular function is using $\alpha = \frac{1}{\sqrt{2}}(x + \mathrm{i}p)$. Replace z in Eq. (C.12) with $z = 2\alpha$:

$$\begin{cases} W_{mn} = \frac{1}{\pi} e^{-2|\alpha|^2} (-1)^m \sqrt{\frac{m!}{n!}} (2\alpha^*)^{n-m} L_m^{n-m}(4|\alpha|^2), & n \geq m, \\ W_{mn} = \frac{1}{\pi} e^{-2|\alpha|^2} (-1)^n \sqrt{\frac{n!}{m!}} (2\alpha)^{m-n} L_n^{m-n}(4|\alpha|^2), & n < m. \end{cases} \tag{C.14}$$

We can also define a radial and an angular variable

$$w = 2(x^2 + p^2), \quad \tan\phi = \frac{p}{x}, \tag{C.15}$$

giving

$$z = \sqrt{2}(x + \mathrm{i}p) = \sqrt{2}|x + \mathrm{i}p|e^{\mathrm{i}\phi} = \sqrt{2}\sqrt{x^2 + p^2}e^{\mathrm{i}\phi} = w^{1/2}e^{\mathrm{i}\phi}. \tag{C.16}$$

Inserting this in (C.12) gives another common representation:

$$\begin{cases} W_{mn} = \frac{1}{\pi} e^{-\frac{w}{2}} (-1)^m \sqrt{\frac{m!}{n!}} w^{\frac{n-m}{2}} e^{\mathrm{i}(n-m)\phi} L_m^{n-m}(w), & n \geq m, \\ W_{mn} = \frac{1}{\pi} e^{-\frac{w}{2}} (-1)^n \sqrt{\frac{n!}{m!}} w^{\frac{m-n}{2}} e^{\mathrm{i}(m-n)\phi} L_n^{m-n}(w), & n < m. \end{cases} \tag{C.17}$$

Bibliography

[1] P. W. Shor, "Polynomial time algorithms for prime factorization and discrete logarithms on a quantum computer," SIAM J. Sci. Statist. Comput. **26**, 1484 (1997), arXiv:quant-ph/9508027 .

[2] S. Lloyd and S. L. Braunstein, "Quantum computation over continuous variables," Phys. Rev. Lett. **82**, 1784–1787 (1999).

[3] S. L. Braunstein and P. van Loock, "Quantum information with continuous variables," Rev. Mod. Phys. **77**, 513–577 (2005).

[4] A. Mari and J. Eisert, "Positive wigner functions render classical simulation of quantum computation efficient," Phys. Rev. Lett. **109**, 230503 (2012).

[5] H. Goldstein, C. Poole, and J. Safko, *Classical Mechanics*, 3rd ed. (Addison Wesley, 2002).

[6] J. D. Jackson, *Classical electrodynamics*, 3rd ed. (Wiley, 1999).

[7] M. Göppert-Mayer, "Über elementarakte mit zwei quantensprüngen," Annalen der Physik **401**, 273–294 (1931).

[8] R. Loudon, *The Quantum Theory of Light*, 3rd ed. (Oxford University Press, 2000).

[9] J. Garrison and R. Chiao, *Quantum Optics*, Oxford Graduate Texts (OUP Oxford, 2008).

[10] H. Breuer and F. Petruccione, *The Theory of Open Quantum Systems* (OUP Oxford, 2007).

[11] D. Walls and G. Milburn, *Quantum Optics* (Springer Berlin Heidelberg, 2008).

[12] C. Gerry and P. Knight, *Introductory Quantum Optics* (Cambridge University Press, 2004).

[13] P. Meystre and M. Sargent, *Elements of Quantum Optics* (Springer Berlin Heidelberg, 1998).

[14] M. Orszag, *Quantum Optics*, Advanced texts in physics (Springer, 2016).

[15] H. J. Carmichael, *Statistical Methods in Quantum Optics 2: Non-Classical Fields* (Springer Berlin Heidelberg, 2008).

[16] C. W. Gardiner and M. J. Collett, "Input and output in damped quantum systems: Quantum stochastic differential equations and the master equation," Phys. Rev. A **31**, 3761–3774 (1985).

[17] C. Gardiner and P. Zoller, *Quantum Noise: A Handbook of Markovian and Non-Markovian Quantum Stochastic Methods with Applications to Quantum Optics*, Springer Series in Synergetics (Springer, 2004).

[18] C. W. Gardiner, A. S. Parkins, and P. Zoller, "Wave-function quantum stochastic differential equations and quantum-jump simulation methods," Phys. Rev. A **46**, 4363–4381 (1992).

[19] A. Doherty and H. Mabuchi, *Optical Microcavities*, edited by K. Vahala (World Scientific Publishing Company, 2004) Chap. Atoms in Microcavities: Quantum Electrodynamics, Quantum Statistical Mechanics, and Quantum Information Science.

[20] X. Mao, ed., *Stochastic Differential Equations and Applications* (Woodhead Publishing, 2011).

[21] Y. V. Prokhorov and A. N. Shiryaev, *Probability Theory III: Stochastic Calculus*, Encyclopaedia of Mathematical Sciences, Vol. 45 (Springer Berlin Heidelberg, 1998).

[22] C. Gardiner, *Handbook of stochastic methods*, 3rd ed., Springer Series in Synergetics (Springer, 2004).

[23] H. Wiseman and G. Milburn, *Quantum Measurement and Control* (Cambridge University Press, 2010).

[24] H. M. Wiseman, "Quantum theory of continuous feedback," Phys. Rev. A **49**, 2133–2150 (1994).

[25] A. Barchielli, "Continual measurements in quantum mechanics and quantum stochastic calculus," in *Open Quantum Systems III: Recent Developments*, edited by S. Attal, A. Joye, and C.-A. Pillet (Springer Berlin Heidelberg, Berlin, Heidelberg, 2006) pp. 207–292.

[26] K. Jacobs and D. A. Steck, "A straightforward introduction to continuous quantum measurement," Contemporary Physics **47**, 279–303 (2006).

[27] K. Kraus, A. Böhm, J. Dollard, and W. Wootters, *States, effects, and operations: fundamental notions of quantum theory*, Lecture notes in physics (Springer-Verlag, 1983).

[28] A. Peres, *Quantum Theory: Concepts and Methods*, Fundamental Theories of Physics, Vol. 57 (Springer, 1995).

[29] A. F. Kockum, *Quantum optics with artificial atoms*, PhD thesis (Department of Microtechnology and Nanoscience, Applied Quantum Physics Laboratory, Chalmers University of Technology, 2014).

[30] T. A. Brun, "A simple model of quantum trajectories," American Journal of Physics **70**, 719–737 (2002).

[31] U. Leonhardt and H. Paul, "Measuring the quantum state of light," Progress in Quantum Electronics **19**, 89 – 130 (1995).

[32] H. M. Wiseman and G. J. Milburn, "Quantum theory of field-quadrature measurements," Phys. Rev. A **47**, 642–662 (1993).

[33] H. Carmichael, *An Open Systems Approach to Quantum Optics*, v. 18 (Springer Berlin Heidelberg, 1993).

[34] P. Kloeden and E. Platen, *Numerical Solution of Stochastic Differential Equations*, Stochastic Modelling and Applied Probability (Springer Berlin Heidelberg, 2011).

[35] D. Clements and B. Anderson, "Well-behaved ito; equations with simulations that always misbehave," IEEE Transactions on Automatic Control **18**, 676–677 (1973).

[36] G. Maruyama, "Continuous markov processes and stochastic equations," Rendiconti del Circolo Matematico di Palermo **4**, 48 (1955).

[37] D. J. Higham., "An algorithmic introduction to numerical simulation of stochastic differential equations," SIAM Review **43**, 525–546 (2001).

[38] E. Wigner, "On the quantum correction for thermodynamic equilibrium," Phys. Rev. **40**, 749–759 (1932).

[39] M. Hillery, R. F. O'Connell, M. O. Scully, and E. P. Wigner, "Distribution functions in physics: Fundamentals," Physics Reports **106**, 121–167 (1984).

[40] T. L. Curtright, D. B. Fairlie, and C. K. Zachos, *A Concise Treatise on Quantum Mechanics in Phase Space* (World Scientific Publishing, 2013).

[41] R. Hudson, "When is the wigner quasi-probability density non-negative?" Reports on Mathematical Physics **6**, 249 – 252 (1974).

[42] H. Walther, "Resonance Fluorescence of Two-Level Atoms," Advances in Atomic Molecular and Optical Physics **51**, 239–272 (2005).

[43] H. J. Kimble and L. Mandel, "Theory of resonance fluorescence," Phys. Rev. A **13**, 2123–2144 (1976).

[44] A. Blais, R.-S. Huang, A. Wallraff, S. M. Girvin, and R. J. Schoelkopf, "Cavity quantum electrodynamics for superconducting electrical circuits: An architecture for quantum computation," Phys. Rev. A **69**, 062320 (2004).

[45] I.-C. Hoi, C. M. Wilson, G. Johansson, J. Lindkvist, B. Peropadre, T. Palomaki, and P. Delsing, "Microwave quantum optics with an artificial atom in one-dimensional open space," New Journal of Physics **15**, 025011 (2013).

[46] A. Wallraff, D. I. Schuster, A. Blais, L. Frunzio, R.-S. Huang, J. Majer, S. Kumar, S. M. Girvin, and R. J. Schoelkopf, "Strong coupling of a single photon to a superconducting qubit using circuit quantum electrodynamics," Nature **431**, 162–167 (2004).

[47] C. M. Wilson, G. Johansson, A. Pourkabirian, M. Simoen, J. R. Johansson, T. Duty, F. Nori, and P. Delsing, "Observation of the dynamical Casimir effect in a superconducting circuit," Nature **479**, 376–379 (2011).

[48] I.-C. Hoi, A. F. Kockum, L. Tornberg, A. Pourkabirian, G. Johansson, P. Delsing, and C. M. Wilson, "Probing the quantum vacuum with an artificial atom in front of a mirror," Nature Physics **11**, 1045–1049 (2015), arXiv:1410.8840 .

[49] F. Mallet, M. A. Castellanos-Beltran, H. S. Ku, S. Glancy, E. Knill, K. D. Irwin, G. C. Hilton, L. R. Vale, and K. W. Lehnert, "Quantum state tomography of an itinerant squeezed microwave field," Phys. Rev. Lett. **106**, 220502 (2011).

[50] O. Astafiev, A. M. Zagoskin, A. A. Abdumalikov, Y. A. Pashkin, T. Yamamoto, K. Inomata, Y. Nakamura, and J. S. Tsai, "Resonance Fluorescence of a Single Artificial Atom," Science **327**, 840 (2010), arXiv:1002.4944 .

[51] A. Kenfack and K. Życzkowski, "Negativity of the wigner function as an indicator of non-classicality," Journal of Optics B: Quantum and Semiclassical Optics **6**, 396 (2004).

[52] B. R. Mollow, "Power spectrum of light scattered by two-level systems," Phys. Rev. **188**, 1969–1975 (1969).

[53] R. H. Brown and R. Q. Twiss, "Interferometry of the intensity fluctuations in light. i. basic theory: The correlation between photons in coherent beams of radiation," Proceedings of the Royal Society of London A: Mathematical, Physical and Engineering Sciences **242**, 300–324 (1957).

[54] R. J. Glauber, "The quantum theory of optical coherence," Phys. Rev. **130**, 2529–2539 (1963).

[55] H. J. Carmichael and D. F. Walls, "Proposal for the measurement of the resonant stark effect by photon correlation techniques," Journal of Physics B: Atomic and Molecular Physics **9**, L43 (1976).

[56] H. J. Kimble, M. Dagenais, and L. Mandel, "Photon antibunching in resonance fluorescence," Phys. Rev. Lett. **39**, 691–695 (1977).

[57] M. Hofheinz, H. Wang, M. Ansmann, R. C. Bialczak, E. Lucero, M. Neeley, A. D. O'Connell, D. Sank, J. Wenner, J. M. Martinis, and A. N. Cleland, "Synthesizing arbitrary quantum states in a superconducting resonator," Nature **459**, 546–549 (2009).

[58] A. Vogt, "Position and momentum distributions do not determine the quantum mechanical state," in *Mathematical Foundations of Quantum Theory*, edited by A. R. Marlow (Academic Press, 1978) pp. 365–372.

[59] A. Orlowski and H. Paul, "Phase retrieval in quantum mechanics," Phys. Rev. A **50**, R921–R924 (1994).

[60] K. Vogel and H. Risken, "Determination of quasiprobability distributions in terms of probability distributions for the rotated quadrature phase," Phys. Rev. A **40**, 2847–2849 (1989).

[61] D. T. Smithey, M. Beck, M. G. Raymer, and A. Faridani, "Measurement of the wigner distribution and the density matrix of a light mode using optical homodyne tomography: Application to squeezed states and the vacuum," Phys. Rev. Lett. **70**, 1244–1247 (1993).

[62] A. I. Lvovsky and M. G. Raymer, "Continuous-variable optical quantum-state tomography," Rev. Mod. Phys. **81**, 299–332 (2009).

[63] Z. Hradil, "Quantum-state estimation," Phys. Rev. A **55**, R1561–R1564 (1997).

[64] J. Sakurai and J. Napolitano, *Modern Quantum Mechanics* (Addison-Wesley, 2011).

[65] A. I. Lvovsky, "Iterative maximum-likelihood reconstruction in quantum homodyne tomography," Journal of Optics B: Quantum and Semiclassical Optics **6**, S556 (2004).

[66] J. S. Neergaard-Nielsen, *Generation of single photons and Schrödinger kitten states of light*, PhD thesis (Center for Quantum Optics, Niels Bohr Institute, 2008).

[67] Z. Hradil, J. Rehacek, J. Fiurasek, and M. Jezek, *Quantum State Estimation (Lecture Notes in Physics)*, edited by M. Paris and J. Rehacek (Springer, 2004).

[68] W. P. Schleich, *Quantum Optics in Phase Space* (Wiley-VCH Verlag GmbH & Co. KGaA, 2005).

[69] J. E. Moyal, "Quantum mechanics as a statistical theory," Mathematical Proceedings of the Cambridge Philosophical Society **45**, 99–124 (1949).

[70] Z. Y. Ou and H. J. Kimble, "Probability distribution of photoelectric currents in photodetection processes and its connection to the measurement of a quantum state," Phys. Rev. A **52**, 3126–3146 (1995).

[71] C. Cohen-Tannoudji, J. Dupont-Roc, and G. Grynberg, *Photons and Atoms: Introduction to Quantum Electrodynamics* (Wiley, 1997).

[72] M. Martin-Martinez, "Lecture on relativistic quantum information," (2017), institute for Quantum Computing, University of Waterloo.

[73] E. Platen and N. Bruti-Liberati, *Numerical Solution of Stochastic Differential Equations with Jumps in Finance*, Vol. 64 (Springer Berlin Heidelberg, 2010) Chap. Stochastic Expansions.

[74] H. Groenewold, *On the principles of elementary quantum mechanics* (Rijks-Universiteit te Utrecht., 1946).

[75] M. S. Bartlett and J. E. Moyal, "The exact transition probabilities of quantum-mechanical oscillators calculated by the phase-space method," Mathematical Proceedings of the Cambridge Philosophical Society **45**, 545–553 (1949).

[76] A. Wünsche, "Laguerre 2d-functions and their application in quantum optics," Journal of Physics A: Mathematical and General **31**, 8267 (1998).